Mathematical and Experimental Study for Waves and Pattern Dynamics: Focused on Animal Locomotion and Belousov-Zhabotinsky Reaction

明治大学大学院先端数理科学研究科

2013 年度

博士学位請求論文

Mathematical and Experimental Study for Waves and Pattern Dynamics: Focused on Animal Locomotion and Belousov-Zhabotinsky Reaction

波とパターンダイナミクスに関する数理的・実験的研究

–生物の運動とベローソフ・ ジャボチンスキー反応を例にして–

学位請求者　現象数理学専攻

岩本　真裕子

Abstract

A mathematical model which captures essences of matters is a great tool in understanding complex phenomena observed in nature and society surrounding us. In this dissertation, I focused on waves and pattern dynamics as a clue to figure out various phenomena, and aimed to reveal the mechanism of generating a phenomenon using a mathematical model. Especially, two cases of waves and pattern dynamics observed in nature are covered, i.e., wave patterns which have some function for maintenance of life, and patterns which are formed as a result of wave propagation. The former study has a purpose to find how wave patterns act in the phenomena created by complex interactions between various factors. Conversely, in the latter study, the aim is to verify a process of forming a wave pattern and to elucidate the mechanism. This dissertation deals experimentally and mathematically with two nonlinear phenomena related to waves and pattern dynamics in nature.

The first topic of this dissertation is animal locomotion, in particular focused on adhesive locomotion in gastropods. In this study, a new mathematical model for adhesive locomotion was proposed based on experimental results, and analyzed by mainly numerical calculations. The second topic is spiral reentry in cardiac myocyte which is observed when ventricular fibrillation occurred. In this study I regard this phenomenon as wave behaviors in inhomogeneous excitable media, and the research was advanced using the Belousov-Zhabotinsky (BZ) reaction which is one of the chemical oscillatory reactions toward understanding of the mechanism of spontaneous spiral formation in excitable media. Wave behaviors in inhomogeneous excitable media were investigated experimentally using two kinds of BZ reactions, photosensitive BZ reaction and BZ reaction with catalyzed resin beads, and numerically using modified existing models for BZ reaction, i.e., Oregonator. Brief explanations of each study are given in subsequent context.

Animals choose the locomotion strategies suitable for the situations and their own environments from various kinds of styles including walking, running, crawling, flying, and swimming. To understand a mechanism of motion in animal has been subjected to scientific study for years. However, a mechanism of even simple locomotion styles such as crawling had not been clear perfectly. On the other hand, in the field of recent engineering, it tends to pursue robots mimicking animals for flexibility and environment adaptability which were hard to implement by an existing way. Mechanism elucidation of animal motion is the most crucial issue also in applicative aspect since it is difficult to realize animal-like implementation, which has flexibility and toughness, by absence of a definite mechanism. It is reasonable to assume that there is a fundamental logic in kinematic control system in common

among a variety of locomotion styles. Final goal of this study thus is to find a common logic in mechanism of animal motion. This study focused on adhesive locomotion which is a typical locomotion strategy of mollusk. Gastropods which are called generally univalve shell including snails and abalones was chosen as a model animal.

It has been reported by previous study in adhesive locomotion of gastropods that the significant factors of locomotion mechanism are "propagation of muscular waves" and "interfacial friction against the ground". The former has specific wave patterns which have been classified into mainly four types by wave direction and symmetric property. The latter has been considered to be controlled by lifting the pedal up, or dynamic viscoelasticity of mucus. To lift pedal up in appropriate timing, complex signals from the center would be necessary although the mechanism of lifting is simple in kinetics. A hypothesis of a mechanism of mucus is based on the Denny's experimental result that the mucus of banana slug has two phases, elastic solid and viscous liquid. The relation to muscular contraction waves, however, remains to be explained. Even though most in this field had been qualitative study from observations and experiments, recent researches have become to elucidate quantitative results. The verification using a model which describes essential factors obtained from the quantitative studies is immediately needed. In addition, a series of studies which applied to robotics based on the hypothesis of frictional control of mucus have not described "flexible" muscular contraction waves which should be considered as an important factor, hence, it is still not clear whether the mutual interaction between mucus and muscular contraction could realize efficient locomotion.

This study focused on the hypothesis of dynamic viscoelasticity of mucus reported by Denny from the point of view of automatic frictional control similar to the mechanism of locomotion in earthworm. Based on the matter of previous study, a simple mathematical model which captures essential factors obtained by qualitative observations is proposed, and the physical parameters in the model are estimated by quantitative results from careful experiments. It has been verified by numerical calculations with the model that the mutual interaction between flexible muscular contraction waves and nonlinear dynamic viscoelasticity of the mucus can achieve an efficient locomotion. In this model, the flexible muscle and the property of mucus are described by the self-driven spring, Real-time Tunable Spring (RTS), and hysteresis loop, respectively. It is more real situation compared with the previous models because a movement of an actual natural length is limited by surrounding environments. The important result in this study is that two locomotion styles, direct wave and retrograde wave, which has been understood by different mechanism, can be realized by the same mechanism. I deal with this result as a bifurcation phenomenon, and the preparations toward mathematical analysis are given in the end of this study.

The second topic of this dissertation is wave behaviors on heterogeneous excitable media for contribution on understanding a mechanism of spiral reentry which could induce ventricular fibrillation. Although it had been indicated that heterogeneity of cardiac myocyte would induce spontaneous spiral formation in ventricular fibrillation, the mechanism has not been clear

yet. In this dissertation, I regard action potential in cardiac cells as propagation of excitable waves in heterogeneous excitable field, and discuss it using the Belousov-Zhabotinsky reaction as a model experiment. The aim of this study is to understand the wave behaviors in common in two dimensional heterogeneous excitable media from a perspective to reveal the mechanism of forming spiral reentry. Specifically, the mechanism of spontaneous spiral formation is investigated.

In cardiomegalia that is one of the characteristic of the heart which ventricular fibrillation occurred, it has been reported that prolongation of action potential duration is induced inhomogeneously at each part of ventricle, and a change would occur in the gap junction which connects electrically and metabolically between cardiac cells. In cardiac muscle whose excitability is reduced, decrease of connection between cells by decrease of gap junction would be a cause of local conduction delay and disruption. On the other hand, existence of an obstacle and vulnerability of wave have been already indicated as the mechanism of spontaneous spiral formation in BZ reaction system. The suggested mechanism which requires interaction of two waves, however, can not elucidate the mechanism of spiral reentry of a solitary wave. To find out a bottom mechanism behind the phenomenon, heterogeneity of cardiac myocyte was classified into two types, i.e., heterogeneity of excitability by inhomogeneous distribution in cell activity, and heterogeneity of propagation by anisotropy in array of gap junctions. The two types of heterogeneity would be regarded as inhomogeneity of reaction and diffusion in BZ reaction system, thus the study was performed by the two systems of BZ reaction.

In photosensitive BZ reaction which realized an inhomogeneity of reaction, three typical wave behaviors were observed with a increase of ratio of heterogeneity, i.e., blocked wave propagation, spiral formation, and planar wave propagation. Moreover, from the results of spiral formation, we found that the heterogeneity locally generated unidirectional sites, which became the origin of the spiral wave. Numerical calculations with the Oregonator model which modified for our experiment have verified that these three kinds of wave propagation are observed typically, and unidirectional path was generated around a spiral core depending on the structure created by heterogeneity of cells. It is also revealed numerically that this unidirectional propagation was generated by gradient of inhibitor.

In the experiment of the BZ reaction with catalyzed resin particles which realized inhomogeneity of diffusion, typical three wave behaviors were also observed, and there was an existence of unidirectional propagation to generate a spiral wave. A time delay and propagation failure of waves are indicated as a cause of generating unidirectional path. Finally, it has been revealed in all system of heterogeneity including the numerical simulation with the FitzHugh-Nagumo model that three types of wave behaviors can be observed typically, and unidirectional path is always observed at a location generating spiral core when spiral waves are formed. This study discussed unidirectional propagation related to a chemical diode as a probable cause of spiral formation.

Acknowledgment

I would like to deeply thank first to Prof. Daishin Ueyama who have accepted me as a doctoral student. I had always interesting discussions with him, and he gave me so much useful advices and supports for getting the opportunities of discussions and presentations. He also provided me mental support finely. I think that it is thanks to Prof. Ueyama that three years of my doctoral course became extremely positive and fulfilling days.

I am also most grateful to my dissertation team fellows; special thanks to Prof. Ryo Kobayashi of Hiroshima University who has supported me since I was a student in faculty of science at Hiroshima University. He gave me a chance to begin a new life by accepting me kindly as a master student after three years of my graduation of university. In addition I also thank for his understanding of my opinion I want to go on to doctoral course, and acceptance of my Ph.D. sub-advisor. I think I was lucky, because he always put appropriate pressure on me, and I have looked at his positive and happy attitude against study. I also say thanks to Lecturer Suematsu J. Nobuhiko who has supported me not only as a senior researcher in Hiroshima University but also as sub-advisor in Meiji University. He told me all knowledge of experiment carefully from scratch although I had no experience with chemical experiment. Moreover he told me a pleasure as well as a difficulty of chemistry experiment research. He gave me a lot of time for discussion about experiments. I owe it all to him that the research including my experiment was published as a paper after two years of beginning chemical experiment. I would like to thank Prof. Masayasu Mimura for always caring about me as my sub-adviser, as the GCOE leader, and as the leader of MIMS center. He created ideal working environment for concentrating in study, put his effort in development of young researchers. Above all, looking at his attitude of always undertaking research with the utmost energy was a comfortable pressure for me, and gave me a energy for advancing study.

I would like to thank for many people who have met in broad area of research, and my researches have been supported by various funds. In the field of animal locomotion, I would like to thank Assoc. prof. Atsushi Tero (Kyushu University) and Assist. prof. Masakazu Akiyama (Hokkaido University) for meaningful discussions about the mechanism of crawling locomotion by mucus at the early stages of this study. I would like to thank Prof. Toshiyuki Nakagaki and Dr. Itsuki Kunita (Hokkaido University) for the interesting experiment and field work, and Dr. Toshiya Kazama (Hiroshima University) for the useful discussions and giving me a lot of knowledge about biology experiment. This study about animal locomotion was supported by Meiji University Global COE Program"Formation and Development of Mathematical Sciences Based on Modeling and Analysis"

and Core Research for Evolutional Science and Technology (CREST) of Japan Science and Technology Agency (JST) "Alliance for Breakthrough between Mathematics and Sciences." In the field of experimental research with Belousov-Zhabotinsky reaction, I have lots of new meeting. I would like to thank Dr. Shu-ichi Kinoshita and Mr. Keita Tateishi for useful discussions in Young Project, and Lecturer Kohta Ikeda and Assoc. prof. Tohru Wakasa (Kyushu Institute of Technology) for giving us a mathematical perspective. I also would like to thank Prof. Kenneth Showalter (West Virginia University), Assoc. prof. Hiroyuki Kitahata (Chiba University), Prof. Satashi Nakata (Hiroshima University), Prof. Takashi Amemiya (Yokohama National University), and Tomohiko Yamaguchi (The National Institute of Advanced Industrial Science and Technology) for great discussions on several conferences and meetings, especially, Gordon Research Conference in Colby college. This study about wave behaviors in heterogeneous excitable media was supported by Young Project of Meiji University Global COE Program "Formation and Development of Mathematical Sciences Based on Modeling and Analysis" in 2011 and 2012. In addition, in the field of theoretical and numerical research on escape behavior under a panic, although it does not include in this dissertation, I would like to thank Lecturer Akiyasu Tomoeda, Mr. Kohta Suzuno, Mr. Tsubasa Masui, and Dr. Siew Hai Yen for the pleasant discussions and giving me a wide vision of study. I also would like to thank the members of Suematsu lab including Dr. Akiko Nakamasu, Miss Mai Kaihara, Miss Kurina Tateno, Mr. Soichiro Inoue, Mr. Takayoshi Shimizu, and Mr. Suguru Shizuka for the useful discussions on my research from a variety of different angles in the seminar.

Moreover, I would like to thank people who spent the days together at 3rd building in ikuta and nakano campus including Mr. Masahiro Yamaguchi, Assoc. prof. Hirofumi Izuhara (Miyazaki University), Dr. Chiaki Miura (The Graduate University of Advanced Studies), Dr. Ryoko Okajima, Dr. Kenta Yashima (The Graduate University of Advanced Studies), Dr. Kenta Odagiri, Dr. Takuya Machida, and Assoc. prof. Ryusuke Kon (Miyazaki University) for many useful discussions and meaningless talking. I also appreciate to office clerks of MIMS, GCOE, and AMS of Meiji University, and MLS of Hiroshima University for lots of supports to progress my study. Especially, I would like to thank people who have still supported me since I was a student of Hiroshima University including Ms. Mayumi Hata, Ms. Noriko Toyota, Ms. Yoko Nakamura, Ms. Kikuko Yanada, and Ms. Mari Nakamura for giving me many pleasure and advises for my life. I send my most sincere thanks for lots of meetings and kindly supports to complete this dissertation.

Finally, I thank my family from the bottom of my heart for always supporting me mentally.

Contents

List of Figures

List of Tables

CHAPTER 1

General Introduction

In this dissertation I focus on "waves and pattern dynamics". Especially, I will discuss two main topics, i.e., "animal locomotion" in Chapter 2 and "waves in chemical system" in Chapter 3, that I was really interested in. In the first section, Section 1.1, of this chapter, I mention my research motivations, and why I have started study in the different field. Then I introduce variety of waves and pattern dynamics in nature in Section 1.2. I describe the guideline to address this study in Section 1.3

1.1. Motivation –Significance of Modeling–

1.1.1. Motivation to Research. I have been interested in "movement", what is more, the motion observed with my own eyes makes it look more exciting. Actually, we are fully surrounded by "movement". The wind is blowing, the water is flowing, and the phases of the moon will change. A seed shoots out buds and it grows up. A flower will bloom someday and the harvest season comes around. Furthermore, we, living creatures, have also "movement". Birds fly to the sky, fishes in the sea are swimming, and there are many walking and running mammals. The interesting point of movement is that it can be observed temporally as well as spatially. Although my heart exists in the same portion of my body all the time, if it would see temporally, my heart is beating and the heartbeat maintains my life. That is to say, there is a rhythm in the beat and breathing. Rhythm is one of important factors in shaping "movement". Rhythmic movement (oscillation) has a temporal alteration, but it is repeated periodically. Nature, especially the phenomena of life, are full of rhythm, such as circadian rhythm cycle and cell division.

We human beings have tried in the past to figure out secrets of nature and obtained a lot of information. In the today's information society, we human beings have our pride and arrogance of the highest creature, and we have delusions that we know all the answers. However it is, of course, an illusion. In various situations, we might face to a high ability of nature, and also be aghast at diverse performances of non-humans. We are always overwhelmed by the force of nature. They really are surviving, without getting lazy, to reproduce their own species to the next generation. I am sure their obtained ways to survive are far beyond human's imagination. Hence, we should confront a lot of still hidden wonders of the natural world.

Now, we humans are at a crossroads. With the development of science and technology, our life have become convenient and the world have been small. While the physical distance shrinks, however, the psychological distance gets farther away. Before I enrolled in the doctoral program, on March

11, the Great East Japan Earthquake occurred. Although I experienced the Great Hanshin Earthquake in Kyoto when I was a elementary school student, I learned anew fear of tsunami and the size of the earthquake. Over 10 years after the Great Hanshin Earthquake, the world has become smaller, people all over the world have thought, been worried, and cared about someone who have never seen. It is sure everyone thought "What is that I can do?". Each looked for "something" which they could, and did it in their own way. Then, we should consider something in anticipation of the future from the viewpoint of scientists even if we are junior scientists. Would our research be helpful to something? Could the science make people happy? Could the science protect people from a misfortune? Human history is also the history of science. Science sometimes hurt and killed people. However, I guess, science made many people smile. We study believing that our researches will possibly be able to contribute to a happy world in future, or surely be able to. Although it may not be direct, we would like to work which someone becomes a smiling face as a result.

As the method to push ahead with my researches, I decided to believe in what I can see in front of me. Nature and phenomena will tell us something, and always raise a new question to us, e.g., "Do you know this mechanism?", and "Do you understand our feelings?" I believe certainly that we would be able to understand something that is invisible by communication with the phenomena visible. Therefore, my motivation never be that "An interesting thing will happen if the model changes a little bit." First, there is a phenomenon, then we start to study by it, and we are aimed at understanding it.

1.1.2. How to Build a Mathematical Model. Now, I would describe how to build mathematical models based on [Burghes and Borrie, 1981, 1990], which play an important role in this paper. What is important is always to go back to fundamentals and to capture the essential of things. I introduce the concepts needed to build a mathematical model. The main process to model problems in real world is illustrated in Figure 1.1.

The problems here mean to give an explanation about several observed data, to predict something about it, or to reach a decision. To realize it, we make a lot of simplified assumptions, and rewrite an actual problem to a mathematical problem. At that time, it is necessary to clarify what is the important variables, and to make an assumption on the premise of relationship between these variables. By constructing a mathematical model from the assumptions and the relationship, we can get a certain mathematical problems in general. Then, we solve the appropriate variables using mathematical techniques suitable for it.

It needs, furthermore, to re-translate the solution to the language of real problem. And it requires an attempt to verify the model, i.e., to check whether the theoretical solution agrees with observational results of actual phenomenon. If there is a good correlativity, the model gives the phenomenon the theoretical explanation, and also it gives us a advanced prediction, or a advice for a decision. Conversely, if there is no suitable correlativity between theoretical results and observation results, we must go back to assumptions of the model, and make a decision to revise any assumptions, or

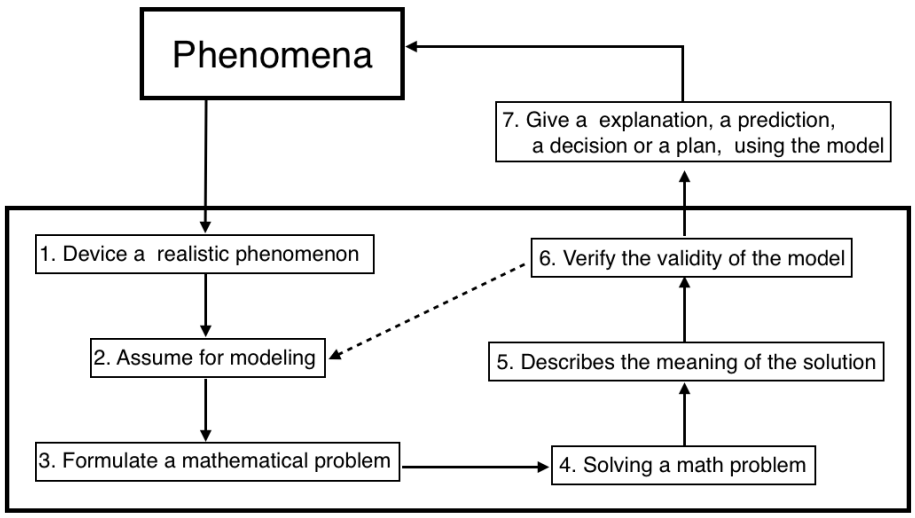

FIGURE 1.1. Main process to model problems in real world, based on [Burghes and Borrie, 1981, 1990].

add some assumptions. Then, we need to consider through this circulation route to confirm whether a new model could adequately describe a real problem. The tops of Figure 1.1 (1, 6, 7) describe a real world, and the bottoms (3, 4) describe a mathematical world. The middle ones act to connect these two world. Most mathematical education relate only to (4), although it is sometimes dealt with (1, 2, 3) formally in the field of applied mathematics. In any case, there is nothing to advance into (5,6,7).

Previously the authors [Burghes and Borrie, 1981, 1990] have said that it is difficult to understand for younger students that mathematics act the important role on solution of many problems faced in modern sciences, technology, and society until the relationship from (1) to (7) is placed importance in mathematical education. They also emphasize that most models do not go through such a well-defined way actually. The defined way is only to give any ideas in relationship between a problem in real world and a mathematical technique to solve it. Most important is the two process of translation, i.e., the first is the process of translation to mathematical problem from a real phenomenon, and the second is to a real problem from results of mathematical solution.

1.1.3. Requirement for Modeling. Modeling means to construct a model in a broad sense. *Daijirin*, the famous japanese dictionary, explains that "modeling" has the following three meaning: building a model based on design ideas, showing spacial effect by making a body and substances to statue, or by shading a picture, and observation learning. What is in common among the three meanings? I guess that is there is an object, i.e., actual or imaginary material and behavior of observer, additionally, to re-create it. Would the re-production be an goal in modeling? In fact, I would think otherwise. The way I understand what is expected of modeling is to re-create simply with capturing essences of the object, to be beyond our imaginings, and more importantly, to feedback to someone or something. It

has no meaning if modeling does not meet these three elements. Furthermore I believe that the same is true of modeling in the field of mathematical sciences.

Here let me quote the word of the famous person. "If we all did the things we are capable of doing, we would literally astound ourselves" (Thomas A. Edison). When we all did the things which we are capable of doing, it will be beyond our imaginations. When we accepted the things which is beyond our imaginations, it will fall into a category of our imaginations. Then, we get additional things which we can do, and moreover, we will be able to obtain a result which is beyond our imaginations. Development of sciences is exactly such a iteration. Modeling is the method for going beyond the compass of imagination, and it is also the tool for controlling the result which was beyond its imagination into a category of our imaginations.

1.1.4. Significance of Modeling. I believe that communication is important for development of science. Nature do not speak, even so, they would talk to us as phenomena. Moreover there is an absolutely necessary communication, i.e., talking with people. In fact, however, there is a significant hurdle here, therefore we should overcome difference in culture. Science cannot develop anymore without cross-cutting method. Although it is surely better to continue rudimentary researches in closed field, interface between different fields is required for development of science which makes the world happy. Fortunately, I could have a lot of interactions with researchers in various field in promoting two main topics picked up for this dissertation. I feel really lucky.

However, the communication with researchers in other fields are still not easy although it would have become better than in the past. I felt so, because I was always asked before the first talking, "What is your specialty?" Discussion never start unless people confirm the other person's culture. I guess it is strange, and I feel accused of that you will not allow me to become your friend until I answer about "Where are you from?" People, of course even if they are not scientists, build an emotional barrier before they talk. For what purpose? For protecting yourself? For attacking the others? The person who build a wall in dialogue is always myself. If I break down my own barrier, the others would surely open their heart. However, I am not even able to answer such an orthodox question as, "What is your field?" properly, put simply, I feel there is no speciality for me. Indeed, I can gain something by not making a wall. I would like to do anything, i.e., mathematics, numerical calculation, chemical experiment, and biological experiment. My research motivation is not to enhance my skills, but rather to understand phenomena in front of me. Using any means to attain my goal, I would like to understand phenomena, i.e., communications with phenomena.

Common language is needed for communications with phenomena similar to that with researchers in various fields. In modern, English is well known to be the common world language. I believe that modeling is the language for interface. Modeling makes a problem simple, and helps to capture the essence of phenomenon. In communication with the others, both mathematicians and experimentalists are connected by intermediate

medium i.e., modeling. Needless to say, it would depend on each speciality how to treat and develop modeling.

Furthermore, we are sure that modeling must point new direction, not just be the role of language or intermediate medium. That is to say, modeling acts the role similar to playmaker of soccer. When we would like to understand what we have seen, in spite of that we can see, we might not be able to understand. There, we look for the unseen essence behind phenomena by modeling. By modeling and analysis, we could gain "what should see" among a lot of invisible things. Exactly, modeling plays a commanding role which directs our course. When people in different cultures communicate, cultural friction occurs regrettably. Friction can, however, generate propulsive force if the directions of movement are the same, although it blocks each other if the directions are in opposite. I believe that model is obviously a playmaker who indicates the direction in discussions among researchers.

1.2. Wave in Nature

1.2.1. What is Wave? It would not be an exaggeration to say that the world is made of waves. Everywhere we can see a wave. For instance, a wave which seen in the sea, a wave of earthquake, and audience wave of soccer stadium. Also, there are a lot of waves which is invisible, that is, sound waves, light waves, radio waves, and microwave. It is often that it is necessary to consider a wave when we try to understand a phenomenon. Here, we would like to ask a simple question, "what is a wave?" As physically, a wave or a undulation is defined as the phenomenon which is spatially propagated the periodic changes on some physical quantity. It is not called "wave" when a point oscillates temporally, but when the oscillation propagates to proximate media. That is to say, a wave has spatial spread.

We would like to focus on "wave" among something of moves. Because of spatial spread, waves would show various patterns if we slice a phenomenon temporally like a strobe picture. Furthermore, the pattern will change with time, i.e., it is movement. Interestingly, the phenomena of moving patterns formed by waves is widely seen in nature. However, what is the meaning of the pattern? Why is it such a pattern? Is there a role to play?

I propose that patterns in nature generated by waves could be classified mainly into two groups. The first is that some useful function could be performed by the pattern moving. Then, the second group is that the patterns had generated as a specific result, and whether for good or bad, moving patterns influence something on something. Whatever the case, I believe that patterns in nature have the meaning. In the subsequent sections, I would introduce "various patterns generated by waves" which is able to see in nature.

1.2.2. Spatial Wave Patterns Formed by Living Matters. Many patterns formed by waves are seen around us. Most interesting for us would be complex patterns which organisms produce [Ball, 2011].

Dictyostelium discoideum is a kind of cellular slime molds, is an amoeboid unicellular organism, who live in the soil. The meaning of "unicellular" is having a single cell, but it means "simple, stupid" when it is said for a

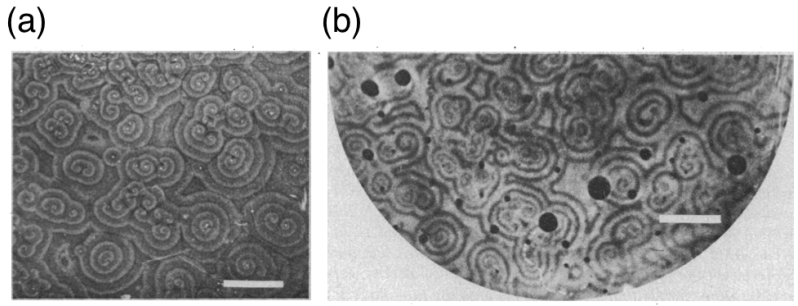

FIGURE 1.2. (a) Organized waves of cell movement during aggregation in *D. discoideum*, (b) fluorographic image of cyclic AMP waves, quoted from Figure 1 and Figure 2 of [Tomchik and Devreotes, 1981], respectively. Calibration bar is 1 cm, respectively.

person. Yet, many researches reported that unicellular creatures are neither simple nor stupid. *D. discoideum* is one of that. Facing starvation they make the multicellular body suitable more for stringent conditions by gathering and combining lots of unicellular bodies. It has been reported that Acrasin, which is a low-molecular-weight substances secreted by the cell which sensed starvation, gives other cells the command of aggregation. It is known that acrasin of *D. discoideum* is cyclic adenosine monophosphate (cAMP). The surrounding cells gather by positive chemotaxis, which is the nature of creatures moving to high concentration region depending on concentration gradient, against acrasin. In the earlier stage of this aggregation, the patterns such as Figure 1.2 are generated in the colony. It is interesting to note that no cells in the situation of easily being able to access to food have the nature of both secreting, and reacting to cAMP. That is to say, the stress of starvation produces a change in the nature of cells. This phenomenon is a example of that the patterns had generated as a specific result for being alive. In various creatures, this cAMP is known to act as the role of second messenger which transmits signals of outside cells to inside. From this common point, slime mold is of assistance in studying about transmission dynamics of many diseases from cholera to tuberculosis.

Examples of pattern formation by chemotaxis are also found in bacteria. Figure 1.3 is the patterns which appeared in colony of *Escherichia coli* grown in semi-solid agar. *E. coli* forms the complex patterns of colony by aggregation in response to chemical signal, aspartate, which is generated by the cell themselves as a metabolic substance [Budrene and Berg, 1991]. Geometric alterations in pattern occur by the difference of culture material principally. Figure 1.4 is other example of pattern formation in bacteria, *Bacillus subtilis*, and it shows target pattern and diffusion-limited aggregation (DLA) pattern [Fujikawa and Matsushita, 1989]. In this case, the alteration in pattern is generated by nutrient and surface moisture. Similar to the pattern formation in *D. discoideum*, these patterns are the results for optimal formation of colony.

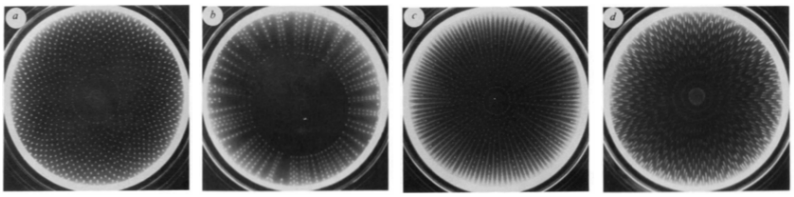

FIGURE 1.3. Patterns formed by *E. coli* in semi-solid agar, quoted from Figure 1 of [Budrene and Berg, 1991], (a) sunflower-like arrays of spots, (b) radial arrays of spots, (c) radial arrays of spots and stripes, and (d)spots with radial tails arrayed in chevrons.

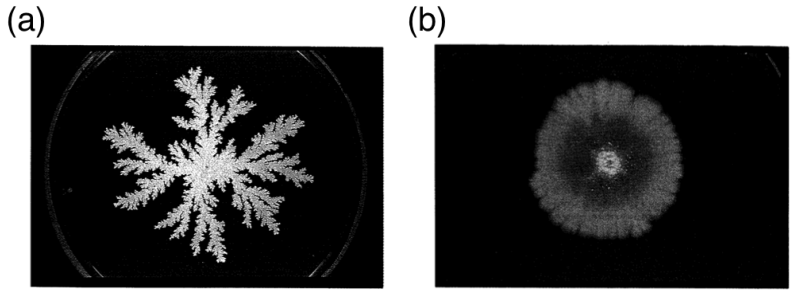

FIGURE 1.4. Patterns formed by *B. subtilis* in semi-solid agar. (a) DLA-like colony pattern which is formed in the condition of nutrient deficiency and low moisture surface, (b) smooth and round pattern which is formed in the condition of nutrient-rich and low moisture surface, quoted from Figure 1 and Figure 4 of [Fujikawa and Matsushita, 1989], respectively.

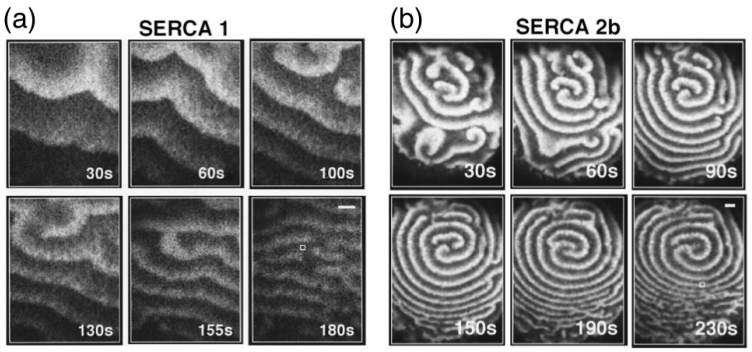

FIGURE 1.5. Repetitive Ca^{2+} wave activity in an oocyte overexpressing Ca^{2+} ATPase ((a)SERCA 1 and (b)SERCA 2a) shows wave dispersion, quoted from Figure 2a and Figure 4a of [Lechleiter et al., 1998], respectively.

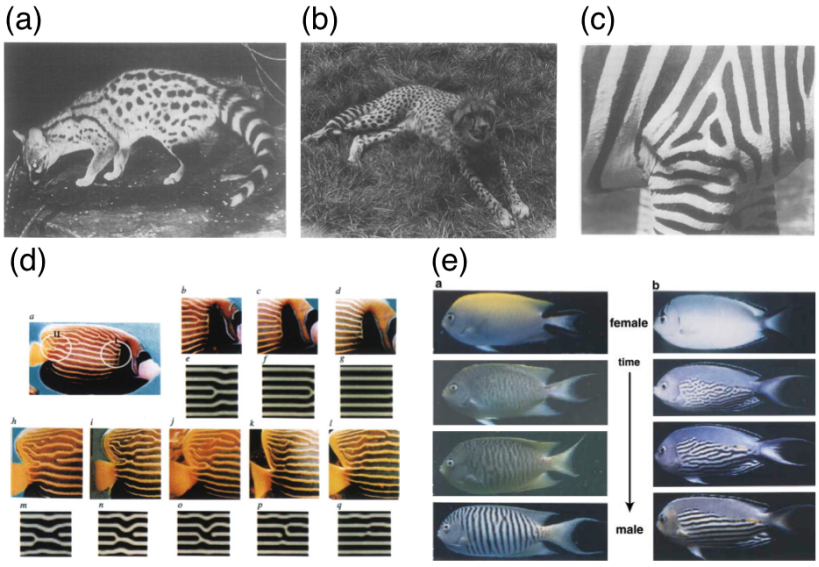

FIGURE 1.6. Patterns seen in animal coat. (a) Spot and stripe pattern of genet (*Genetta genetta*), (b) Spot pattern of cheetah (*Acinonyx jubatis*), and (c) Scapular stripes on foreleg of a mountain zebra (*Equus zebra zebra*), quoted from Plate I, Plate II, and Plate IV of [Murray, 1981], respectively. (d) Rearrangement of the stripe pattern of emperor angelfish (*Pomacanthus imperator*) and computer simulation with Turing mechanism, quoted from Figure 2 of [Kondo and Asai, 1995]. (e) The transition of stripe formation in the skin of swallowtail angelfish (*Genicanthus melanospilos*) and watanabei angelfish (*Genicanthus watanabei*) during their sex change, quoted from Figure 1 of [Shoji et al., 2003].

It is known that, when eggs of higher organisms including humans were fertilized, waves of calcium ions Ca^{2+} propagates on the surface of oocytes. Although the purpose of such a wave is not clear, it is regarded as the preparation for embryo growing. Most of these waves are simple ripples which propagate from one side to another side. It is however generated by reaction diffusion processes, so more complex patterns, e.g., spiral pattern, may be generated. Figure 1.5 is a spiral wave of calcium observed on the surface of *Xenopus laevis* oocytes [Lechleiter et al., 1998].

We can hardly discuss pattern formations in nature without taking Alan Turing into account. Turing demonstrated in 1952 that spatial heterogeneous patterns could be formed from completely homogeneous field [Turing, 1952]. It is more than sixty years ago from now, so this discovery would have been a great surprise. Many animal species have a characteristic pattern as shown in Figure 1.6, respectively, and the patterns of their surface skin are spatially larger in scale than the size of individual cells. Such a pattern is not in any internal structure, but only on the skin. Looking at these patterns would make anyone think that for what, and how this is

generated. Reaction-diffusion model helped to give the answer to this wonder. It showed that spot and stripe patterns could be generated by a simple two-factor chemical system, and explained about various phenomena of biological pattern formation, including animal pigmentation [Murray, 1981; Meinhardt, 1982; Murray, 1989]. Furthermore, Shigeru Kondo, who states flatly that he is a great fan of Turing, reported that not the width between stripes but rather the number of stripes increase in the growth process, and he simulated the process of angel fish using a Turing system model [Kondo and Asai, 1995], as shown in Figure 1.6(d). Focusing on diffusion coefficient in Turing mechanism, Kondo also reported about relationship between growth and the direction of stripe [Shoji et al., 2003]. He always stands at the forefront of this research field on pattern formation of animal skin.

Thinking about patterns of living creature, most people would imagine also the design of shells. Surface of shells we pick up in the coast is decked out in a variety of patterns. Turing mechanism also clarified the wonders of the shell patterns [Meinhardt and Klingler, 1987; Meinhardt, 1982]. The pattern of cone shell as shown in Figure 1.7 was recreated by an activator-substrate model with the addition that the substrate production is inhibited by a hormone-like substance. Hans Meinhardt [Meinhardt and Klingler, 1987] also succeeded in regenerating other various patterns of shells by Turing mechanism. Would these patterns of creature show some result? Otherwise would these have some function? It seems that there can be no definite answer to this problem even now, although a mechanism to generate these patterns was clarified by Turing system. That would be why many researchers continue to be naturally attracted to that as yet.

The idea of Turing pattern is considered beyond the patterns seen in animals. That is an attitude that patterns formed by trees and grasses might be also understood as Turing pattern. In W National Park of Niger, plants generate the pattern [Klausmeier, 1999; Valentin et al., 1999] and its patterns are called Tiger bush as shown in Figure 1.8. Tiger bush was reported for the first time by W.A. Macfaden [Macfadyen, 1950], and then these patterns are observed in Niger, Burkina Faso, Somalis, Somaliland, Ethiopia, Israel, and Mexico where are semi-desert region. To understand such phenomena in nature, Christopher [Klausmeier, 1999] built a Turing-like model in 1999, and showed with numerical simulation a striped pattern of vegetation going up slowly slope. The growth of vegetations is relying on scarce water resources and their ability to receive rainwater and prevent water from flowing down in slope. The regions where grass concentrates act an activator for growth locally, since they prevent dammed water from flowing out. Conversely, these regions act an inhibitor in long-distance since they would take away water from the below ground of slope. The phenomenon is, exactly, able to understood based on the idea of Turing pattern. It is to say that these patterns of vegetation are the results of various factors from the environment.

Spiral pattern can be sometimes bad news. It is a spiral re-entry [Jalife et al., 1998; Shajahan et al., 2011] seen in heart as shown in Figure 1.9. Ventricular fibrillation, which is one of the causes of sudden death, is related that regular traveling wave of action potential in heart converted to

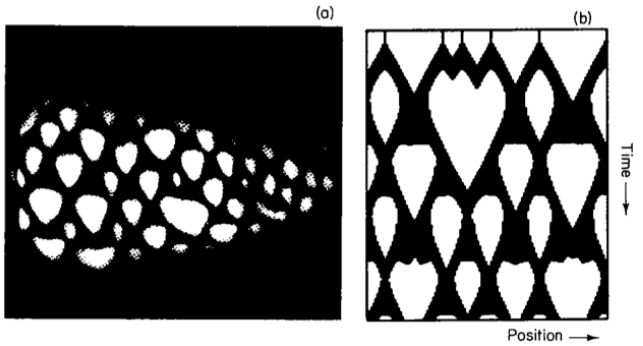

FIGURE 1.7. Pigment pattern on tropical sea shell. (a) Cone shell (*Conus marmoreus*) and (b) the calculation result with an activator-substrate model, quoted from Figure 9 of [Meinhardt and Klingler, 1987].

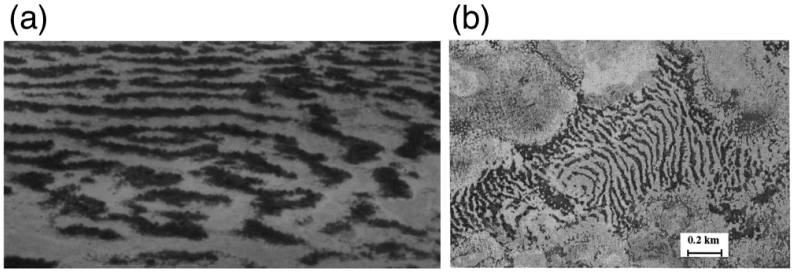

FIGURE 1.8. Typical type of banded vegetation pattern near Niamey, in Niger quoted from (a) Figure 1 of [Klausmeier, 1999] and (b) Figure 1a of [Valentin et al., 1999].

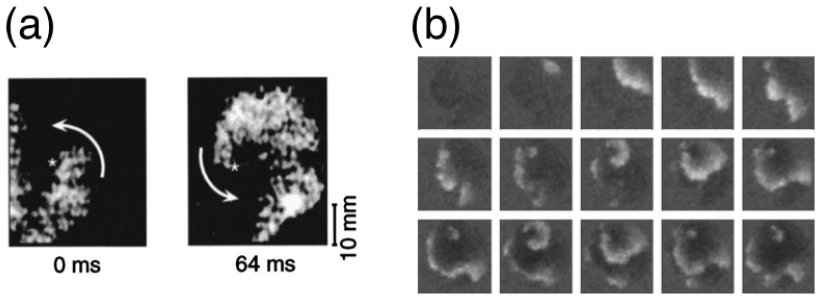

FIGURE 1.9. Spiral waves in cardiac muscle. (a) A counterclockwise rotating spiral wave recorded from a thin sheet of dog epicardial muscle using a video camera and a voltage sensitive dye, quoted from Figure 3a of [Jalife et al., 1998]. (b) A calcium wave in a monolayer culture of chick embryonic heart cells, quoted from Figure 1 of [Shajahan et al., 2011].

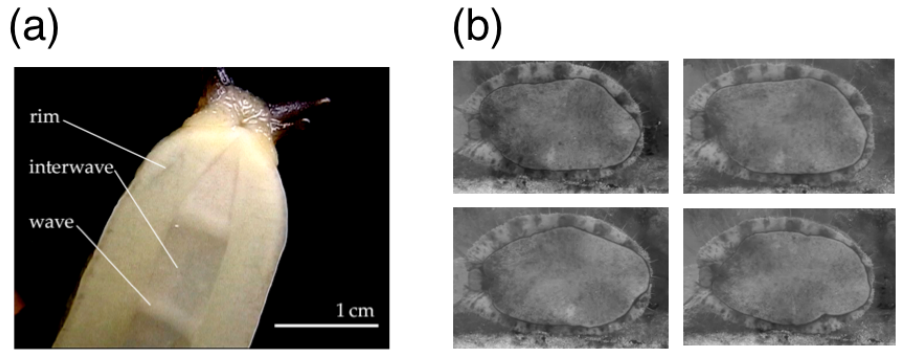

FIGURE 1.10. Wave patterns seen in adhesive locomotion of gastropods, (a) snail (*Limax maximus*) quoted from Figure 1 of [Chan et al., 2005], and (b) abalone (*Haliotis discus discus*), quoted from Figure 6.1 of [Iwamoto, 2011].

spiral waves. In excitable media, the wavelength of spiral waves tend to be shorter than that of target waves, and as a result, spiral waves, are replacing target waves, become dominant if spiral pattern formed once. In fact, it was confirmed that spiral waves are generated in the heart of animals such as rabbit and sheep on the culture substrate and that then ventricular fibrillation occurs [Gray and Jalife, 1996; Jalife et al., 1998; van Capelle et al., 1972]. It is reasonable that spiral wave is one of the pattern states which are generated in excitable media such as heart. However, the cause of spiral occurring has not been clear yet. Although it has been proposed by cellular automata model that the poor communication between cells is one of the causes [Bub et al., 2002a], an detailed answer has not seen anything yet. In order to find out why the spiral re-entry occurs, we have explored using chemical reaction and a mathematical model. Details leave to Chapter 3.

Though most people tend to focus on its seashell in thinking about patterns of univalve shell, the patterns, actually, can be seen in not only its shell but also soft body part as shown in Figure 1.10. What a wonderful creature to have patterns in the whole body! The pattern seen in its soft body part will be studied in detail in Chapter 2.

1.2.3. Spatial Wave Patterns Formed by Non-Living Matters. It seems that these periodic oscillatory phenomena and patterns are peculiar to living organisms because that are commonly seen in them. However, we can also found wonderful patterns that are created by waves in non-living system.

Patterns of waves created by atmosphere are fantastic and magnificent. For example, tropical cyclones that occur in the summer sea every year, including hurricanes and typhoons, have the structure of spiral. Tropical cyclone is that groups of cumulonimbus clouds are systemized, and rotates around its center. It is said that its rotation relates to centrifugal force and the Coriolis force, and that the direction of rotation is counterclockwise in the northern hemisphere, in contrast, is clockwise in the southern. How is a collection of cumulonimbus clouds systemized to a tropical cyclone? In the

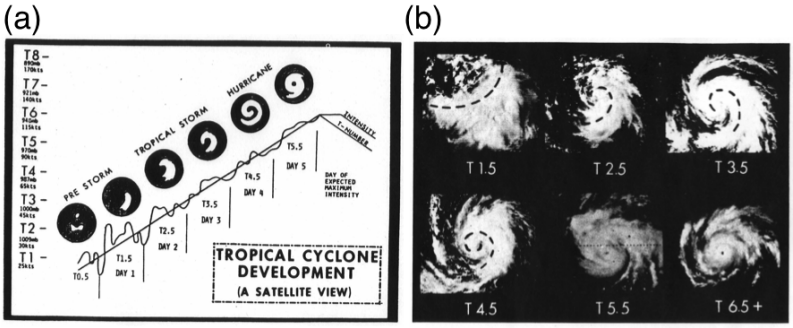

FIGURE 1.11. Dvorak method using T-number for measuring pressure center and maximum wind speed, quoted from (a) Figure 1 and (b) Figure 2 of [Dvorak, 1984], respectively. (a) Model of tropical cyclone development used in intensity analysis. (b) Examples of tropical cyclone cloud patterns at each stage of development.

process of systemization of clouds, it is known that periodic atmospheric condition which alternates between the development of cumulonimbus and the development of low pressure (called "CISK: conditional instability of the second kind") is needed, but the mechanism of forming tropical cyclone is not clear yet. However, the patterns give us various information. Meteorologist Vernon F. Dvorak [Dvorak, 1984] of NOAA (The National Oceanic and Atmospheric Administration) in the United States published in 1984 a method of measuring the maximum wind speed and central pressure from the image of the pattern as shown in Figure 1.11, and its improvements are used now.

Although tropical cyclone is the phenomenon which moves on the earth changing its pattern, there is the pattern which is seen at the same place. When cold winds blow in every winter, the vortex pattern is seen in the lee of Cheju (Jeju) Island as shown in Figure 1.13 [Jensen and Agee, 1978]. This is called Kármán vortex, because Theodor von Kármán of Hungarian showed its stability. Kármán vortex street is generated when an obstacle is placed in flow, or when a solid is moved in fluid. Its alternus vortex has occurred since Jeju Island acts the role of an obstacle in the flow of atmosphere.

Without satellite photos, that is, when we looked up at the sky, clouds show us various patterns. For example, it is well-known that the shape of clouds such as shown in Figure 1.12 is generated by kelvin-Helmholtz instability. Kelvin-Helmholtz instability is the concept of fluid dynamics that instability of fluid is generated when each layered fluid which has different density moves horizontally in different speed. At the interface, density and vorticity become inhomogeneous and disturbance grows, and then the movement of fluid is destabilized. Also in atmosphere, its instability is generated at the interface which has density difference (or difference of temperature or atmosphere pressure) and velocity difference. In the case of the interface between layers with and without clouds, we can see its pattern because the interface generated by instability appears as the shape of clouds. Kelvin-Helmholtz instability is very familiar for Japanese. The shape of waves

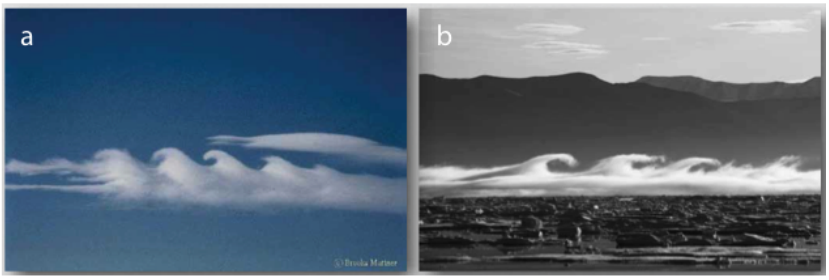

FIGURE 1.12. Kelvin-Helmholtz billows (a) by clouds and (b) by a fog layer, quoted from Figure 1a and 1b of [Smyth and Moum, 2012], respectively.

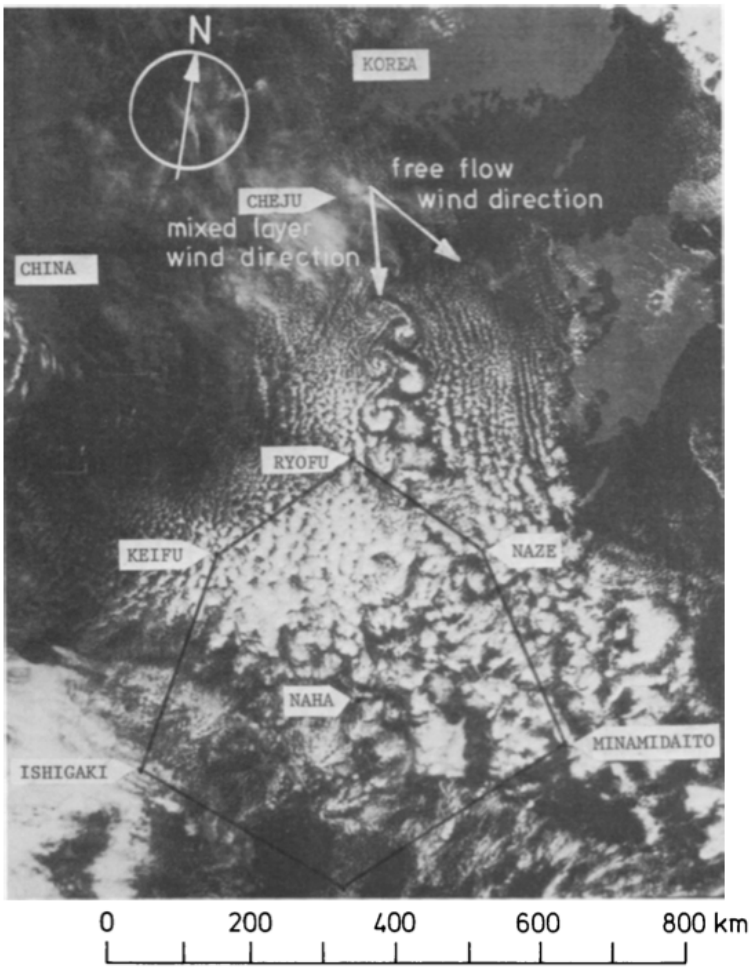

FIGURE 1.13. Kármán vortex street extending downwind of Cheju (Jeju) Island into the East China Sea, quoted from Figure 2 of [Jensen and Agee, 1978].

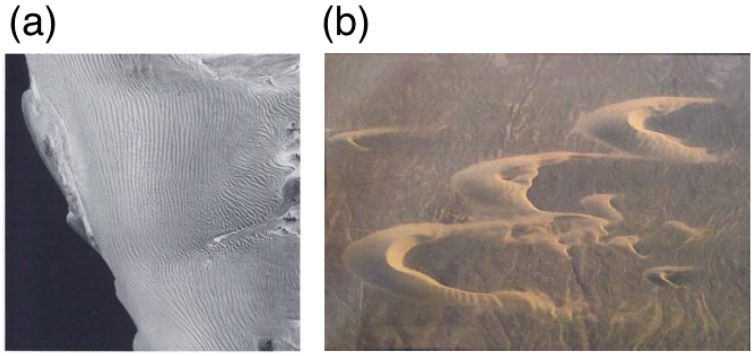

FIGURE 1.14. Pattern formation seen in dune. (a) Landsat image of the central parts of the Namib Sand Sea, quoted from Plate 1 of [Lancaster, 1995]. (b) Crescent-shaped barchan sand dunes in the desert between Chimbote and Casma on the coast of Peru, quoted from Figure 1 of [Schwämmle and Herrmann, 2003].

seen in *The Great Wave off Kanagawa* drawn by Hokusai, that is exactly Kelvin-Helmholtz instability.

On vast ground, there are also patterns created in nature. In the desert, linear pattern are seen in general as shown in Figure 1.14(a) [Lancaster, 1995]. Such a pattern in dune is considered as one of the activator-inhibitor systems. Slightly elevated hill of sand is formed by accumulation of particles blowing in the wind. Dunes and sand ripples take in more sand from the air, and further promote its growth. The large dunes, conversely, suppress sands to accumulate on its vicinity of downwind by acting as a wall. Balance between the two processes makes a certain distance between the sand dunes. Various patterns, e.g., star dunes, barchan dunes (Figure 1.14(b) [Schwämmle and Herrmann, 2003]) are also seen on desert all over the world.

Examples of pattern are also appeared in some rocks. Figure 1.15 is an example in which the pattern of the ring can be seen in carbonate siltstones (calcisiltites). Many people would be surprised by the beauty of this pattern generated spontaneously in nature. A cause of this ring pattern is explained as one of Liesegang phenomena. Such a ring pattern of iron oxide are a common secondary chemical structure found in many permeable, igneous, metamorphic and sedimentary rocks that have undergone weathering. Liesegang ring formed when oxygen in ground water diffused into polyhedra containing soluble ferrous iron in pore water.

As indicated by the name, this phenomenon was reported by Raphael Eduard Liesegang who is German chemist in 1896. Liesegang found this phenomenon, i.e., continuous phases (spacing law) in test tube and continuous rings such as tree ring on flat plate, using a silver nitrate solution and gelatin gel soaked with potassium dichromate. The similar reaction is also observed in cylinder tube of cobalt salt plus gelatin as shown in Figure 1.16. This phenomenon is that cobalt hydroxide $Co(OH)_2$ precipitated from ammonia aqueous NH_4OH diffused into a gel medium of cobalt ion

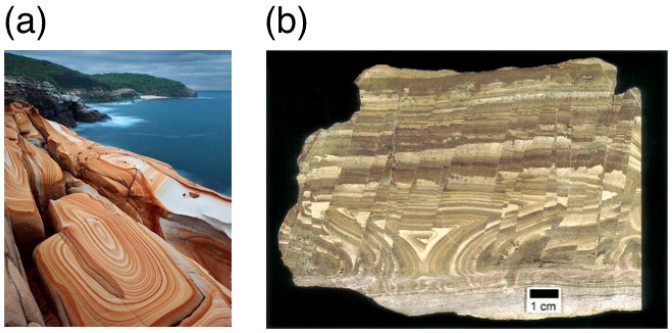

FIGURE 1.15. (a) Liesegang rings at bouddi national park in New South Wales, Australia. (b) Pattern of Liesegang bands in a calcisiltite, quoted from Figure 1 of [McBRIDE, 2003].

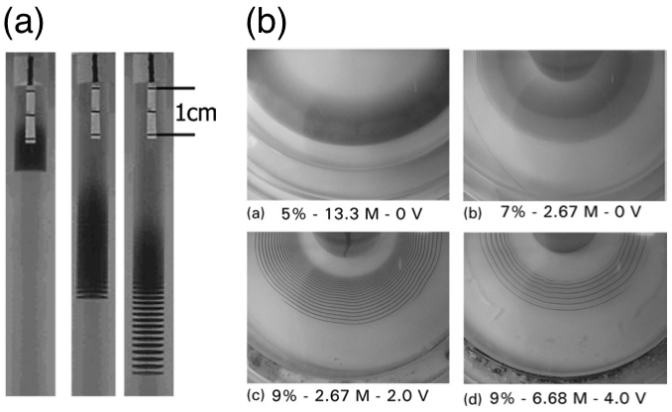

FIGURE 1.16. $Co(OH)_2$ Liesegang patterns. (a) $Co(OH)_2$ bands from Co^{2+} and NH_4OH, propagating down a tube, and (b) 2D patterns in the special petri dish, quoted from Figure 1 and 5 of [Shreif et al., 2004], respectively. In 2D experiments, $[Co^{2+}]$ was set constant, and the gel concentration, $[NH_4OH]$ and the applied voltage were changed as indicating on the figure.

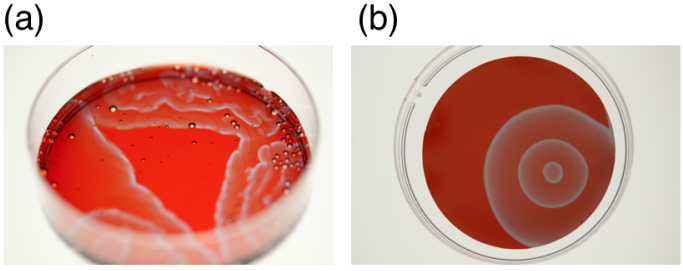

FIGURE 1.17. The spatial patterns of BZ reaction with ferroin as a catalyst, (a) in a petri dish and (b) on a membrane filter (target pattern).

Co^{2+}. The blue $Co(OH)_2$ bands seemingly migrate down a 1D vertical tube (Figure 1.16(a)), because the salt re-dissolves at the top of the pattern in a synchronized manner with the band formation by precipitation at the bottom. In 2D experiments, it was done in the presence of a electric field. Then, the ring like tree ring was observed, and the interval between rings would change depending on $[NH_4OH]$, the gel concentration, and the applied voltage as shown in Figure 1.16(b). Studies on Liesegang phenomenon are developing still, and various mathematical models have been proposed.

Belousov-Zhabotinsky (BZ) reaction is something that should not be forgotten in talking about patterns in chemical system, that is the most famous reaction as the patterns seen in chemical reaction. BZ reaction is one of the oxidation-reduction reaction of malonic acid with metallic catalyst such as cerium and ferroin, and is well-known as a typical example of oscillatory reaction. It is the spatial the patterns, i.e., target pattern (Figure 1.17(b)) and spiral pattern, that made BZ reaction famous. This reaction is characterized by having an excitable state depending on concentration of each material, or light intensity. In Chapter 3, I will research a mechanism of spiral re-entry occurred on heart, using the feature that BZ reaction is one of the excitable media.

As a feature of the chemical reaction showing such patterns, the presence of autocatalytic mechanism has been pointed out. It is said that, under this mechanism, a chemical reaction can become oscillatory. However, it is reported also in the chemical reaction that autocatalytic mechanism is clearly absent. It is, for example, in a chemical reaction that changes carbon monoxide to carbon dioxide with platinum as a catalyst. CO molecule and the oxygen atom merely bind and make CO_2. Though, It was reported that depending on temperature and partial pressures of the reactants, the reaction rate can become oscillatory or even chaotic [Ertl, 1991]. Furthermore, spatially and temporally, the concentration distributions of the adsorbed species on the surface can form patterns including spiral and target patterns as shown in Figure 1.18. Although the other examples of patterns which are generated on the surface of a metallic catalyst such as Pd, Rh and Ir were also reported, the more interesting examples are in a bimetallic catalyst. Bimetallic catalysts can play a remarkable role in heterogeneous catalysis, because mixed two metals can potentially achieve a catalytic performance superior to single ones. One can find rate oscillations and chemical wave patterns comprising target patterns, pulse trains, and rotating spiral waves in the catalytic H_2+O_2 reaction on a Rh(111) surface after alloying with Ni, as shown in Figure 1.19. The oscillatory behavior is attributed to periodic changes in the composition of the bimetallic surface alloy causing concomitant variations in catalytic activity. The study on detailed mechanism of excitation/oscillation which occurred on a Rh/Ni surface is in progress now.

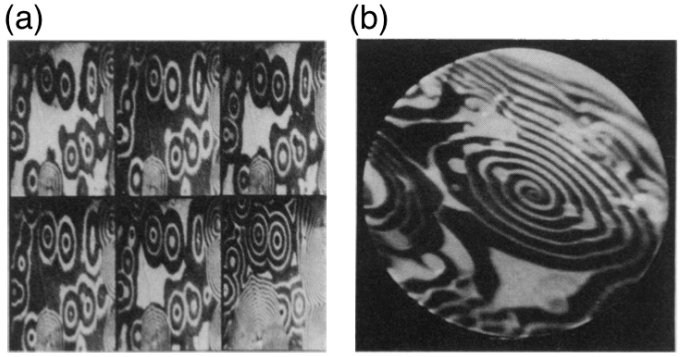

FIGURE 1.18. Spatio-temporal pattern formation in the catalytic oxidation of CO on Pt(110). (a) Target pattern and (b) spiral wave pattern, quoted from Figure 9 and 8 of [Ertl, 1991], respectively.

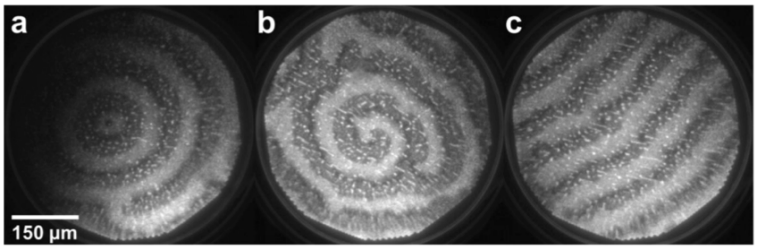

FIGURE 1.19. PEEM (photoemission electron microscopy) images of (a) target pattern, (b) rotating spiral waves, and (c) pulse trains on a biometallic Rh(111)/Ni surface, quoted from Figure 2 of [Lovis et al., 2012]. The bright structures of μm size distributed over the surface are NiO particles.

1.3. Research Subject and Guideline for Dissertation

As we have seen, there are lots of patterns generated by living creatures in nature. I classify these patterns into the following two categories, as mentioned before, the first is that it acts as the role of specific function, and the second is that it is a result for something to optimize. In the latter case, it can have direct and indirect influence on living creatures by moving, in a positive or negative way. In the first case, these patterns have been left through the process of natural selection. What does this mean? It is a fact that has been optimized. Organisms have sought how to live efficiently, hence it would be considered that there is a tip to enrich our future. In the second case, although the pattern was generated as a result of optimization, it is important that this pattern can have effects on something, whether good or bad. Particularly, if it has had a bad influence, the situation is serious. Understanding the function and mechanism of these patterns, it can be said to be the keyword of one in which we are to live better.

However, study using organisms is difficult, in the way that more time is needed, and there are several limitations. So, we should focus on the pattern

generated by non-living matters. Given the conditions occurring patterns of non-living matters, it can be seen relationships between the patterns of living creatures and non-living creatures. Through the experiments of non-living matters, it is gained a further understanding of the patterns by living creatures. Then, it is a mathematical model to act an important role in the process of promoting these researches. Using a mathematical model enables us to capture an essential factor and to consider what factors are important, and how large influences have.

I focused on the patterns seen in locomotion of organisms as the first case. A mechanism of locomotion in living creatures including we human beings, remains to be explained despite it seems easy to be achieved. It would be considered that the mechanisms adopted by organisms are optimized results through natural selection. I wonder our research could contribute to society if this mechanism would be clarified. The significant view point here is to believe that there is a common logic which is hidden in the mechanism of locomotion styles in animal. Hence I would deal with adhesive locomotion which is the simplest style, and explore its mechanism. In Chapter 2, I would study about a mathematical research for adhesive locomotion in gastropods.

Next, as the second one, I focused on the spiral patterns seen in the heart. What conclusion will await us by this pattern? It is death. Conversely, if we could prevent this pattern from generating, one of the cause of death would disappear. Using the advantage that the heart is an excitable medium, we focused on BZ reaction as excitable media as well. In Chapter 3, I would verify the process of forming spiral waves, and reveal the mechanism of spiral re-entry in the heart using experiments of chemical reaction and mathematical models. Moreover, I mention a supposed method for eliminating the cause of spiral.

In Chapter 4, I would conclude each phenomenon in the global view point, and describe about future works.

CHAPTER 2

Role of Wave Patterns in Animal Locomotion

"How do animals move?" Many scientists have been thinking about an answer for this question. There are various styles in animal locomotion, e.g., walking, running, crawling, swimming, and flying. Including zoologists and biologists, researchers in various fields had explored a mechanism of each style. The complexity of biological structure being a contributing negative factor, a mechanism of the locomotion style which seems easily is still unclear.

In the field of engineering, in parallel, robots mimicking the shapes and the movements of animals had been developed. Unfortunately, the control method of these robots is such as describing a trajectory of a joint part, so it was unable to mimic a real mechanism. It was difficult for this method to adapt surrounding environment as animals always do. In the recent robotics field, seeking implementation of environmental adaptability and flexibility, it tends to pay attention to robots close to animals more, i.e., the control methods are being changed from centralized control to autonomous decentralized control, and the devices are from hard to flexible. However, in the current situation where motion mechanism is lacking, it is difficult to achieve the implementation of the robot flexible and tough against its environment like animals. In fact, elucidation of the mechanism movement has become the most important issue in practical applications.

From the perspective that there is a underlying common logic hidden in various and complex styles of movements, I tried to uncover the logic from a simple style. In this study, we focused on "adhesive (crawling) locomotion" which is a typical form of mollusk. I selected gastropods including snails and abalones as a model organism which move by crawling, they are called "univalve shell" in general, and have the most species in the mollusk.

In this chapter, the previous study about adhesive locomotion are covered in the next section, and I will mention an importance of the friction against the ground in adhesive locomotion using a simple model in section 2.2. In section 2.3, I would model adhesive locomotion with mucus in gastropods, and in section 2.4, describe the results of computer simulations with our model. I would analyze the locomotion styles as bifurcation phenomenon from a mathematical view point in section 2.5, and discuss in section 2.6 the mechanism of adhesive locomotion in gastropod. Finally I summarize this study and describe about future works in section 2.7.

2.1. Introduction: Adhesive Locomotion

Adhesive locomotion is one of the most fundamental locomotion strategies for many animals without extremities, including amoeba, snakes (Figure 2.1(a)), and earthworms (Figure 2.1(b)). Gastropods such as snails (Figure 2.1(c)), slugs and abalone (Figure 2.1(d)) are also able to crawl steadily by propagating periodic muscular waves (alternating contraction and expansion) along their ventral foot in contact with the substrate [Miller, 1974b; Lissmann, 1945a; Gray, 1968; Jones and Trueman, 1970]. Gastropods interact with the substrate through the mucus released from their pedal foot. It is known generally that gastropod pedal mucus is produced to adjust humidity and salinity [Grimm-Jorgensen et al., 1986]. On the other hand, most researchers believe that the nonlinear rheological properties of mucus have an important role in locomotion [Denny, 1980b; Denny and Gosline, 1980; Denny, 1980a, 1981]. Understanding the locomotion mechanism of gastropods has been an interesting subject for biologists and biophysicists for over a century [Parker, 1917; Barr, 1926, 1927; Lissmann, 1945b; Jones, 1973; Miller, 1974a; Trueman, 1983; Alexander, 1992a; Donovan and Carefoot, 1997; Alexander, 2002; Lai et al., 2010]. In recent years, from the perspective of designing bio-mimicry robots, adhesive locomotion has become a subject of renewed interest among engineers [Chan et al., 2005; Lauga and Hosoi, 2006; Ewoldt et al., 2007] and physicists [Tanaka et al., 2011]. Although physical observations and physiological knowledge of gastropod crawling locomotion exists, the interaction mechanisms between the muscular waves and the physical features of mucus remain to be sufficiently elucidated.

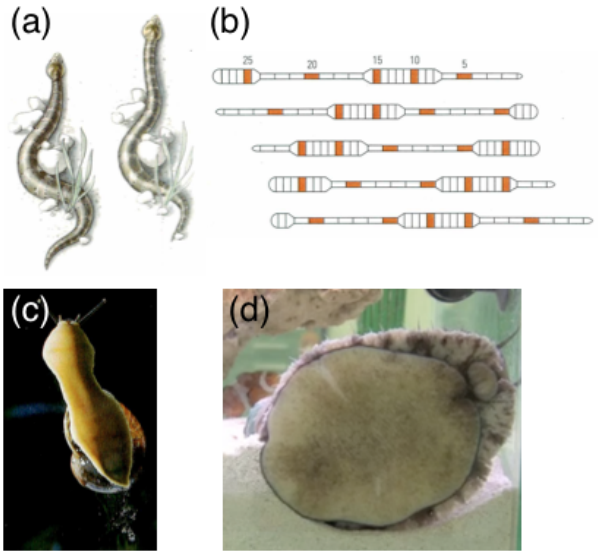

FIGURE 2.1. Animals that move by crawling, (a) snake, (b) earthworm, and (c) snail, quoted from [Alexander, 1992b], respectively. (d) Abalone which had been raised in the laboratory when I was a master course student, quoted from Figure 4.1 of [Iwamoto, 2011].

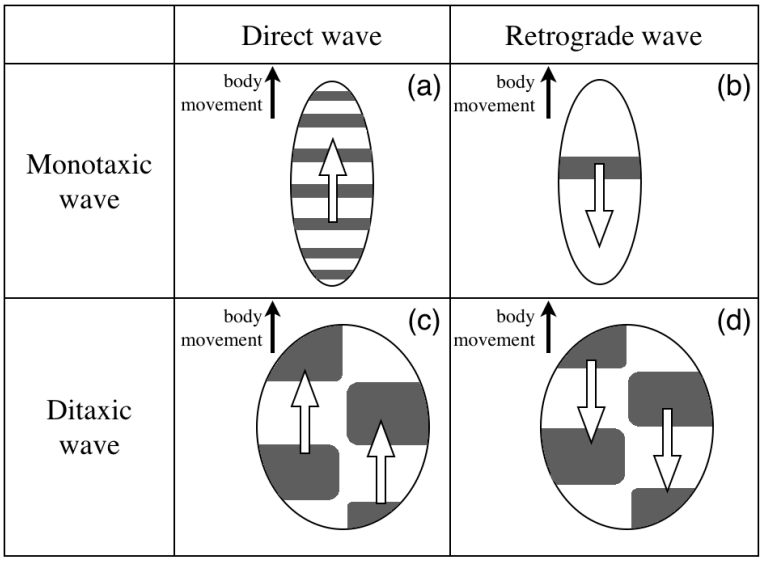

FIGURE 2.2. Sketch of the wave patterns of muscular contraction (or elongation). There are the four typical examples, (a) monotaxic direct wave, (b) monotaxic retrograde wave, (c) ditaxic direct wave, and (d) ditaxic retrograde wave.

2.1.1. Classification of Locomotion by Wave Patterns. Although it has long been known that many gastropods crawl on hard substrates using the actuation of muscular pedal waves along the sole of their foot, many of the earlier studies are simply records of visual observations [Simroth, 1879; Lister, 1694; Parker, 1911]. Dubois and Vles classified the waves observed in the pedal foot of gastropods into two types according to their direction of propagation [Dubois and Vles, 1907]. Direct waves (Figure 2.2(a) and (c)) were defined as moving in the same direction as the movement of the animal. Retrograde waves (Figure 2.2(b) and (d)), by contrast, were defined as those moving in the opposite direction to that of the animal. Furthermore, regardless of their direction, waves are classified as "monotaxic" when a single wave spans the animal's foot (Figure 2.2(a) and (b)) and "ditaxic" when two waves alternately span their foot (Figure 2.2(c) and (d)) [Miller, 1974b].

Several early studies confirmed that the waves along a gastropod's pedal foot are concavities, as evidenced by the distortion of air bubbles in mucus underneath the foot [Parker, 1911] and observations of the frozen sample of a slug during crawling [Jones, 1973]. Lissmann was the first to study the kinematics and dynamics of gastropod locomotion in detail, and this enabled improvements in experimental techniques [Lissmann, 1945a,b]. Lissmann studied three characteristic species: *Helix pomatia* (monotaxic direct waves: Figure 2.2(a)), *Haliotis tuberculata* (ditaxic direct waves: Figure 2.2(c)), and *Pomatias elegans* (ditaxic direct waves: Figure 2.2(c)). Note that Lissmann considered that the movement of *Pomatias elegans* is by alternating contraction and elongation of muscle rather than by some muscular waves. He proposed that there were a number of forces involved in gastropod crawling

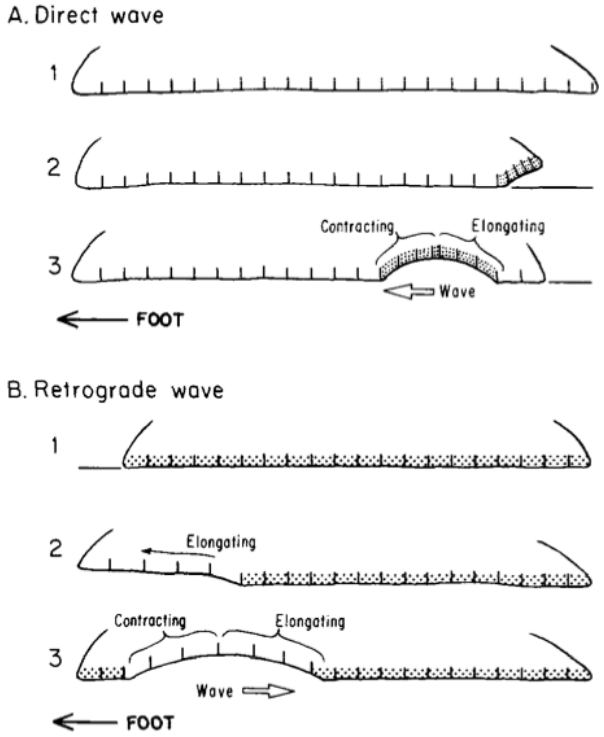

FIGURE 2.3. A simple mechanism of direct and retrograde waves, quoted from Figure 2 of [Miller, 1974a]. A: Direct wave. (1) The pedal adheres to the substratum at maximum extension, (2) the rear foot is longitudinally contracted and (3) the contracted part propagates forward. B: Retrograde wave. (1) the foot is attached along its shortest length, (2) the front of the foot is maximally extended forward and (3) the extended part propagates backward.

locomotion, including external sliding friction in the form of both drag and slip.

The simple mechanism of the difference between direct and retrograde waves was clarified by Jones and Trueman [Jones and Trueman, 1970], after Lissmann [Lissmann, 1945b] and Miller [Miller, 1974a]. The described mechanism of direct waves (Figure 2.3A) is as follows: the pedal foot is adhesive to the substratum at maximum extension, then forward movement will occur when the foot is longitudinally contracted and the contracted part propagates forward. That is, migration of the center of gravity occurs in the contracted part of the foot. In contrast, the mechanism of retrograde waves (Figure 2.3B) is as follows: when retrograde waves occur, the pedal foot is attached along its shortest length, and then the foot is maximally extended forward and the extended part propagates backward. That is, migration of the center of gravity occurs in the extended part of the foot. A great deal of experimental information about pedal locomotory waves was

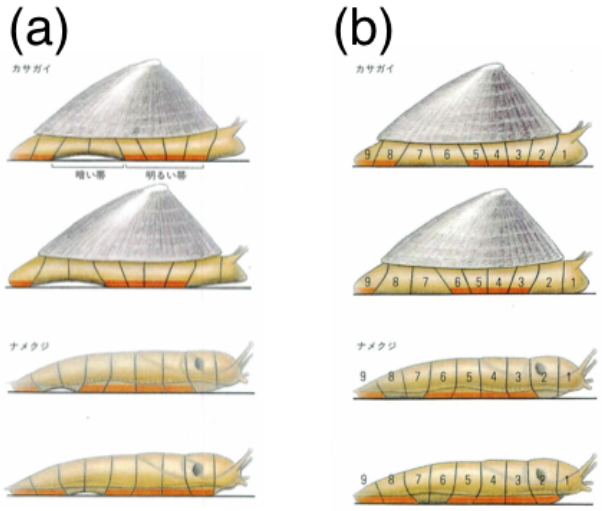

FIGURE 2.4. Images of muscular contraction and elongation, and control of interfacial friction. It has been considered that animals would control the friction against the ground by (a) lifting up a part of their foot, or (b) without lifting up, quoted from [Alexander, 1992b], respectively.

coherently organized by Miller [Miller, 1974a,b]. The key to solving the frictional mechanism, enabling the creation of the propulsive force, was shown by subsequent studies.

The previous researches on worm-like peristaltic locomotion [Alexander, 2002; Zimmermann et al., 2009; Bolotnik et al., 2011; Chernous'ko, 2011; Steigenberger and Behn, 2012; Zimmermann et al., 2013; Tanaka et al., 2011; Gray and Lissmann, 1938] is crucial in proceeding the study about the mechanism of adhesive locomotion in gastropods. Especially, the studies using a simplified mathematical model of a chained body in a resistive medium, including the case of few degrees of freedom, indicated that directional migration of mass center of body could be realized by nonlinear nonsymmetric frictional forces [Zimmermann et al., 2009; Bolotnik et al., 2011; Chernous'ko, 2011; Steigenberger and Behn, 2012; Zimmermann et al., 2013; Tanaka et al., 2011]. Friction mechanism of actual earthworms who move by retrograde waves was solved: anisotropic chaetae which protruded from shortened segments acts the role of a spike. The important thing in the case of earthworms is that a system of friction against surrounding environment is controlled without central signals. This is an intelligent mechanism for primitive creatures, then it would be reasonable that gastropods also have an automatic control system of friction. What is the structure of friction control in gastropods?

2.1.2. The Role of Pedal Mucus. Mark Denny was the first person to reveal the properties of the pedal mucus in crawling locomotion [Denny, 1980b]. Before that, it has been considered that the friction against the contact area is controlled by lifting up a muscular contraction part from

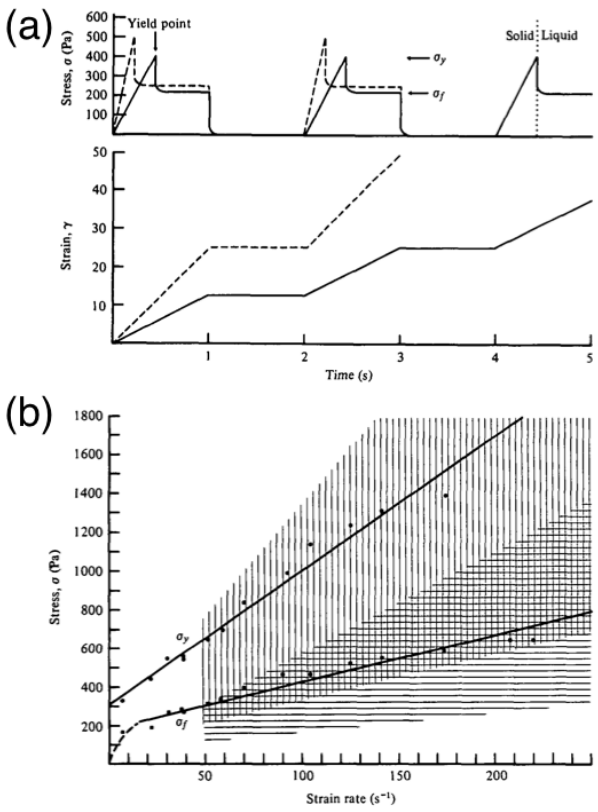

FIGURE 2.5. The characteristics of *Ariolimax columbianus* pedal mucus at large strains, quoted from Figure 9 and 10 of [Denny and Gosline, 1980], respectively. (a) The strain control and the consequent forces against the strain. The mucus yields at a stress σ_y and a strain of approximately 5. The mucus 'heals' if allowed to rest unstressed. (b) A plot of yield stress σ_y and flow stress σ_f, which are linear with respect to strain rate.

the ground in direct wave motion, or a elongation part in retrograde wave motion, as shown in Figure 2.4(a). In short, it has long been thought that the contact region is anchored on the ground and the separated region from the ground moves in the direction of cephalocaudal axis. Denny concluded, however, that the pedal waves of the foot remain attached to the substrate through the pedal mucus when the gastropod crawls along a surface, based on the observation that no concavities were found in frozen samples of the foot of the Pacific banana slug (*Ariolimax columbianus*). That is, as shown in Figure 2.4(b), animals would move keeping their foot on the ground without lifting up their foot. If it is the fact, How could they make a moving part? As the answer for this question, what Denny focused on was the mucus which is filled between the foot and the ground.

It is reasonable that the mucus plays a significant role in maintaining firm adhesion and smooth sliding locomotion. However, Denny thought there must be important role of mucus in movement more. Denny [Denny,

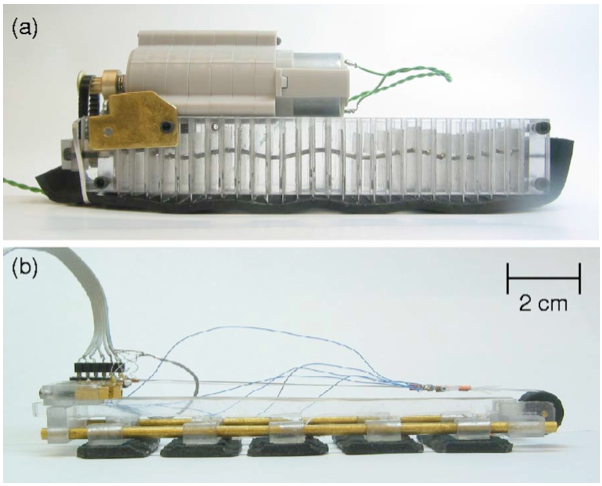

FIGURE 2.6. Photographs of two prototype crawler robots, (a) Retrograde crawler and (b) Direct crawler, quoted from Figure 2 of [Chan et al., 2005]. The direct crawling device can climb a vertical wall.

1980b,a] and Gosline [Denny and Gosline, 1980] collected the mucus of Pacific banana slugs (*Ariolimax columbianus*), and measured the rheological properties, including the finite yield stress, of the pedal mucus using a cone-plate rotary viscoelasticity measuring instrument. As shown in Figure 2.5, they measured a stress to the corresponding strain at a constant strain rate. Then, they found that the mucus has a specific viscoelasticity such as the following. First, when the strain was small, the torque was linear with respect to deformation. That is, the mucus behaved as an elastic solid. The mucus was found to yield ("Yield point" in Figure 2.5(a)) when the deformation exceeded some threshold value σ_y, and the torque became a constant value σ_f regardless of the amount of strain. According to Figure 2.5(b), the threshold value σ_y and this torque σ_f are linear with respect to the strain velocity, that is, mucus behaves as a viscous liquid. Thereafter, the increase in strain stops. More importantly, after a certain period of time, healing time, the mucus recovers its elastic property.

Hence, Denny reached the important conclusions that the unusual viscoelastic nature of pedal mucus acts as the friction control against the substratum in the generation of the animal's driving force [Denny, 1980a,b]. In particular, Denny studied the mechanics of the thin layer of mucus by quantitatively comparing experimentally measured stress in pedal mucus to order-of-magnitude approximations based on the measured yield stresses of the fluid [Denny, 1981]. It is widely accepted that mucus is absolutely essential for adhesion and lubrication of the pedal foot. It is unclear, however, how the propulsive force is generated by mucus.

Coming into the 2000s, engineers began to research the mechanical studies that could support and expand on Denny's hypothesis. Chan et al. [Chan et al., 2005] constructed mathematical models of adhesive and lubrication on a thin layer of viscous fluid, and tested the efficacy of these mechanisms using

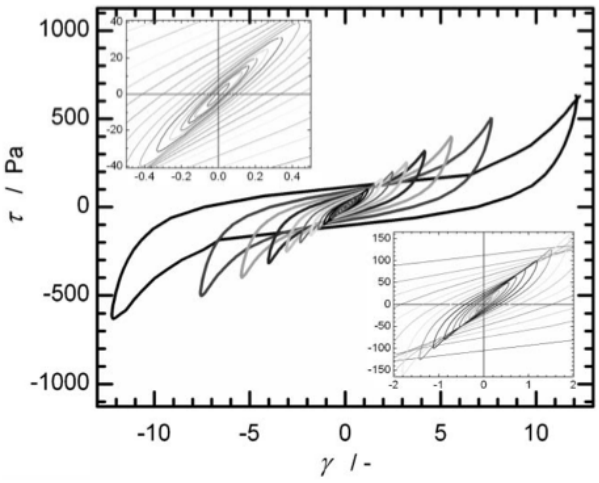

FIGURE 2.7. Lissajous curves resulting from the large amplitude oscillatory shear tests using pedal mucus from *Limax maximus*, quoted from Figure 9 of [Ewoldt et al., 2007].

two robotic snails as shown in Figure 2.6. Their rheological model indicates that movement using direct waves is achieved by the effectiveness of mucus without the foot lifting, although it is impossible to achieve movement using retrograde waves in a similar situation. They tried, however, to clarify the mechanism of crawling locomotion under the properties of mucus by putting a strong emphasis on concepts from fluid dynamics [Lauga and Hosoi, 2006]. Hence, their model could be criticized for being a hard-body model, as they could not describe certain physical characteristics of gastropods, such as their soft foot and the flexible contractions of muscle. Also the disadvantage of the models is that the wave motion is prescribed independently of the underlying muscle mechanics. It seems reasonable that their conclusions, in the process toward clarifying the locomotion mechanism, are at least partly true.

2.1.3. Latest Study on Crawling Locomotion. Rheological characteristic of pedal mucus of snail and synthetic complex fluids have been measured [Ewoldt et al., 2007], and they have investigated the key features for a complex fluid to be useful in adhesive locomotion with direct waves with a model like the Chan's direct crawler robot. Figure 2.7 is the Lissajous curves resulting from shear test using pedal mucus of gastropod. Compared with the synthetic fluids, the pedal mucus exhibits a strongly nonlinear response leading up to a yield point.

It was Lai et al. [Lai et al., 2010] who raised an question to a part of the conventional wisdom about the possibility of generating locomotion by the properties of mucus. They believed that an undeveloped technique dating from [Denny, 1980b] had observed results suggesting that gastropods do not lift up their foot during crawling locomotion. By a series of careful experiments as shown in Figure 2.8, they reported that garden snails (*Helix aspersa*) lift their foot by up to 70 μm in locomotion. Detailed features of

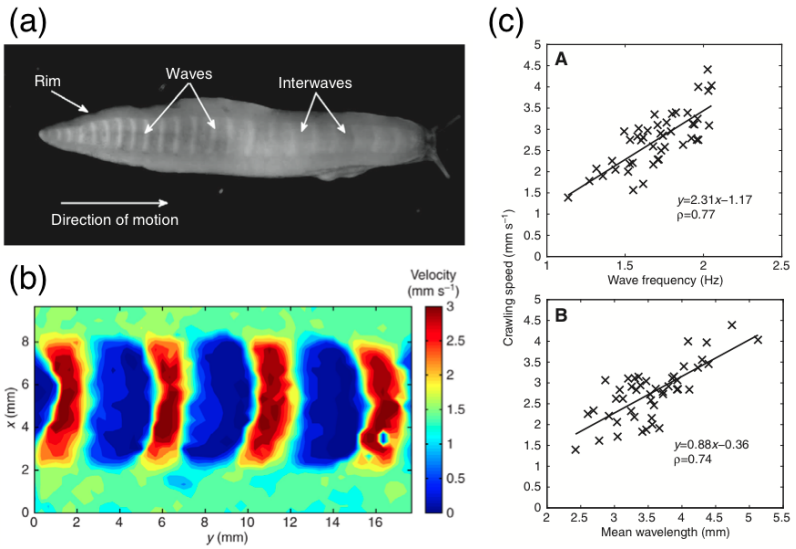

FIGURE 2.8. Results of detailed experiments, quoted from Figure 1, 8, and 10 of [Lai et al., 2010], respectively. (a) The ventral surface of *Ariolimax californicus* moving on a glass surface. (b) Velocity contour map of a part of the ventral surface. The waves (red), interwaves (blue) and rim (pale green/yellow) can be distinguished by their different velocity magnitudes. (c) The crawling speed correlated positively with (A) wave frequency and (B) wavelength.

the wavelength and wave velocity, which had not previously been revealed, were also reported. Yet it is clear that mucus exists under a gastropod's pedal foot. Their study cannot explain how the properties of mucus do not contribute at all to the generation of propulsive force on crawling locomotion, because the possibility that the cavity between the rough surfaces of the foot and the substrate is filled with mucus cannot be ruled out.

A new simplified mathematical model of peristaltic locomotion was proposed by Tanaka et al. [Tanaka et al., 2011]. This aimed to provide a clear answer to the relationship between the velocity of locomotion and the role of anchoring. Their numerical calculations showed the remarkable result that the locomotion direction of the animal is a controllable factor determined by changing the anchoring timing. This is dependent on the phase of the muscle (contraction or elongation) during its periodic regular contraction motion. This recent study means that it is possible to elucidate sufficiently the mechanism of crawling locomotion by direct waves and retrograde waves through the same model. Their model, which describes the flexible physical features of gastropods, can be regarded as more animal-like. However, it is regrettable that their study is only a generalization under the implicit assumption that animals can control their anchoring friction against the substrate. Although their study lacks the important key to how the animals actually realize this anchoring control, they obtained the significant result

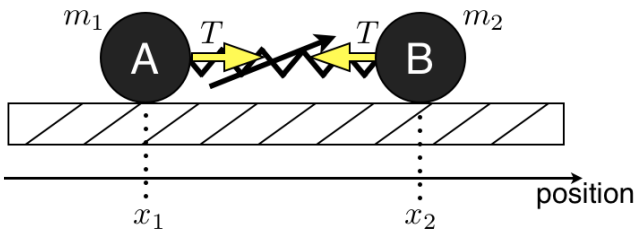

FIGURE 2.9. Simplest model of spring-mass system. Particle A and B are connected by an active spring. m_1 and m_2 are mass, and x_1 and x_2 are position of each particle, respectively. T is spring tension.

that the difference between the direct wave and retrograde wave mechanism depends only on the timing of the anchoring.

2.1.4. Aim of This Study. The aim of this study is to prove that crawling locomotion is achieved by the interaction between the propagation of soft-bodied muscular waves reported by many scientists [Miller, 1974b; Lissmann, 1945a; Trueman, 1983; Lai et al., 2010] and the properties of pedal mucus reported by Denny et al. [Denny, 1980b,a; Denny and Gosline, 1980]. This study is more realistic and practical because it verifies how the anchoring is implemented, though this is the subject of subsequent, continued research by Tanaka et al. [Tanaka et al., 2011]. In the pursuit of this aim, a simple mathematical model for crawling locomotion is proposed. In this model, the behavior of mucus is switched between elasticity and viscosity, depending on the force generated by the soft-bodied muscular waves. In parallel, the propulsive force for locomotion is generated by the states of the mucus. The model, which describes the interaction between animals and their environments, is close to the situation that occurs in nature. Our results indicate that crawling locomotion is achieved by this mutual interaction, and that the hysteresis property of mucus is essential to the realization of locomotion. It is also indicated that both direct wave and retrograde wave locomotion are realized by the same mechanism. In our model, the difference in the timing of anchoring, as previously shown by Tanaka et al. [Tanaka et al., 2011], can be determined by the properties of mucus and muscle. This means there is no need for animals to control the timing of anchoring. Next, I will mention an importance of the friction against the ground in adhesive locomotion.

2.2. Importance of Friction Control in Locomotion: Using Simplest Model

Before beginning to explain our model in concrete terms, the importance of friction control in the study of a mechanism of crawling locomotion would be mentioned. In this section, the simplest model of spring-mass system as shown in Figure 2.9 is dealt with. Note that it is assumed that a spring has an active nature. What situation would be needed for achieving valid motion in this two-mass system?

2.2.1. Case of Same Coefficients of Kinetic Friction. As shown in Figure 2.9, in the case of the two particles A and B, which have a mass of m_1 and m_2, being connected by a spring, the equations of motion of A and B are expressed as the following,

$$m_1\ddot{x}_1 = T - \alpha_1\dot{x}_1, \tag{2.2.1}$$

$$m_2\ddot{x}_2 = -T - \alpha_2\dot{x}_2, \tag{2.2.2}$$

where x_1, x_2 $(x_1 < x_2)$, T, α_1, and α_2 are positions of particle A and B, spring tension, coefficients of kinetic friction of A and B, respectively. Symbol $\cdot$ over a variable means differentiation with respect to t. Tension T would alternate temporally since an active spring is assumed.

Now, it is assumed that a mass of particles is too small enough, i.e., $m_1 \ll 1$, $m_2 \ll 1$. Then inertial force could be ignored, i.e., $m_1\ddot{x}_1 \approx 0$, $m_2\ddot{x}_2 \approx 0$. What we should consider is a time variation of center of mass $(x_1 + x_2)/2$, then both sides of each equation (2.2.1) and (2.2.2) are added as follows,

$$0 = -\alpha_1\dot{x}_1 - \alpha_2\dot{x}_2,$$

$$\Leftrightarrow \ \alpha_1\dot{x}_1 + \alpha_2\dot{x}_2 = 0. \tag{2.2.3}$$

Here, consider the case of the two coefficients of kinetic friction being the same value, i.e., $\alpha_1 = \alpha_2 = \alpha(t) > 0$, so the equation becomes as follows,

$$\dot{x}_1 + \dot{x}_2 = 0,$$

$$\Leftrightarrow \ \frac{d}{dt}(x_1 + x_2) = 0.$$

The velocity of center of mass is,

$$\frac{d}{dt}\left(\frac{x_1 + x_2}{2}\right)$$

$$= \frac{1}{2}\frac{d}{dt}(x_1 + x_2) = 0.$$

It is confirmed easily that center of mass can not move in the case of the same coefficient of kinetic friction.

2.2.2. Case of Distinct Coefficients of Kinetic Friction. As explained in the previous section, it was found that this system is impossible to move in the case of the same friction coefficient. What does this system need for achievement of movement? Movement is that center of mass proceeds in positive or negative direction of x-axis in Figure 2.9. Hence, symmetry breaking of force acting to two particles would be expedient.

Now, it is assumed that the two coefficients of kinetic friction have distinct positive values, i.e., $\alpha_1 \neq \alpha_2$ ($\alpha_1,\ \alpha_2 > 0$), the equation (2.2.3) is as follows,

$$\alpha_1 \dot{x_1} + \alpha_2 \dot{x_2} = 0,$$

$$\Leftrightarrow \ \frac{d}{dt}(\alpha_1 x_1 + \alpha_2 x_2) = 0,$$

$$\Leftrightarrow \ \frac{d}{dt}\Big(\frac{\alpha_1 x_1 + \alpha_2 x_2}{\alpha_1 + \alpha_2}\Big) = 0.$$

That is confirmed that the velocity of the internally dividing point $(\alpha_1 x_1 + \alpha_2 x_2)/(\alpha_1 + \alpha_2)$ between particle A and B is always zero, so internally dividing point can not move. This means that the whole body can not move in both directions.

2.2.3. Friction Control for Achievement of Locomotion. In fact, what this system needs for achieving locomotion is a switching of friction as well as symmetry breaking of it. Therefore, it is assumed that frictional coefficients α_1 and α_2 have two states, $\underline{\alpha}$ (low friction) and $\overline{\alpha}$ (high friction), where $0 < \underline{\alpha} < \overline{\alpha}$, and these states would change under the following conditions,

(2.2.4) **Contracting mode** $\dot{x_1} > 0, \dot{x_2} < 0 \ \Rightarrow \alpha_1 = \underline{\alpha}$ and $\alpha_2 = \overline{\alpha}$,

(2.2.5) **Expanding mode** $\dot{x_1} < 0, \dot{x_2} > 0 \ \Rightarrow \alpha_1 = \overline{\alpha}$ and $\alpha_2 = \underline{\alpha}$.

Put simply, in contracting mode as shown in Figure 2.10(a), the frictional coefficient of x_1 is set to a small value, and that of x_2 to a large one. Conversely, in expanding mode as shown in Figure 2.10(b), the frictional coefficient of x_1 is set to a large value, and that of x_2 to a small one. Here, the following simply proves that it is possible to achieve locomotion by such a switching of frictional coefficient.

At the time t, let the force acting a particle be $f(t)$ in the case of contracting model: $\underline{\alpha} = \alpha_1 < \alpha_2 = \overline{\alpha}$. Consider the force acting each

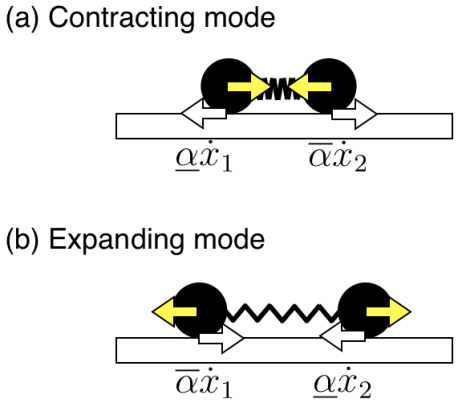

FIGURE 2.10. Two states of frictional coefficient. (a) Contracting mode: $\alpha_1 = \underline{\alpha}, \alpha_2 = \overline{\alpha}$. (b) Expanding mode: $\alpha_1 = \overline{\alpha}, \alpha_2 = \underline{\alpha}$.

particle,

$$\alpha_1 \dot{x_1} = f(t),$$

$$\alpha_2 \dot{x_2} = -f(t).$$

Both sides of each equation are added for erasing $f(t)$ as follows,

$$\alpha_1 \dot{x_1} + \alpha_2 \dot{x_2} = 0,$$

$$\Leftrightarrow \ \underline{\alpha} \dot{x_1} + \overline{\alpha} \dot{x_2} = 0,$$

$$\Leftrightarrow \ \dot{x_2} = -\frac{\underline{\alpha}}{\overline{\alpha}} \dot{x_1}. \tag{2.2.6}$$

Conversely, in the case of expanding mode: $\underline{\alpha} = \alpha_2 < \alpha_1 = \overline{\alpha}$, consider the force acting each particle,

$$\alpha_1 \dot{x_1} = -f(t),$$

$$\alpha_2 \dot{x_2} = f(t).$$

Both sides of each equation are added for erasing $f(t)$ as follows,

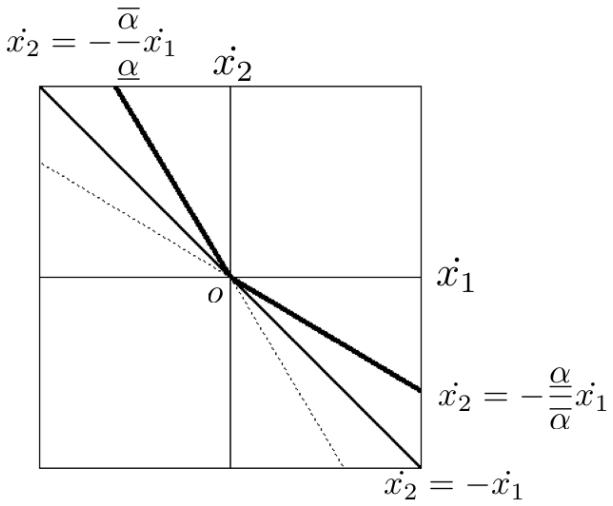

FIGURE 2.11. Phase diagram of $\dot{x_1}$ and $\dot{x_2}$.

$$\alpha_2\dot{x_2} + \alpha_1\dot{x_1} = 0,$$

$$\Leftrightarrow \ \overline{\alpha}\dot{x_1} + \underline{\alpha}\dot{x_2} = 0,$$

$$\Leftrightarrow \ \dot{x_2} = -\frac{\overline{\alpha}}{\underline{\alpha}}\dot{x_1}. \tag{2.2.7}$$

Hence, it found by the equations (2.2.6) and (2.2.7) that the inequality $\dot{x_1} + \dot{x_2} \geq 0$ is always true as shown in Figure 2.11, note that equality holds when $\dot{x_1} = \dot{x_2}$. That is to say, the velocity of center of mass always satisfies the following,

$$\frac{d}{dt}\left(\frac{x_1 + x_2}{2}\right)$$

$$= \frac{1}{2}\frac{d}{dt}(x_1 + x_2) \geq 0.$$

It was confirmed that the gravity can move in a positive direction.

As just confirmed, it is important for achieving of movement to control a friction against the substrate. It is reasonable to consider that animals achieve crawling locomotion by controlling an interfacial friction corresponding to their environment and situation for anchoring in an optimal state.

2.3. Modeling of Adhesive Locomotion

The aim of this study is to verify the locomotion mechanism by the mutual interaction between periodic muscular wave propagation and the unusual physical properties of pedal mucus. This mechanism was implicitly suggested by Denny et al. [Denny, 1980b; Denny and Gosline, 1980]. Toward the achievement of this aim, we construct a simple mathematical model that is sufficient to capture the essence of this mechanism, based on the experimental results reported by many scientists [Miller, 1974b; Lissmann, 1945a; Trueman, 1983; Parker, 1911] as well as Denny et al. [Denny, 1980b; Denny and Gosline, 1980]. Our mathematical model is considered an improvement over the model of peristaltic motion proposed by Tanaka et al. [Tanaka et al., 2011]. We now explain the details of our model [Iwamoto et al., 2013]. There are two critical factors in this hypothesis of the locomotion mechanism—the propagation of muscular waves and the nonlinear properties of pedal mucus.

2.3.1. Muscular Wave Propagation. Muscular waves are observed during the crawling locomotion of a wide variety of mollusks as many scientists have reported [Miller, 1974b; Lissmann, 1945a; Parker, 1917; Barr, 1926, 1927; Trueman, 1983; Alexander, 1992a; Donovan and Carefoot, 1997; Parker, 1911]. One of the key functions for generating self-driven force is to excite muscular contraction and then propagate the region as a wave. Essentially, with a few exceptions such as the rim of slugs, during locomotion, the ventral foot consists of the moving (slipping) regions and the adhesive (anchoring) regions. A one-dimensional model is sufficient for the aim of our study, which is to verify whether directional crawling locomotion is achieved.

It is reasonable to use an active spring to describe the flexible muscle of a mollusk-like gastropod. A muscle has two phases, contraction and relaxation, and its self-driven movement is realized by the actin–myosin system based on control signals. If a spring can change its natural length in real time, it is an active device, i.e., it can realize self-driven movement. It is taken for granted that the device also moves passively because it is a spring. Such an idea has already been proposed in a mathematical model of movement in slime mold [Kobayashi et al., 2006] and in earthworm [Tanaka et al., 2011], and, aside from this, analogous devices have been developed in robotics, such as the Real-time Tunable Spring (RTS) pioneered by Umedachi et al. [Umedachi et al., 2007].

There are two types of active springs who change its natural length; one is a hinged spring assumed by Tanaka's model [Tanaka et al., 2011] as shown in Figure 2.12(a), and the other is a reeling one with a motor used in this study as shown in Figure 2.12(b). There is not so much of a difference essentially between these two devices because both of them have self-driven and describe a flexible body. The difference is the way to change its natural length; in the case of a hinged spring, only the apparent length is changed by opening angle of the hinge, and in contrast, in the case of a reeling spring with a motor, the actual length is changed.

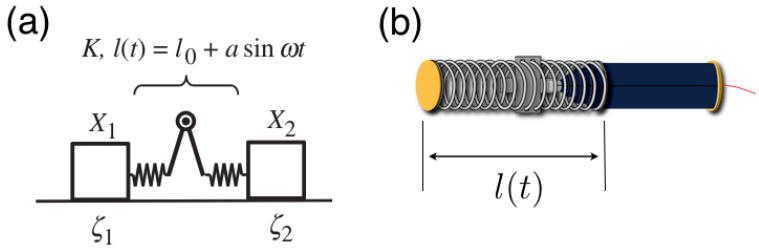

FIGURE 2.12. Image sketches of two types of active springs: (a) hinged spring quoted from Figure 1(c) of [Tanaka et al., 2011], and (b) reeling spring with a motor developed by [Umedachi et al., 2007].

The description of force generated by a spring makes a difference by the difference between hinged and reeled ones, even if the natural length $l(t)$ at the time t is controlled similarly as following;

$$l(t) = l_0(1 + \alpha \sin \omega t). \tag{2.3.1}$$

where l_0, α, and ω are an average length of natural length, contraction rate, and wave frequency, respectively. In the case of hinged ones, the length of parts of springs is not change even though the apparent length would be changed, hence the force acting on a segment generated by the spring is described as follows,

$$F_h(t) = \kappa_h(x_1 - x_0 - l(t)), \tag{2.3.2}$$

where x_0 and x_1 are segments connected by a hinged spring. In this case κ_h represents the spring constant. On the other hand, in the case of a reeling spring with a motor, the force is a bit different from the case of a hinged spring. In generally, a spring becomes soft when the natural length is long, and vice versa. Therefore, in the case that its natural length can change, it is reasonable to consider that the spring coefficient would vary, i.e., that is inversely proportional to its natural length as follows,

$$F_r(t) = \frac{\kappa_r}{l(t)}(x_1 - x_0 - l(t)). \tag{2.3.3}$$

In this case κ_r represents the stiffness of a spring determined by materials. This study uses the Real-time Tunable Spring (RTS) [Umedachi et al., 2007] such as Figure 2.12(b) to mimic muscle in the mathematical model of this study, with a view to it being utilized in the robot.

To mimic actual animals, we consider a multi-segment model, as in Figure 2.13, that can express the propagation of muscular waves. Now, we

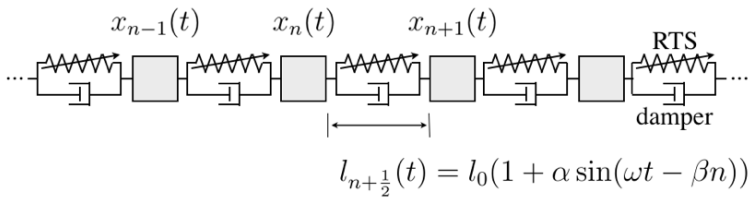

FIGURE 2.13. Modeling of the ventral foot of gastropods. Each segment is connected by a Real-time Tunable Spring (RTS) and a damper.

assume that the animal's ventral foot is divided into $(N+1)$ segments. Similar to the method of the previous studies [Ewoldt et al., 2007; Bolotnik et al., 2011; Zimmermann et al., 2013; Tanaka et al., 2011], we configure the spring to repeatedly contract and elongate. In our mathematical model, such an active spring is achieved by periodically controlling the natural length of RTS. The natural length of the $(n + 1/2)$th RTS, which is one of the elements connected to the nth and $(n + 1)$th segments at time t, is

$$l_{n+\frac{1}{2}} = l_0(1 + \alpha \sin(\omega t - \beta n)). \tag{2.3.4}$$

Using specific properties of the animal's foot, we set $l_0 = L/N$ and $\beta = 2\pi W/N$, where L is the length of the whole foot and W is the number of waves along the foot. The muscular force $F_{n+\frac{1}{2}}$ acting on the nth segment generated by the $(n + 1/2)$th RTS and damper is described using $l_{n+\frac{1}{2}}$ as follows:

$$F_{n+\frac{1}{2}} = \kappa_{n+\frac{1}{2}}\left(\frac{x_{n+1} - x_n}{l_{n+\frac{1}{2}}} - 1\right) + q_{n+\frac{1}{2}}(\dot{x}_{n+1} - \dot{x}_n), \tag{2.3.5}$$

where x_n is the position of the nth segment in the direction of movement, and $\cdot$ over a variable means differentiation with respect to t. The first term is an elastic force generated by RTS and the second term is the damping force. Coefficients $\kappa_{n+\frac{1}{2}}$ and $q_{n+\frac{1}{2}}$ are constants, and $\kappa_{n+\frac{1}{2}}$ which has the dimension of force means the stiffness of a spring, determined from materials.

2.3.2. Dynamic Viscoelastic Properties of Pedal Mucus. The second essential factor is the physical properties of pedal mucus reported by Denny et al. [Denny, 1980b; Denny and Gosline, 1980]. Put simply, gastropod pedal mucus has two states, elastic solid and viscous liquid. It is known that the mucus is primarily composed of water, mucopolysaccharides and glycoproteins [Kim et al., 2010].

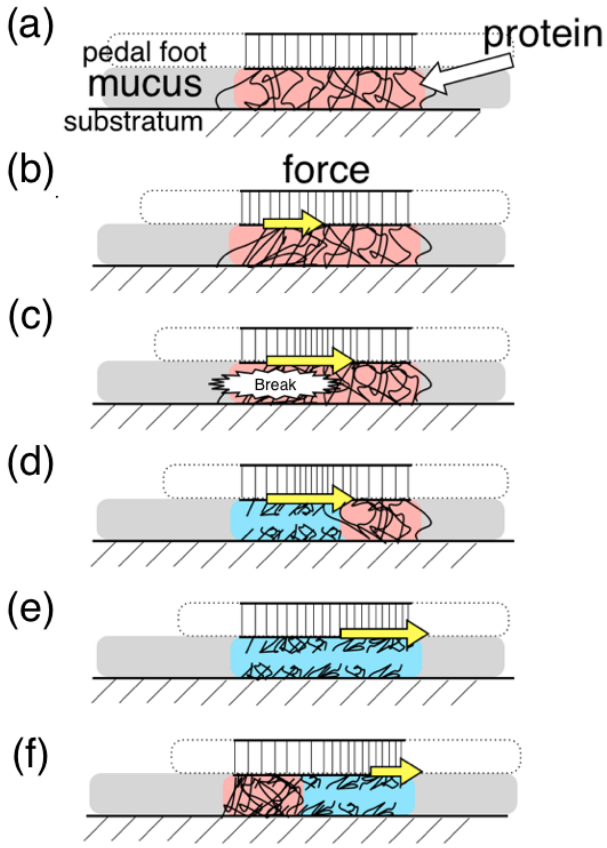

FIGURE 2.14. Image sketch of mucus dynamics under stress. First an animal does not move, so (a) mucus behaves as elastic solid (red), then (b) muscular wave comes. By mucus being stretched by muscular contraction, (c) chemical bond breaking in mucus occurs, i.e., the mucus yields. After yield occurred, (d) mucus behaves as viscous liquid (blue), and (e) the region of viscous liquid expands by muscular wave moving. (f) Muscular wave passes, then re-coupling is occurred. After a certain period of time, mucus recovers its elasticity, i.e., the condition of mucus is back to (a).

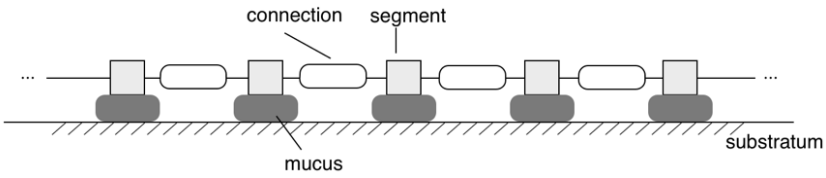

FIGURE 2.15. Pedal mucus under each segment has two properties, elastic solid and viscous liquid.

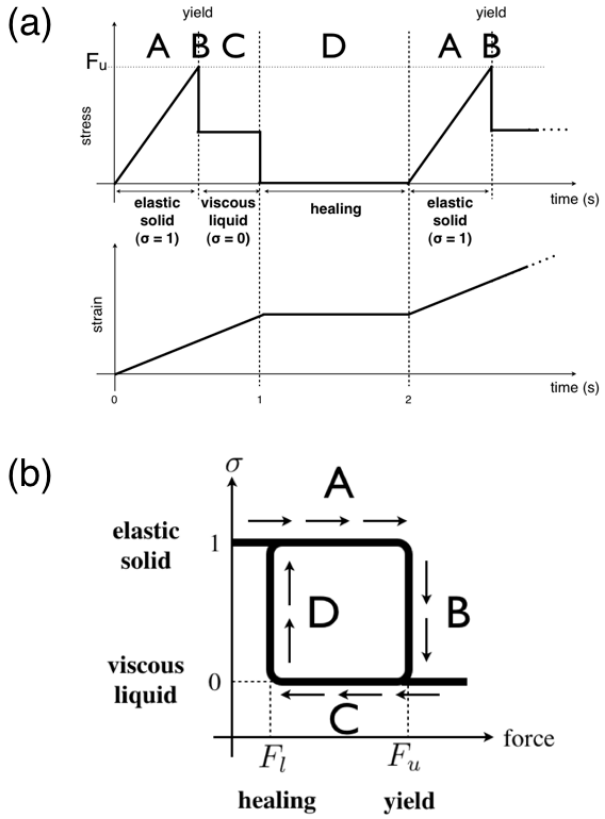

FIGURE 2.16. Modeling for pedal mucus. (a) Outline of one of the results in Denny's experiments [Denny, 1980b; Denny and Gosline, 1980]. The parameter F_u who is the threshold when mucus changes its property from elasticity to viscosity corresponds to yield stress. The states A, B, C, and D correspond to that in hysteresis loop (b), respectively. (b) Internal hysteresis loop of pedal mucus. The parameter F_l who is the threshold from viscosity to elasticity corresponds to a stress when it stops to strain mucus. Variable σ represents the state of the mucus. When $\sigma = 1$, the mucus behaves as an elastic solid. If the external force on a segment increases (A) and reaches F_u, the mucus yields (B) and behaves as a viscous liquid $\sigma = 0$. When $\sigma = 0$, if the external force on a segment decreases (C) below F_l, the mucus recovers its elasticity $\sigma = 1$ (D).

Based on the results of Denny's measurement, the image sketch of mucus dynamics under stress is pictured as Figure 2.14. Chemical bond which has been coupled in the elastic state of the mucus breaks when the muscular contraction waves came. After the wave passed through this region, the elasticity of the mucus is recovered by re-coupling of chemical bond although it takes a small amount of time.

Now, we assume that mucus is divided into $(N+1)$ parts similar to pedal foot as in Figure 2.15. An outline of Denny's experiment [Denny, 1980b] is

as follows. The mucus of Pacific banana slugs (*Ariolimax columbianus*) was collected, and its torque against deformation was measured using a cone-plate rotary viscoelasticity measuring instrument.

First, when the strain was small, the torque was linear with respect to deformation, as in Figure 2.16(a)A. That is, the mucus behaved as an elastic solid. The mucus was found to yield (Figure 2.16(a)B) when the deformation exceeded some threshold value, and the torque became a constant value regardless of the amount of strain as in Figure 2.16(a)C. According to data reported by Denny [Denny, 1980b], this torque is linear with respect to the strain velocity, that is, mucus behaves as a viscous liquid. Thereafter, the increase in strain stops. More importantly, after a certain period of time, healing time, the mucus recovers its elastic property (Figure 2.16(a)D $\rightarrow$ A). Now, by defining σ as states of property of mucus, i.e., mucus behaves as elastic solid when $\sigma = 1$, and it behaves as viscous liquid when $\sigma = 0$, it becomes clear that the pedal mucus retains a loop system such as in Figure 2.16(b). When the force acting on it is small, the mucus is an elastic solid ($\sigma = 1$). When the force increases (A) and exceeds an upper threshold F_u, the mucus yields (B). The behavior of the mucus changes significantly, and it immediately becomes a viscous liquid ($\sigma = 0$). When the force decreases (C) below a lower threshold F_l, the mucus recovers its elasticity (D).

2.3.3. Equation of Motion for Adhesive Locomotion. Considering the features mentioned above, the muscular waves and the rheology of mucus, the equation of motion for each segment can be given as follows:

$$m\ddot{x}_n = F_{n+\frac{1}{2}} - F_{n-\frac{1}{2}} - (1-\sigma_n)\mu\dot{x}_n - \sigma_n\gamma(x_n - \overline{x}_n), \tag{2.3.6}$$

where m [kg] is mass of each segment, and the constants μ [N·s/m] and γ [N/m] are the viscosity coefficient and elastic coefficient of the mucus, respectively, and provided that $F_{n-\frac{1}{2}} = 0$ if $n = 0$ and that $F_{n+\frac{1}{2}} = 0$ if $n = N$. In this model, the viscoelastic behavior of mucus as friction is described by modified the Kelvin-Voigt model, where the variable σ_n represents the state of the mucus under the nth segment. In this model, it is assumed that the critical position of the nth segment at the moment when the mucus changes state from a viscous liquid ($\sigma_n = 0$) to an elastic solid ($\sigma_n = 1$), as in Figure 2.16(b)D, is memorized as an anchoring position $\bar{x}_n$. In addition, for realization of the hysteresis loop shown in Figure 2.16(b), the variable σ_n is assumed to satisfy the following conditions:

$$\begin{aligned} &\text{if } \sigma_n = 1 \text{ and } |F_{n+\frac{1}{2}} - F_{n-\frac{1}{2}}| > F_u, \\ &\qquad\qquad\qquad\qquad \text{then } \sigma_n \text{ changes to } 0; \end{aligned} \tag{2.3.7}$$

$$\begin{aligned} &\text{if } \sigma_n = 0 \ \text{ and } \ |F_{n+\frac{1}{2}} - F_{n-\frac{1}{2}}| < F_l, \\ &\qquad\qquad\qquad\qquad \text{then } \sigma_n \text{ changes to 1 and } \overline{x}_n \text{ is set to } x_n. \end{aligned} \tag{2.3.8}$$

Let $x_n = LW^{-1}\tilde{x}_n$ and $t = \omega^{-1}\tilde{t}$, where $\tilde{x}_n$ and $\tilde{t}$ are dimensionless position and time, respectively. Then we can obtain a system of non-dimensional equations in the case of $n \neq 0, N$ as

$$\begin{aligned} \tilde{m}\ddot{\tilde{x}}_n = \tilde{\kappa}\left(\frac{\tilde{x}_{n+1}-\tilde{x}_n}{\tilde{l}_{n+\frac{1}{2}}} - \frac{\tilde{x}_n - \tilde{x}_{n-1}}{\tilde{l}_{n-\frac{1}{2}}}\right) + \tilde{q}(\dot{\tilde{x}}_{n+1} - 2\dot{\tilde{x}}_n + \dot{\tilde{x}}_{n-1}) \\ -(1-\sigma_n)\tilde{\mu}\dot{\tilde{x}}_n - \sigma_n(\tilde{x}_n - \overline{\tilde{x}}_n), \end{aligned} \tag{2.3.9}$$

where some coefficients are assumed constant, $\kappa_{n+\frac{1}{2}} = \kappa$ and $q_{n+\frac{1}{2}} = q$, and dimensionless parameters are obtained as

$$\tilde{m} = m\omega^2\gamma^{-1}, \qquad \tilde{l}_{n+\frac{1}{2}} = 1 + \alpha\sin(\tilde{t} - 2\pi W\frac{n}{N}),$$

$$\tilde{\kappa} = \kappa N(\gamma L)^{-1}, \qquad \tilde{q} = q\omega\gamma^{-1}, \qquad \tilde{\mu} = \mu\omega\gamma^{-1}.$$

The two mucus thresholds, the yield point and the healing point, can be similarly represented as dimensionless parameters as

$$\tilde{F}_l = F_l W(\gamma L)^{-1}, \quad \tilde{F}_u = F_u W(\gamma L)^{-1}.$$

Now the order of $\tilde{m}$ is vanishingly small compared with the other dimensionless coefficients, so that means it can be assumed that the inertial force is negligible. This assumption is reasonable in the mechanism of locomotion for gastropods and their relatives. The nondimensional equations are then as follows:

$$\begin{aligned} &(1-\sigma_n)\mu\dot{x}_n + \sigma_n(x_n - \overline{x}_n) \\ &\quad = \kappa\{\frac{x_{n+1}-x_n}{l_{n+\frac{1}{2}}} - \frac{x_n - x_{n-1}}{l_{n-\frac{1}{2}}}\} + q(\dot{x}_{n+1} - 2\dot{x}_n + \dot{x}_{n-1}). \end{aligned} \tag{2.3.10}$$

where the tildes are omitted for simplicity, and they will be also omitted in later discussions. Equation (2.3.10) is temporally discretized using a finite difference method in order to perform numerical calculations. We confirmed that solutions to the resultant simultaneous equations always exist, because the tridiagonal matrix is diagonally dominant as described in the next section.

2.3.4. Formulas for Numerical Calculations. To perform the numerical calculations, the dimensionless equation (2.3.10) is discretized using a finite difference method as making no assumption as to $\kappa_{n+\frac{1}{2}}$ and $q_{n+\frac{1}{2}}$:

$$\begin{aligned}
&(1-\sigma_i^j)\mu\frac{x_i^j - x_i^{j-1}}{\delta t} + \sigma_i^j(x_i^j - \overline{x}_i^j) \\
&= \frac{\kappa_{i+\frac{1}{2}}}{l_{i+\frac{1}{2}}}(x_{i+1}^j - x_i^j - l_{i+\frac{1}{2}}) + q_{i+\frac{1}{2}}\left(\frac{x_{i+1}^j - x_{i+1}^{j-1}}{\delta t} - \frac{x_i^j - x_i^{j-1}}{\delta t}\right) \\
&-\frac{\kappa_{i-\frac{1}{2}}}{l_{i-\frac{1}{2}}}(x_i^j - x_{i-1}^j - l_{i-\frac{1}{2}}) - q_{i-\frac{1}{2}}\left(\frac{x_i^j - x_i^{j-1}}{\delta t} - \frac{x_{i-1}^j - x_{i-1}^{j-1}}{\delta t}\right),
\end{aligned} \tag{2.3.11}$$

where δt denotes a time step and x_i^j is the position of the ith segment at time j. The following simultaneous equations are obtained by simplifying equation (2.3.11) in the case of $i \neq 0, N$:

$$\begin{aligned}
&-\left(\frac{\kappa_{i+\frac{1}{2}}}{l_{i+\frac{1}{2}}} + \frac{q_{i+\frac{1}{2}}}{\delta t}\right)x_{i+1}^j - \left(\frac{\kappa_{i-\frac{1}{2}}}{l_{i-\frac{1}{2}}} + \frac{q_{i-\frac{1}{2}}}{\delta t}\right)x_{i-1}^j \\
&+\left(\sigma_i^j + \frac{(1-\sigma_i^j)\mu + q_{i+\frac{1}{2}} + q_{i-\frac{1}{2}}}{\delta t} + \frac{\kappa_{i+\frac{1}{2}}}{l_{i+\frac{1}{2}}} + \frac{\kappa_{i-\frac{1}{2}}}{l_{i-\frac{1}{2}}}\right)x_i^j \\
&= -\kappa_{i+\frac{1}{2}} + \kappa_{i-\frac{1}{2}} + \sigma_i^j\overline{x}_i^j - \frac{q_{i+\frac{1}{2}}}{\delta t}x_{i+1}^{j-1} \\
&+\frac{(1-\sigma_i^j)\mu + q_{i+\frac{1}{2}} + q_{i-\frac{1}{2}}}{\delta t}x_i^{j-1} - \frac{q_{i-\frac{1}{2}}}{\delta t}x_{i-1}^{j-1}.
\end{aligned} \tag{2.3.12}$$

Solutions of these simultaneous equations always exist, because the tridiagonal matrix is diagonally dominant. The simultaneous equations are solved easily using LU decomposition. As the special case, the simultaneous equations for the segments at the end points of the body are given as follows:

$$\begin{aligned}
&-\left(\frac{\kappa_{0+\frac{1}{2}}}{l_{0+\frac{1}{2}}} + \frac{q_{0+\frac{1}{2}}}{\delta t}\right)x_1^j + \left(\sigma_0^j + \frac{(1-\sigma_0^j)\mu + q_{0+\frac{1}{2}}}{\delta t} + \frac{\kappa_{0+\frac{1}{2}}}{l_{0+\frac{1}{2}}}\right)x_0^j \\
&= -\kappa_{0+\frac{1}{2}} + \sigma_0^j\overline{x}_0^j - \frac{q_{0+\frac{1}{2}}}{\delta t}x_1^{j-1} + \frac{(1-\sigma_0^j)\mu + q_{0+\frac{1}{2}}}{\delta t}x^{j-1}
\end{aligned} \tag{2.3.13}$$

(2.3.14)

$$\left(\sigma_N^j + \frac{(1-\sigma_N^j)\mu + q_{N-\frac{1}{2}}}{\delta t} + \frac{\kappa_{N-\frac{1}{2}}}{l_{N-\frac{1}{2}}}\right) x_N^j - \left(\frac{\kappa_{N-\frac{1}{2}}}{l_{N-\frac{1}{2}}} + \frac{q_{N-\frac{1}{2}}}{\delta t}\right) x_{N-1}^j$$
$$= \kappa_{N-\frac{1}{2}} + \sigma_N^j \overline{x}_N^j + \frac{(1-\sigma_N^j)\mu + q_{N-\frac{1}{2}}}{\delta t} x_N^{j-1} - \frac{q_{N-\frac{1}{2}}}{\delta t} x_{N-1}^{j-1}.$$

TABLE 2.1. Data of physical features in animals obtained from [Denny, 1980b; Denny and Gosline, 1980; Lai et al., 2010; Iwamoto, 2011].

	Denny & Gosline (Banana slug)	Lai (Banana slug, garden slug)	Iwamoto (Japanese abalone)
wave frequency [Hz]		1.0-2.5	0.02-0.2
crawling speed [mm/s]		1.0-5.0	0.4-2.84
body length [mm]		7-280	60-90
number of waves		6-23	1.5-2.0
wave speed [mm/s]		1.5-3.28	1.26-15.0
speed ratio (crawling / wave)		0.33-1.0	0.12-0.33
extension rate			0.5-0.85
wave length [mm]		2.5-5.5	30-60
viscosity [Pa s]	3.0-5.0		
stress against strain [Pa]	300 (against 1 Hz)		
thickness of mucus [μm]		70	

TABLE 2.2. Physical features in the model. The values of animal were obtained from [Denny, 1980b; Denny and Gosline, 1980; Lai et al., 2010; Iwamoto, 2011].

parameters in the model	animals	for the model
W (number of waves)	1 - 23	1 - 23
L (body length)	$7 - 280 \times 10^{-3}$ [m]	50×10^{-3} [m]
N (division number)	-	50
l_0 (average natural length)	-	L/N $= 1 \times 10^{-3}$ [m]
width of foot	-	1×10^{-2} [m]
area of foot	-	$l_0 \times$width $= 1 \times 10^{-5}$ [m^2]
thickness of mucus	50×10^{-6} [m]	50×10^{-6} [m]
γ (Modulus of Elasticity)	stress is 400 Pa when strain is 5	$\frac{\text{stress}\times\text{area}}{\text{thickness}\times\text{strain}}$ $= \frac{400\times1\times10^{-5}}{50\times10^{-6}\times5}$ $= \frac{400}{25} = 16$ [N/m]
α (ratio of contraction)	0.4 - 0.85	0.5 (0.1-0.9)
ω (wave frequency)	0.02 - 2.5 [Hz]	0.1 [Hz]
μ (viscosity)	3 - 5 [Pa·s]	$\frac{5[\text{Pa·s}]\times\text{area}[\text{m}^2]}{\text{thickness}}$ $= \frac{5\times1\times10^{-5}}{50\times10^{-6}}$ $= 1$ [N·s/m]
F_u (yield point)	400 - 1800 [Pa]	400 Pa $\times$ area [m^2] $= 400 \times 1 \times 10^{-5}$ $= 4 \times 10^{-3}$ [N]
κ (stiffness of spring)	-	
q (damping coefficient)	-	
F_l (healing point)	-	
m (mass of a segment)	-	$\ll 1$

TABLE 2.3. Parameter setting

$\tilde{\gamma}$	5.0×10^{-3}
$\tilde{\kappa}$	1.0
$\tilde{q}$	5.0×10^{-3}
$\tilde{F_u}$	$0.1 - 1.0 \times 10^{-2}$
$\tilde{F_l}$	5.0×10^{-6}

Scaling of each parameter can be estimated from previous study [Denny, 1980b; Denny and Gosline, 1980; Lai et al., 2010; Iwamoto, 2011]. Table 2.1 is a arrangement the data of these researches. To apply into mathematical model, some adjustments in a unit need such as Table 2.2.

Furthermore, in dimensionless equation, three parameters, κ, q and F_l, are unknown in animals. There, we estimate only two dimensionless parameters which use well known values.

$$\tilde{\gamma} = \gamma\omega\mu^{-1} = \frac{1[N \cdot s/m] \times 0.1[Hz]}{16[N/m]} = 0.00625 \approx 5.0 \times 10^{-3}, \tag{2.3.15}$$

$$\tilde{F_u} = F_u W(\mu L)^{-1} = \frac{4 \times 10^{-3}[N] \times 1}{16[N/m] \times 50 \times 10^{-3}[m]} = 5.0 \times 10^{-3}. \tag{2.3.16}$$

On the other hand, we simulate with mucus model setting parameter values as Table 2.3, so our calculations are reasonable.

In the next section, these simultaneous equations with time evolution are solved using numerical methods.

2.4. Numerical Calculations

It is assumed that the initial state of the mucus under each segment is $\sigma_n = 1$ (elasticity), because the animals are adhering to the substratum when the locomotion begins. Numerical simulations are carried out with the estimated scale of some physical feature quantities from previous research [Denny, 1980b; Denny and Gosline, 1980; Lai et al., 2010; Iwamoto, 2011] mentioned in Table 2.2 and 2.3.

2.4.1. Realization of Adhesive Locomotion. Figure 2.17(a) shows chronological snapshots and Figure 2.18(a) shows the spatiotemporal dynamics of a simulation using $F_u = 0.35 \times 10^{-2}$, $F_l = 0.001 \times 10^{-2}$, $\kappa = 1.0$, and $q = 0.005$. The mucus under each segment shifts its state (viscosity or elasticity) on a moment-to-moment basis by being pushed and pulled depending on the muscular contraction and expansion. From the results with

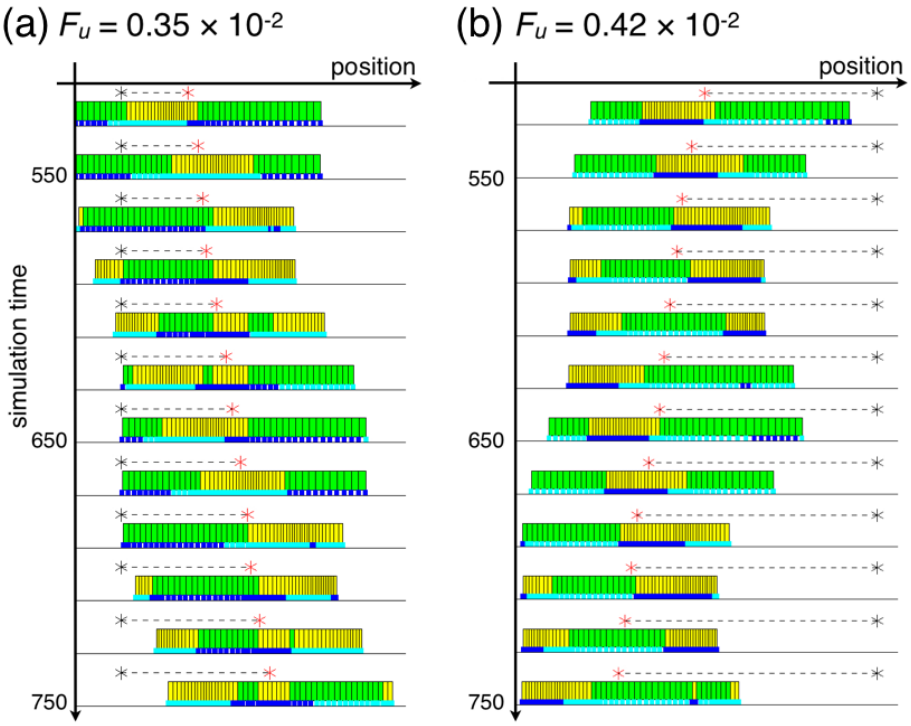

FIGURE 2.17. Chronological snapshots of simulations carried out with $F_l = 0.001 \times 10^{-2}$, $\kappa = 1.0$, and $q = 0.005$. In each foot segment, the green regions represent expanded muscle and the yellow represents contracted muscle compared to the average length of the RTS. Light blue regions are viscous liquid (slipping) and dark blue represents elastic solid (anchoring) in the mucus under each segment of foot. Black and red markings show the position of the center at the initial time and subsequent times, respectively. (a) Direct wave: $F_u = 0.35 \times 10^{-2}$. The waves of contraction propagate in a positive direction and the whole body moves in the same direction. (b) Retrograde wave: $F_u = 0.42 \times 10^{-2}$. The waves of expansion propagate in a positive direction, but the whole body moves in the opposite direction.

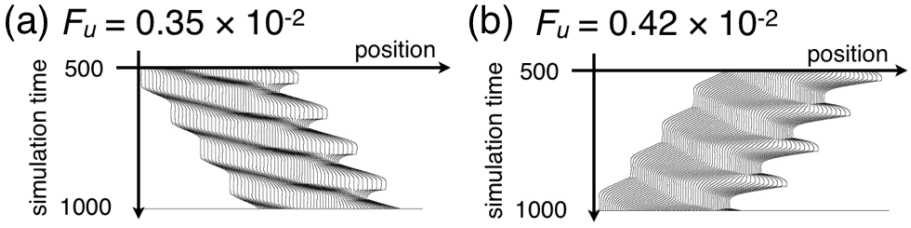

FIGURE 2.18. Time series plots of the position of each segment using the same parameters as in Figure 2.17(a) and (b).

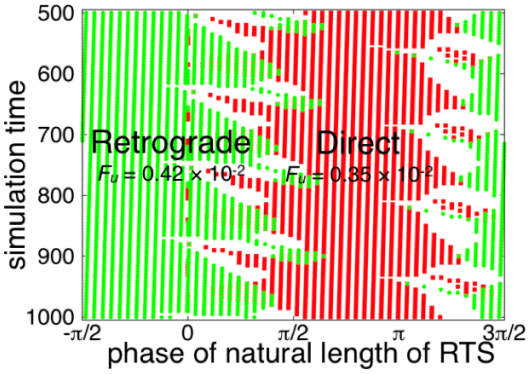

FIGURE 2.19. Phase plots of the natural length of RTS $l(t)$ when the mucus behaves as an elastic solid (anchoring), i.e., it indicates the phase of the adhesive region of the foot. The red plots show the results with the same parameters as in Figure 2.17(a), and the green are with the same parameters as in Figure 2.17(b).

these parameter values (Figure 2.17(a) and Figure 2.18(a)), it seems that segments of expanded muscle are anchored. In other words, the regions of contracted muscle move along the body.

Figure 2.17(b) shows chronological snapshots and Figure 2.18(b) shows the spatiotemporal dynamics of a simulation using $F_u = 0.42 \times 10^{-2}$, $F_l = 0.001 \times 10^{-2}$, $\kappa = 1.0$, and $q = 0.005$. Put simply, the change from Figure 2.17(a) and Figure 2.18(a) is just the value of F_u. Figure 2.18(b) shows with perfect clarity that retrograde wave locomotion is achieved. In this case, it seems that anchoring occurs around the regions of muscle contraction (Figure 2.17(b)). Hence, the regions of muscle expansions move along the body.

2.4.2. Direct Wave and Retrograde Wave. Figure 2.19 is the result of plotting each phase of the natural length of RTS when each segment is anchored. The result shows that a small change in the value of the yield point can completely change the phase of anchoring.

Why the anchoring phase changed? It would be explained by the two possible situations which the mucus yields, that is because we consider absolute value of the force in evaluating. It means the mucus has the two yield points, positive and negative values, and hence it is possible to exceed the threshold F_u in both contraction and elongation of a spring. We can obviously see these situations in Figure 2.20, which is the temporal plots of natural length and actual length of RTS (upper), and force (lower) acting a segment located in the middle of body ($n = 25$). The panels (a) and (b) are in the cases of direct wave and retrograde wave. By the upper graph of (a), we can see that the anchoring occurred in elongated state of a spring. Also, the place which has the actual spring been able to follow the natural length is in the viscous state of mucus, i.e., the contracted state of a spring. It is confirmed by the graph of the force that the jump B of hysteresis loop system as shown in Figure 2.16 happened in the positive value F_u. That is to

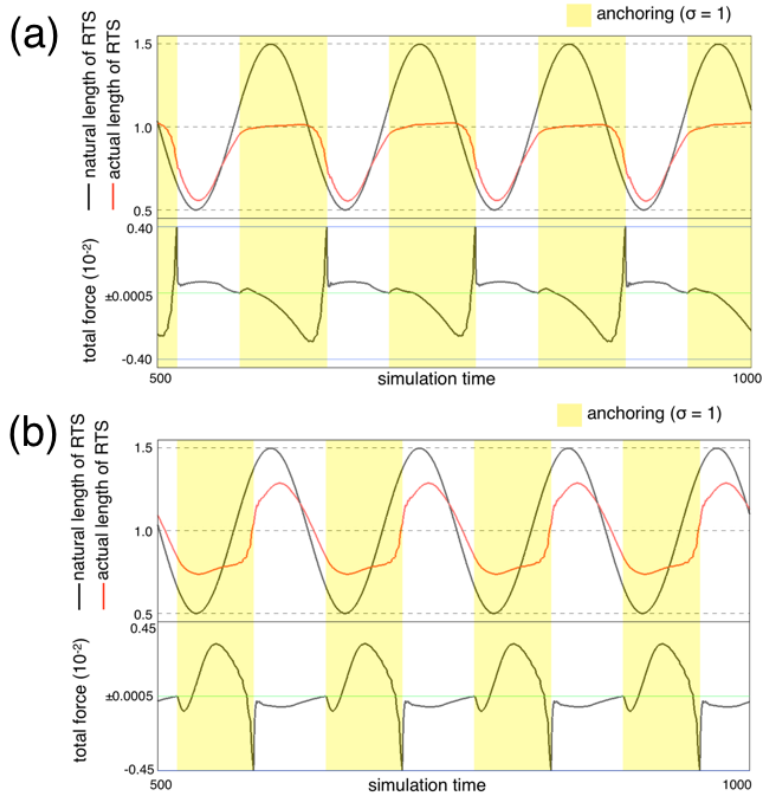

FIGURE 2.20. Temporal plots of natural length and actual length of RTS (upper), and force (lower) acting the 25th segment. The yellow regions correspond to the timing of anchoring, i.e., it is the time that the state of mucus under the 25th segment was elastic solid ($\sigma = 1$). (a) Direct wave ($F_u = 0.40 \times 10^{-2}, F_l = 0.0005 \times 10^{-2}$, $\kappa = 2.0$, and $q = 0.05$): The jump B of mucus in hysteresis loop as shown Figure 2.16(b) occurs when the force becomes more than F_u. (b) Retrograde wave ($F_u = 0.45 \times 10^{-2}, F_l = 0.0005 \times 10^{-2}$, $\kappa = 2.0$, and $q = 0.05$): The jump B occurs when the force becomes less than $-F_u$.

say, the state of mucus would change from elasticity to viscosity just before RTS achieves the shortest natural length. It is found that the propulsive force is generated by being pushed in the case of direct wave. On the other hand, we can see by upper graph of (b) that the anchoring occurred in contracted state of a spring. In addition, the place where the actual spring can follow the natural length is in the state of elongation. Moreover, the graph of the force shows that the jump B of hysteresis loop system happened in the negative value $-F_u$, i.e., the state of mucus would change from elasticity to viscosity just before RTS achieves the longest natural length. In the case of retrograde wave, the propulsive force is generated by being pulled.

2.4.3. Role of Feature of Mucus in Locomotion. Figure 2.21 is a velocity diagram that examines in detail the effect of some properties of

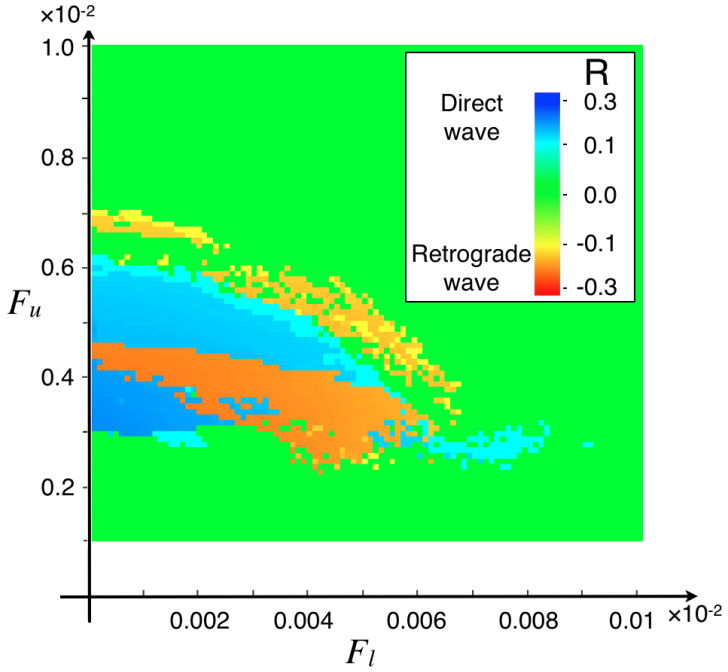

FIGURE 2.21. The effects of properties of mucus on the velocity ratio R for $\kappa = 1.0$, and $q = 0.005$. The color plot of R with respect to F_u and F_l. If the absolute value of R is greater than 0.1, the region is colored blue ($R \geq 0.1$: direct wave) or red ($R \leq -0.1$: retrograde wave).

mucus on motion. Here, the velocity ratio R (= velocity of the center of body / wave velocity) has been calculated. Based on the previous knowledge [Lai et al., 2010; Iwamoto, 2011], we define that an efficient directional motion is achieved when the absolute value of R is more than 0.1. We found in Figure 2.21 that the parameter region of F_u and F_l for achieving a valid locomotion exists. Figure 2.21 clearly shows that regions of both direct and retrograde waves exist. As it turns out, Figure 2.21 indicates that the properties of mucus that influence the motion of the body are both F_u and F_l. In addition, this study examines the influence of the viscosity of the mucus on locomotion.

Figure 2.22 is the result of calculations of R with respect to the viscosity of mucus μ for $F_u = 0.45 \times 10^{-2}$, $F_l = 0.0005 \times 10^{-2}$, $\kappa = 1.0$, and $q = 0.005$. We found that μ makes a significant contribution to locomotion. Our results indicate that the direct wave appears when μ is either smaller than a lower threshold or larger than an upper threshold value. Comparing these two regions of the direct wave, R is larger when μ is smaller. Interestingly, the region of the retrograde wave exists between two regions of direct wave. The diagram shows that the direction determination of the body depends deeply on the viscosity of mucus. Enormousness of μ on the choice of locomotion styles would be clear by Figure 2.23. Also, from Figure 2.23, it is realized that q is of little relevance to the choice of locomotion styles.

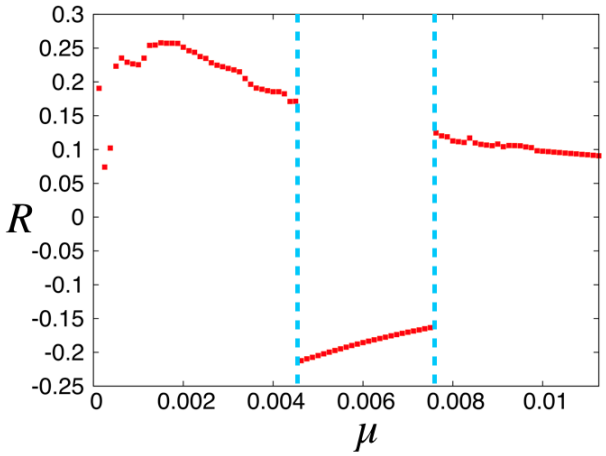

FIGURE 2.22. The effects of properties of mucus on the velocity ratio R for $\kappa = 1.0$, and $q = 0.005$. The plots of R with respect to the viscosity of mucus μ.

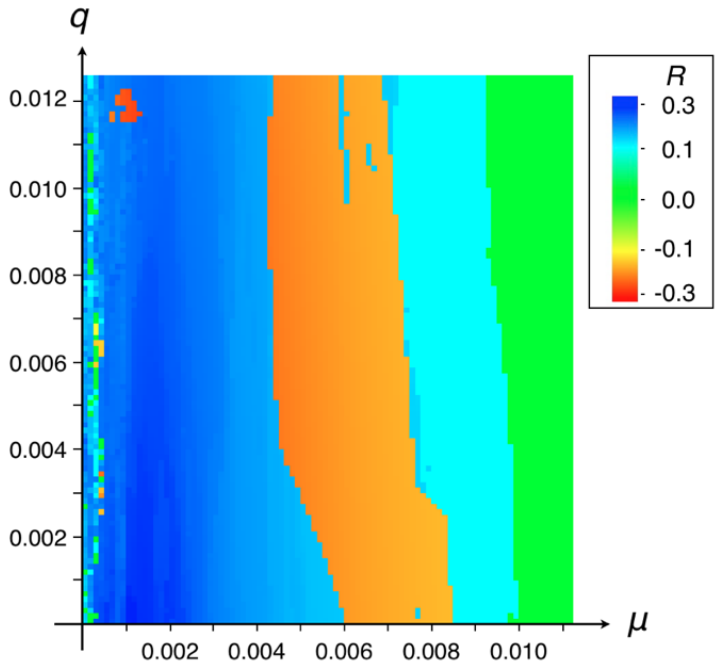

FIGURE 2.23. The effects of properties of mucus on the velocity ratio R. The effect of the viscosity of mucus, μ. In Figure 2.22, it was investigated in the case that $q = 0.005$. The two thresholds for the determination of direction always exist regardless of the value of q.

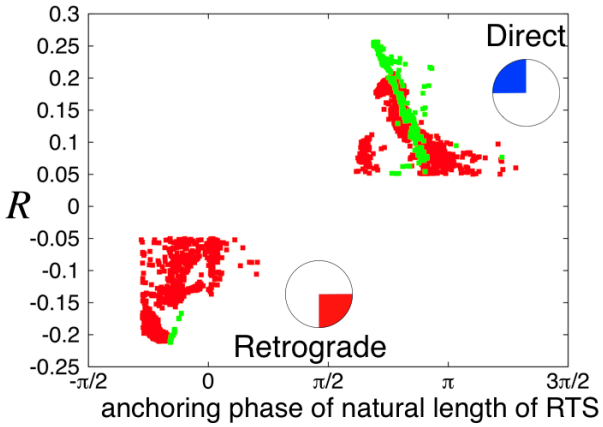

FIGURE 2.24. The effects of properties of mucus on the velocity ratio R for $\kappa = 1.0$, and $q = 0.005$. The relation between anchoring phase and R in the case that the absolute value of R is larger than 0.05. The red plots are obtained by varying F_u and F_l; the green are by varying μ.

The relation between velocity ratio R and the average of the anchoring phase can be seen in Figure 2.24. The natural length is longer (elongation) when the phase ($P = t - 2\pi Wn/N$) satisfies $\sin P > 0$. Conversely, it is in the contracted state when $\sin P < 0$. The results show that the anchoring phase occurs in the state of elongation when the direct wave is chosen and in the state of contraction when the retrograde wave is chosen, i.e., almost anti-phase with respect to the direct wave.

2.4.4. Role of Feature of Muscle in Locomotion. Now, we investigate the influence of muscle features on locomotion style.

Biologically, it would be an interesting finding if the physical features of muscle have implications for determining the direction of the body. Hence, Figure 2.25 shows the effect of muscular parameters. Parameter κ corresponds to stiffness of an active spring and α represents the ratio of contraction and elongation. We found in Figure 2.25 that the parameter region of κ and α for achieving a crawling locomotion exists. Furthermore, it can clearly be discerned that the nature of the muscle affects the determination of the direction of movement.

Figure 2.26 shows the result of changing the anchoring phase, similar to Figure 2.24, in the case of varying the parameters κ and α. The two styles of locomotion are realized by changing the anchoring phase in response to the change in parameters. Moreover, the black lines in Figure 2.25 plot the range of the spring coefficient r_{sc} ($= 2\kappa\alpha/(1-\alpha^2)$), i.e., the difference between the maximum and the minimum value of the spring coefficient. The black lines are only drawn when valid locomotion is achieved, that is, $0.8 \leq r_{sc} \leq 5.2$. We can see that effective locomotion can be realized by the retrograde wave as much as the direct wave when r_{sc} is a relatively small value, $0.8 \leq r_{sc} \leq 2.8$. When the range r_{sc} is larger, $4.0 \leq r_{sc}$, the direct wave is the only feasible strategy.

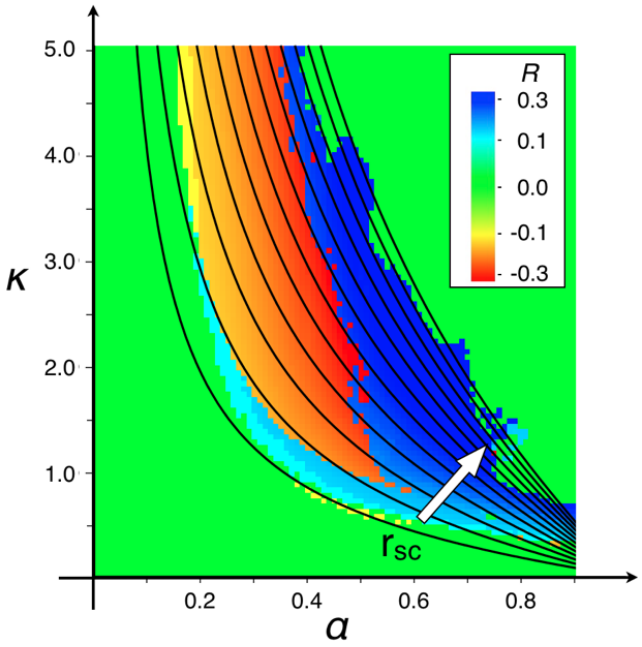

FIGURE 2.25. The effect of muscle features on velocity ratio R. The color plots of R with respect to κ and α. The result is for $F_u = 0.45 \times 10^{-2}$, $F_l = 0.0005 \times 10^{-2}$, and $q = 0.005$. If the absolute value of R is greater than 0.1, the region is colored blue ($R \geq 0.1$: direct wave) or red ($R \leq -0.1$: retrograde wave). The black lines are plots of the range of spring coefficient of RTS r_{sc}, and the white arrow indicates a positive direction. The plotted range of black line is $0.8 \leq r_{sc} \leq 5.2$.

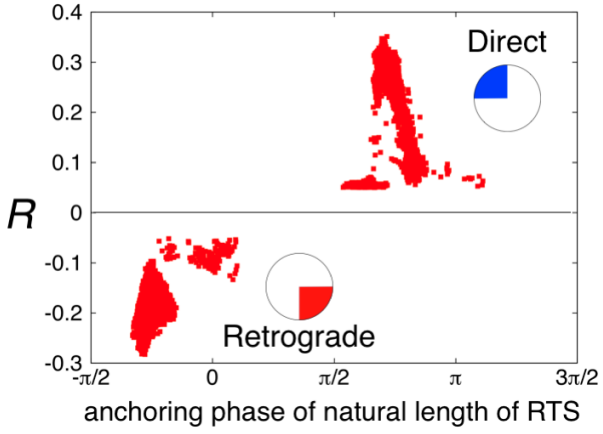

FIGURE 2.26. The effect of muscle features on velocity ratio R. (b) The relation between the average of anchoring phase and R in the case that the absolute value of R is greater than 0.05. The plots show results obtained by varying κ and α.

2.4.5. Nonlinearity of Pedal Mucus Influenced on Locomotion. Now I would like to focus on nonlinearity of pedal mucus. In adhesive locomotion, large stresses and strains are imposed upon the material, and thus the nonlinear rheological response of mucus in large amplitude oscillatory shear (LAOS) is important key for dynamics of adhesive crawling motion.

Lissajous' figure of strain-stress curve is one of the methods to examine nonlinearity of viscoelastic materials. Before discussing about the feature of mucus in our model, I simply explain a basic way to analysis of Lissajous' figure in rheology. In the case of purely elastic materials, as shown in Figure 2.27(a), there is no difference between the phases of stress and strain. Hence, the strain-stress curve becomes linear, and its gradient is modulus of elasticity in shear. Conversely, in the case of purely viscous fluid, the phase difference between strain and stress is just 90 degrees as shown in Figure 2.27(b), that is, the stress is linear with respect to strain rate. Lissajous' figure of purely viscous fluid is shaped an ellipse which is reduced only in direction of vertical axis compared with circle. The reduction rate in direction of vertical axis expresses viscosity of its material, in particular, a material of the curve with solid line is smooth, and the curve with dot-line is sticky in the strain-stress curve in Figure 2.27(b).

Viscoelastic materials have features of both elastic solid and viscous fluid. The phase difference of viscoelastic materials is more than 0 degree and less than 90 degrees, and the Lissajous' figure in this case becomes a diagonal ellipse as shown in Figure 2.27(c). The area of ellipse of strain-stress curve indicates loss energy, hence, elastic materials do not dissipate energy (heat) when a load is applied then removed. In viscoelastic measurement, these wave is decomposed into elastic and viscous elements, and storage elastic modulus and loss elastic modulus are estimated.

A distortion from an ellipse-like shape in Lissajous' figure shows its nonlinearity. It has been reported by Ewoldt et al. [Ewoldt et al., 2007], as shown in Figure 2.7, that the curve resulting from the LAOS using pedal mucus from *Limax maximus* exhibits a strongly nonlinear response leading up to yield. Especially, the elliptical curves become progressively distorted as the stress amplitude is increased, and its deformation increases sharply at large strains.

Now I would investigate the nonlinearity of mucus in our model. Figure 2.28 is Lissajous' figure of strain-force varying parameters (a) oscillation amplitude of natural length of RTS, α, and (b) yield point of mucus, F_u. In this figure, strain is calculated by actual length over natural length of 25th RTS, and force is obtained as total force acting 25th segment. The curves are classified into three styles of locomotion by color, direct wave (blue and cyan), retrograde wave (red and magenta), and still state (green and yellow). In particular the anchoring phases in each type are also indicated by blue, red, and green. As the same as previous study, as shown in Figure 2.28(a), the curve is like an ellipse at a small amplitude, and a strong nonlinearity appears at a large amplitude. The still state in Figure 2.28(a) has two types, i.e., nonlinearity did not appear since amplitude is too small, or symmetric nonlinearity appeared at a large amplitude. In the case that effectual motion was achieved by direct wave and retrograde wave, that occurs at appropriate

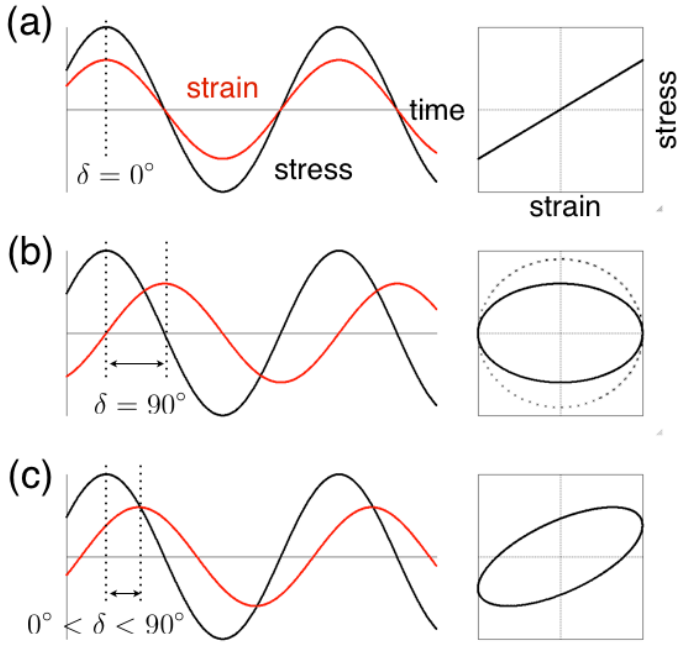

FIGURE 2.27. Dynamic viscoelastic behavior of solid and liquid materials. Phase difference δ varies by materials. (a)Purely elastic solid: $\delta = 0°$, and strain-stress curve is linear. (b)Purely viscous liquid: $\delta = 90°$, and strain-stress curve shapes like a circle. (c)Viscoelastic material: $0° < \delta < 90°$, and strain-stress curve is like an ellipse.

values of α between the two still states, the Lissajous' curve showed a nonlinearity and a strong asymmetrically. Compared between the direct wave states, it is clear that loss energy increases with increase in amplitude.

In the case of fixing $\alpha = 0.5$ and varying F_u, in Figure 2.28(b), a strongly nonlinear response always appeared. Although nonlinearity is clearly important for realization of locomotion, F_u does not influence on nonlinearity, but α does strongly. The effect of yield point appears in asymmetric nature. Also the figure indicates that valid locomotion could be realized when the internal area of the curve is appropriately large.

2.5. Toward Understanding Adhesive Locomotion as Bifurcation Phenomenon

In our numerical results, there is interesting issue from a view point of mathematics concerning the determination of locomotion styles. In phase diagram such as Figure 2.19, 2.21, 2.22, and 2.25, boundary between areas of direct and retrograde waves is clear. Additionally, a discontinuous transition occurs in the boundary. It would be reasonable to understand it as bifurcation phenomenon, but it is difficult to analyze mathematically. Here I describe preparations toward mathematical bifurcation analysis about determination of locomotion styles, direct wave or retrograde wave. First, in

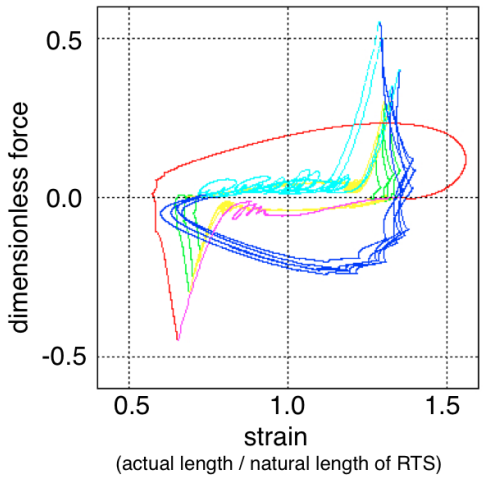

FIGURE 2.28. Lissajous' figure of strain-force curve, varying α for $\kappa = 1.0$, $q = 0.005$, and $F_l = 0.0005 \times 10^{-2}$. The curves are classified into three styles of locomotion, direct wave (blue and cyan), retrograde wave (red and magenta), and still state (green and yellow). Anchoring phases in each type are also indicated by blue, red, and green. Fixing $F_u = 0.45 \times 10^{-2}$ and varying $0.1 \leq \alpha \leq 0.8$. Nonlinear response appears at a large amplitude $\alpha \geq 0.4$.

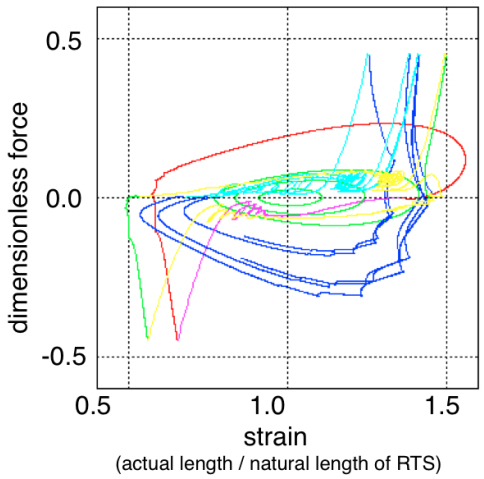

FIGURE 2.29. Lissajous' figure of strain-force curve, varying F_u for $\kappa = 1.0$, $q = 0.005$, and $F_l = 0.0005 \times 10^{-2}$. The curves are classified into three styles of locomotion, direct wave (blue and cyan), retrograde wave (red and magenta), and still state (green and yellow). Anchoring phases in each type are also indicated by blue, red, and green. Fixing $\alpha = 0.5$ and varying $0.20 \times 10^{-2} \leq F_u \leq 0.55 \times 10^{-2}$. Asymmetric property appears at a large yield $0.35 \times 10^{-2} \leq F_u \leq 0.55 \times 10^{-2}$.

next section, let show numerical results of bifurcation phenomenon occurs in boundary.

2.5.1. Initial Value Dependence for Locomotion Style. For understanding transition between direct wave and retrograde wave observed in the phase diagrams, initial value dependence of solution in this model is investigated. Now, each initial value of switching parameter, σ_n, are set to 0 or 1 randomly, although they were set to 1 as a realistic value in above-mentioned simulations.

Figure 2.30 is a bifurcation diagram of relative velocity R with respect to one of the muscular parameters α when the dimensionless parameters are set as $\kappa = 1.0$, $q = 0.005$, $F_l = 0.0005 \times 10^{-2}$, and $F_u = 0.45$. The multiple panels (a) - (f) are typical types of Lissajous' figure of the strain-force curve of 25th segment in each state. When α is small enough not to observe a nonlinearity in Lissajous' figure as the panel (a), the stable state of R is 0. The bifurcation like a super-critical pitchfork bifurcation appears at first with increasing the parameter. That is, the stable state transitions from the ineffective motion (a: monostable) to two branch (c: bistable), after the period of chaotic bistate (b). It is reasonable to predict that there is the unstable branch of ineffective motion in the state of (c). With increasing

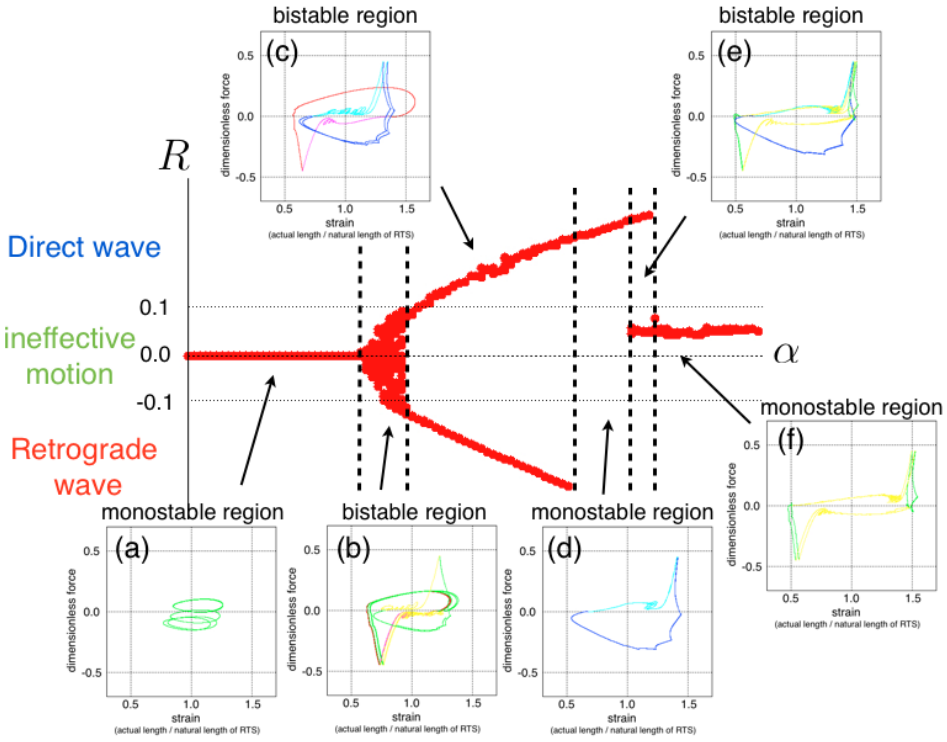

FIGURE 2.30. Bifurcation diagram of R with respect to α when the dimensionless parameters are set that $\kappa = 1.0$, $q = 0.005$, $F_l = 0.0005 \times 10^{-2}$, and $F_u = 0.45$. The range of α is [0,1). A bifurcation like super-critical pitchfork type is appeared.

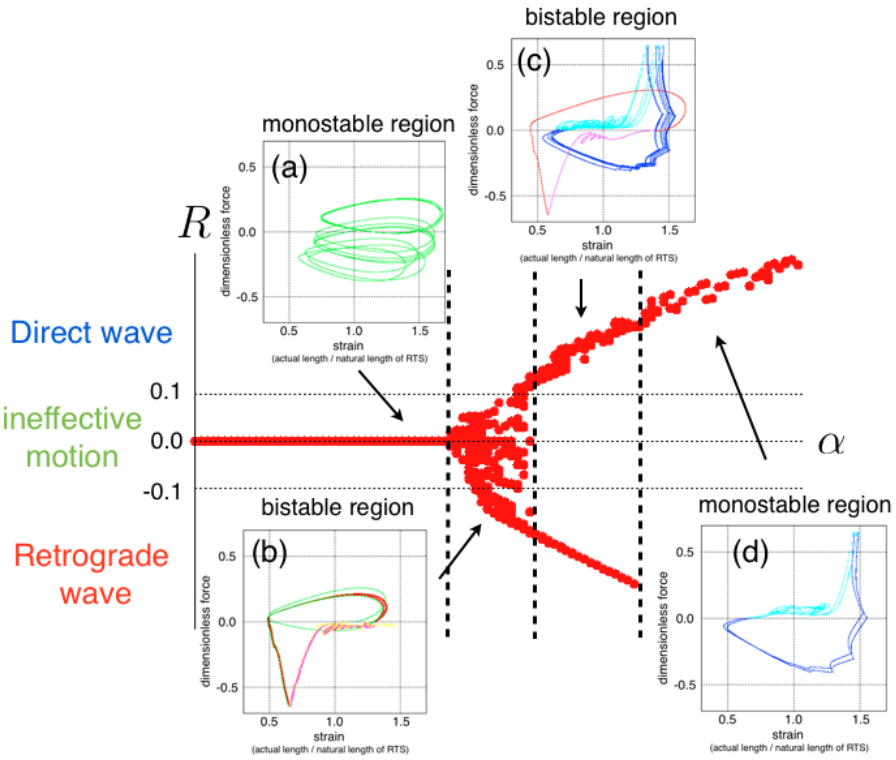

FIGURE 2.31. Bifurcation diagram of R with respect to α when the dimensionless parameters are set that $\kappa = 1.0$, $q = 0.005$, $F_l = 0.0005 \times 10^{-2}$, and $F_u = 0.65$. The range of α is [0,1). A type of super-critical pitchfork is maintained if the value of F_u would be varied.

of α, it appears branches are difficult to understand, although it can be predicted that ineffective motion becomes stable again at the large enough value of α to keep its symmetry (f). It is noteworthy that direct wave can exist as a stable state independently (d) in spite of the fact that retrograde wave cannot as shown in (b) and (c).

It has found that the super-critical pitchfork bifurcation such as Figure 2.30 is maintained even though the parameter F_u was varied. Figure 2.31 is one of the examples in the case of $F_u = 0.65$. Compared with Figure 2.30, a pitchfork bifurcation appeared at a point which moved to the positive direction. Furthermore, a monostable region of ineffective motion (d) and a bistable region of its transition period (c) did not appear.

Similar to α, a bifurcation phenomenon can be found with respect to other parameter. Figure 2.32 is bifurcation diagram of R with respect to κ, which is another muscular feature of pedal foot, when $\alpha = 0.5$. The super-critical pitchfork bifurcation appeared in the diagram with respect to the parameter α. The bistable branches which bifurcated by super-critical bifurcation exist without interruption with increasing of κ.

It can be easily predicted by Figure 2.30 and 2.31 that the bifurcation diagram of κ could be change with increasing of α because it has been

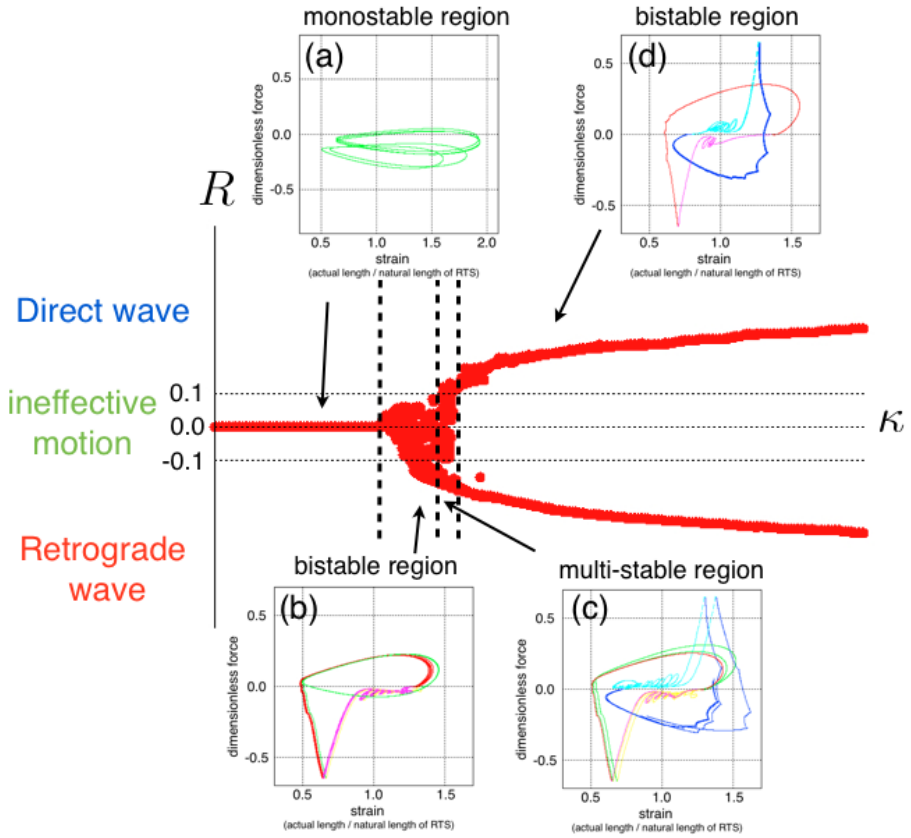

FIGURE 2.32. Bifurcation diagram of R with respect to κ when the dimensionless parameters are set that $\alpha = 0.5$, $q = 0.005$, $F_l = 0.0005 \times 10^{-2}$, and $F_u = 0.65$. The range of κ is [0,3]. A bifurcation of super-critical pitchfork type is appeared.

already found that direct wave is independently stable when α is large. In fact, the bifurcation diagram of κ when $\alpha = 0.8$ as shown in Figure 2.33 is a bit different from Figure 2.32. Although the super-critical pitchfork bifurcation also appeared, the state of retrograde wave becomes unstable with increasing of κ. It is noteworthy, similar to bifurcation diagram of α, that direct wave can exist as a stable state independently (d) in spite of the fact that retrograde wave cannot as shown in (b) and (c). It is, however, more complex to analyze because bistable region of direct and retrograde waves (e) appeared again. To sum up simply, with few exceptions, retrograde wave tends to become difficult to appear as a stable state with increasing of α and κ. That is, it has found by numerical results that direct wave is clearly dominant when α and κ are large.

By the result that there are coexistence regions, the state of stable solution can be classified into seven types as shown in Table 2.4 although the monostable region of retrograde wave, (R) in the table, could not be observed in the diagrams of Figure 2.31, 2.32, and 2.33. Now, to be clear the co-existence of direct and retrograde waves in the border of regions of two

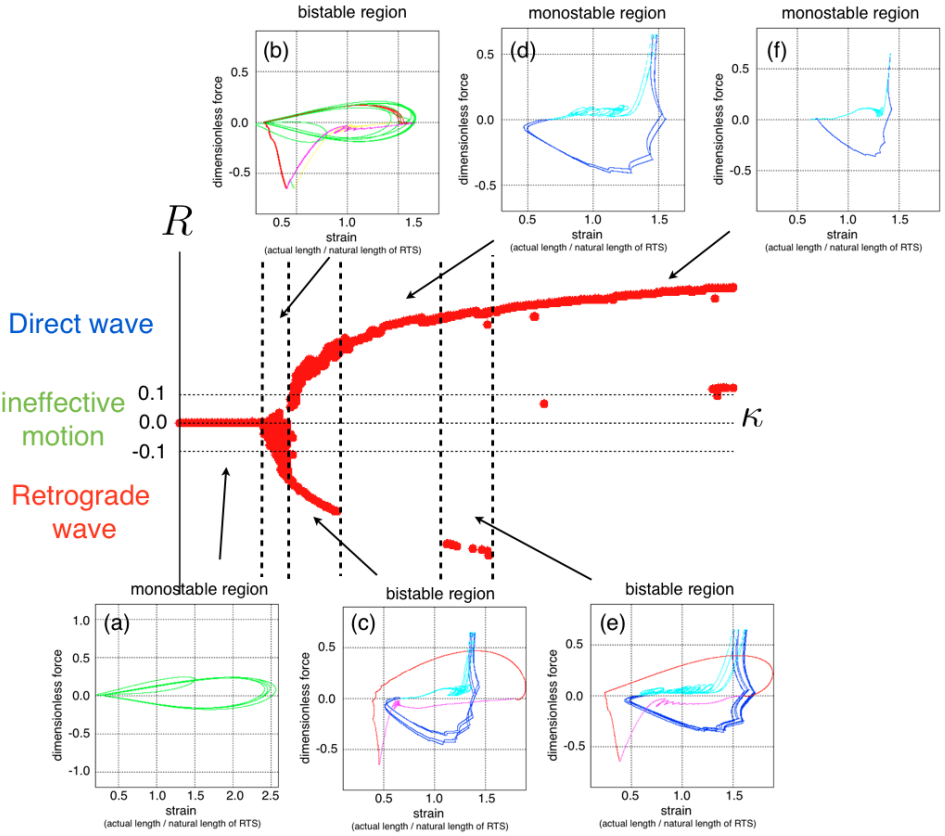

FIGURE 2.33. Bifurcation diagram of R with respect to κ when the dimensionless parameters are set that $\alpha = 0.8$, $q = 0.005$, $F_l = 0.0005 \times 10^{-2}$, and $F_u = 0.65$. The range of κ is [0,3]. The super-critical pitchfork bifurcation appeared, and direct wave becomes dominant with increasing of κ.

locomotion styles, the phase diagram of Figure 2.25 can be used different colors for each stable state as Figure 2.34. It is shown clearly in Figure 2.34 that the state of ineffective motion of Figure 2.25 is totally stable state. Conversely, most of the states of efficient motion of Figure 2.25 are bistable states of direct and retrograde waves. Most significant result is that the monostable state of direct wave has a large region, and non-existence of the monostable state of retrograde wave was confirmed. Looking along α axis, sequence of stable state is maintained as (I) $\rightarrow$ (R+I) $\rightarrow$ (D+I+R) $\rightarrow$ (D+R) $\rightarrow$ (D) $\rightarrow$ (D+I) $\rightarrow$ (I).

Figure 2.35 is phase diagram of stable states in the case of $F_u = 0.65 \times 10^{-2}$. With increasing of the value of F_u, the region of efficient motion tends to expand, and both monostable (D) and bistable (D+I) regions also seem to expand.

On the other hand, it has been already found that the feature of mucus also influence on determination of locomotion style, and a discontinuous transition occurs in the boundary. Here, the bifurcation diagram of R with respect to the dimensionless parameter F_u, which is yield point of the mucus,

TABLE 2.4. The classification of stable state

	Direct wave	Ineffective motion	Retrograde wave
Monostable (D)	Stable	Unstable	Unstable
Bistable (D+I)	Stable	Stable	Unstable
Multistable (D+I+R)	Stable	Stable	Stable
Bistable (D+R)	Stable	Unstable	Stable
Bistable (R+I)	Unstable	Stable	Stable
Monostable (R)	Unstable	Unstable	Stable
Monostable (I)	Unstable	Stable	Unstable

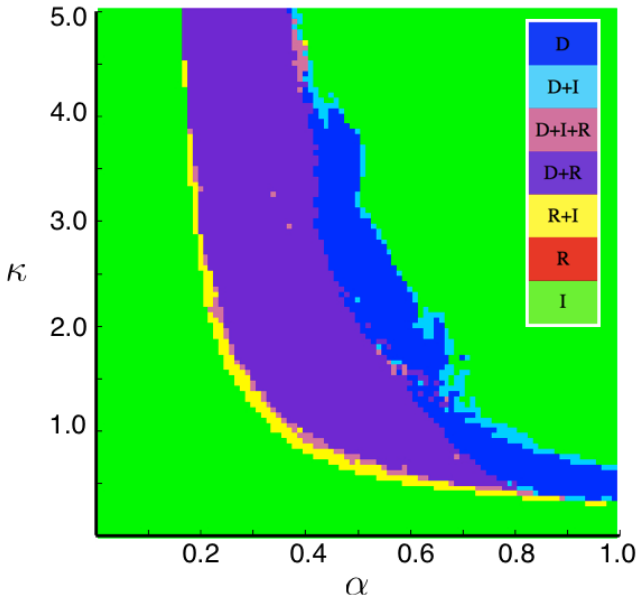

FIGURE 2.34. Phase diagram of stable states with respect to dimensionless parameter α and κ, which used different colors for each stable state of Figure 2.25 into seven states mentioned in Table 2.4. The result is for $F_u = 0.45 \times 10^{-2}$, $F_l = 0.0005 \times 10^{-2}$, and $q = 0.005$. Monostable state of direct wave exist at a larger value of α.

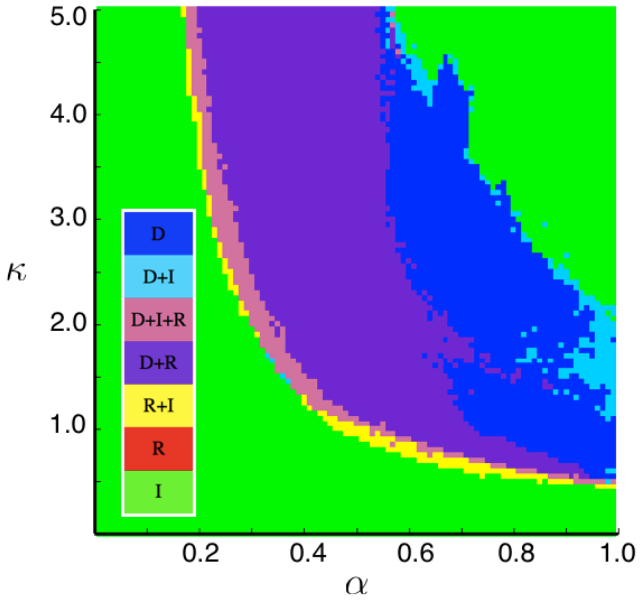

FIGURE 2.35. Phase diagram of stable states with respect to dimensionless parameter α and κ. The result is for $F_u = 0.65 \times 10^{-2}$, $F_l = 0.0005 \times 10^{-2}$, and $q = 0.005$.

is described in Figure 2.36. In contrast to the case of bifurcation diagram with respect to muscular feature, the bifurcation which occurred at a small value of F_u is unusual type. The stable branch of ineffective motion (a) might connect implicitly to the two stable branches (c), direct wave and retrograde wave, by unstable branches. It can be recognized, however, that the second bifurcation which occurred at a large value is similar to subcritical pitchfork bifurcation. Two stable branches of direct and retrograde waves (c) switch stability with the branch of ineffective motion (f) after a chaotic period (d) and (e).

Similar to the case of muscular feature, we can obtain the phase diagram of stable states as shown in Figure 2.37. The calculations are carried out with dimensionless parameters $\alpha = 0.5$, $\kappa = 1.0$, and $q = 0.005$. It is clear that the state of ineffective motion of Figure 2.21 is totally stable state. Looking along F_u axis as far as $F_l = 0.005 \times 10^{-2}$, sequence of stable state tends to maintain as (I) $\rightarrow$ (R+I) $\rightarrow$ (D+I+R) $\rightarrow$ (D+R) $\rightarrow$ (D+I+R) $\rightarrow$ (R+I) $\rightarrow$ (I). Within comparatively large values in F_l, interestingly, bistable state of (D+I) is only dominant among efficient motion. Moreover, We obtained a meaningful result that the monostable state of retrograde wave (R) exists at an appropriate region.

In the next section, I will discuss this study.

2.6. Discussions

We were first able to verify that the crawling locomotion is validly simulated by the mechanism, that is, by the mutual interaction between periodic muscular contraction waves of the soft foot and the specific properties of

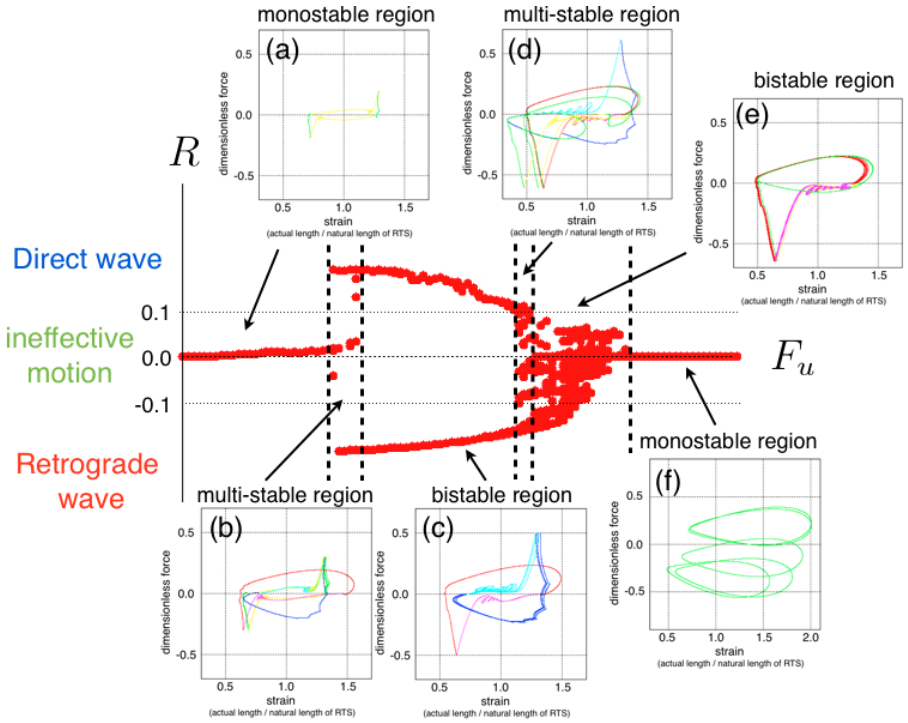

FIGURE 2.36. Bifurcation diagram of R with respect to F_u when the dimensionless parameters are set that $\kappa = 1.0$, $\alpha = 0.8$, $q = 0.005$, and $F_l = 0.0005 \times 10^{-2}$.

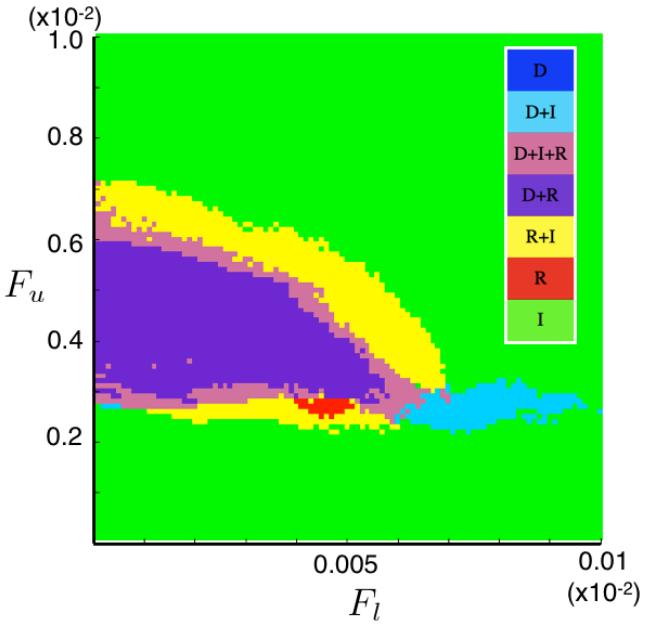

FIGURE 2.37. Phase diagram of stable states with respect to dimensionless parameter F_l and F_u, which used different colors for seven states mentioned in Table 2.4. The result is for $\alpha = 0.5$, $\kappa = 1.0$, and $q = 0.005$.

mucus. At first, the muscle begins to contract and extend periodically, in concert with the phase of the internal oscillators. The mucus under each segment is pulled and pushed depending on the tension induced by the muscular waves. When the tension force acting on the mucus becomes larger, the mucus, which was an elastic solid working to fix the body to the substrate (anchoring), changes to a viscous liquid. After this point, the body segments can move smoothly (slipping). Both the anchoring and the slipping regions exist along the foot. Similar to the muscular wave, the waves of these anchoring and slipping regions propagate.

Furthermore, and intriguingly, two locomotion styles, direct wave and retrograde wave, are realized in our numerical simulation. The simple mechanism of the difference between direct and retrograde waves was clarified by Jones and Trueman [Jones and Trueman, 1970], after Lissmann [Lissmann, 1945b] and Miller [Miller, 1974a,b]. The simplified mechanism of direct waves is as follows: the pedal foot is adhesive to the substratum at maximum extension, then forward movement will occur when the foot is longitudinally contracted and the contracted part propagates forward. That is, migration of the center of gravity occurs in the contracted part of the foot. In contrast, the mechanism of retrograde waves is as follows: when retrograde waves occur, the pedal foot is attached along its shortest length, and then the foot is maximally extended forward and the extended part propagates backward. That is, migration of the center of gravity occurs in the extended part of the foot. These existing mechanisms only described the appearance based on observations that each locomotion style was realized, but did not say about a bottom mechanism, how to be realized. The results of numerical simulation using our mathematical model are an advantage in that these previous mechanisms were realized as a result of considering the underlying essence.

Comparing the results of mathematical model for peristaltic locomotion [Tanaka et al., 2011] makes easy to understand why these two locomotion styles could be realized. Tanaka et al. [Tanaka et al., 2011] claimed that the peristaltic locomotion of both the direct wave and the retrograde wave can be realized if it is possible to change the phase of anchoring. Thus, in the simplest terms, it is necessary to change the anchor phase in order to realize two locomotion styles. We claim, based on our numerical calculations, that it is possible to change the anchor phase by changing only the properties of mucus (Figure 2.19, 2.24), or the features of muscle (Figure 2.26). Our study fully supports Tanaka's conclusions, and, in parallel, we can say that control of friction is not required in the case of spontaneous friction control by mucus, unlike the mechanism of peristaltic locomotion.

Figure 2.20 explains why the anchoring phase would change. The significance here is that the jump B of Figure 2.16, i.e., the moment of the mucus changing from elasticity to viscosity, occurred in what condition of pedal foot. The force can generate by being pushed as well as pulled. In the case of direct wave, the jump B occurs in the segment of foot being pushed. Hence, the mucus becomes the property of viscous liquid before this portion of foot reaches a peak of contraction. Therefore, the elongated parts of their foot are anchored. In the case of retrograde wave, in contrary, the jump

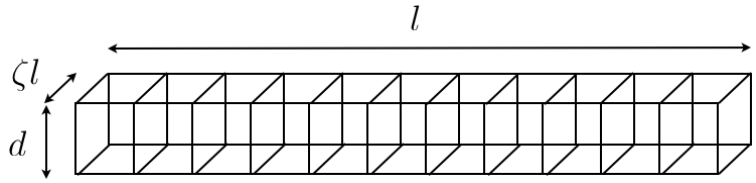

FIGURE 2.38. Image sketch of pedal foot for a continuous model.

B occurs in pulled state of the segment, and the mucus changes to viscous liquid before this portion of foot reaches a peak of elongation. That is, the contracted regions of their foot are anchored.

The choice among two styles is uniquely determined by the parameters related to mucus and muscle basically. However, we already know by our additional numerical calculations mentioned in Section 2.5 that these two locomotion styles are co-existence in the boundary regions between direct and retrograde waves as shown in Figure 2.21, 2.22, 2.23, and 2.25. In this study, the initial conditions of σ_n for all n were set to 1 (elasticity) because we would consider the condition in nature. By this assumption, the parameter regions where the locomotion style suddenly changes exist. From a mathematical viewpoint, the interesting question is why the sign of the velocity inverts immediately when some parameter values are changed. We have found by the bifurcation diagrams such as Figure 2.31, 2.32, and 2.36 that a bifurcation like super-critical pitchfork appears in the case related to muscle, and a bifurcation like subcritical pitchfork appears related to mucus. This problem which originates from a existence of a number of solutions, should be analyzed by improving a description of mucus from discrete to a continuous model and also by decreasing degrees of freedom to three mass system. Toward mathematical explanation of these bifurcation phenomena observed in numerical results, I introduce a spatial continuous model obtained by taking the limit of our discretized model as follows.

As preliminary stage of modification for a continuous model, let consider about relationship between elastic solid and spring constant. Now, as shown in Figure 2.38, I assume that the length and width of pedal are l and ζl, respectively, and the height is d. The spring constant of this elastic solid is $Ed\zeta l/l = \zeta Ed$, where E is the Young's modulus. Dividing the length of this material into $N-1$, the length of each elastic solid becomes $l/(N-1)$, the spring constant k of each material in x-axis thus becomes as following:

$$k = E\zeta ld(N-1)/l = E(N-1)\zeta d$$

Assuming both viscosity η and elasticity ξ of mucus under each segment to be proportional to sectional area,

$$\eta = \zeta l \times \frac{l}{N-1} \times \mu = \frac{\zeta l^2 \mu}{N-1},$$

$$\xi = \zeta l \times \frac{l}{N-1} \times \gamma = \frac{\zeta l^2 \gamma}{N-1},$$

where μ and γ are viscosity and elasticity per unit of area, respectively.

The model with RTS of the muscle and hysteresis loop of the mucus is written by,

$$\begin{aligned}(1-\sigma_i)\eta\dot{u}_i + \sigma_i\xi(u_i - \overline{u}_i) \\ =k\frac{\bar{l}_{i+\frac{1}{2}}}{l_{i+\frac{1}{2}}}(u_{i+1} - u_i - l_{i+\frac{1}{2}}) - k\frac{\bar{l}_{i-\frac{1}{2}}}{l_{i-\frac{1}{2}}}(u_i - u_{i-1} - l_{i-\frac{1}{2}})\end{aligned} \tag{2.6.1}$$

where u_i is the position of ith segment. Variable $l_{i+\frac{1}{2}}$ is natural length of ith RTS controlled as

$$l_{i+\frac{1}{2}} = \frac{l}{N-1}(1 + \alpha \sin\theta_i),$$

where

$$\theta_i = \omega t - \frac{2\pi l}{\lambda}\frac{i}{N-1}.$$

Now we consider a map $u : [0:1] \to \mathbf{R}$ which satisfies $u_i = u(i\delta s)$ is N is large enough, where $\delta s = l/(N-1)$, and the function u is assumed to be smooth. The equation (2.6.1) is rewritten as

$$\begin{aligned}(1-\sigma_i)\dot{u}_i + \sigma_i\frac{\xi}{\eta}(u_i - \overline{u}_i) \\ =\frac{k}{\eta}\frac{\bar{l}_{i+\frac{1}{2}}}{l_{i+\frac{1}{2}}}(u_{i+1} - u_i - l_{i+\frac{1}{2}}) - \frac{k}{\eta}\frac{\bar{l}_{i-\frac{1}{2}}}{l_{i-\frac{1}{2}}}(u_i - u_{i-1} - l_{i-\frac{1}{2}}).\end{aligned} \tag{2.6.2}$$

Each coefficient can be calculated as follows,

$$\frac{\xi}{\eta} = \frac{\zeta l^2 \gamma/(N-1)}{\zeta l^2 \mu/(N-1)} = \frac{\gamma}{\mu},$$

$$\frac{k}{\eta} = \frac{E(N-1)\zeta d}{\zeta l^2 \mu/(N-1)} = \frac{Ed}{\mu}\frac{(N-1)^2}{l^2} = \frac{Ed}{\mu}\frac{1}{(\delta s)^2}.$$

Hence, taking the limit of the right-hand side of the equation (2.6.2),

$$\lim_{N\to\infty}\left(\frac{k}{\eta}\frac{\bar{l}_{i+\frac{1}{2}}}{l_{i+\frac{1}{2}}}(u_{i+1}-u_i-l_{i+\frac{1}{2}}) - \frac{k}{\eta}\frac{\bar{l}_{i-\frac{1}{2}}}{l_{i-\frac{1}{2}}}(u_i-u_{i-1}-l_{i-\frac{1}{2}})\right)$$

$$= \lim_{N\to\infty}\frac{k}{\eta}\bar{l}\left(\frac{u_{i+1}-u_i}{l_{i+\frac{1}{2}}} - \frac{u_i-u_{i-1}}{l_{i-\frac{1}{2}}}\right)$$

$$= \lim_{N\to\infty}\frac{Ed}{\mu(\delta s)^2}\left(\frac{u_{i+1}-u_i}{1+\alpha\sin\theta(s_i)} - \frac{u_i-u_{i-1}}{1+\alpha\sin\theta(s_{i-1})}\right)$$

$$= \frac{Ed}{\mu}\frac{\partial^2 u}{\partial s^2}\left(\frac{1}{1+\alpha\sin\theta(s)}\right).$$

Here we can obtain the continuous model as follows,

$$(1-\sigma)\dot{u} + \sigma\nu(u-\overline{u}) = \frac{Ed}{\mu}\frac{\partial^2 u}{\partial s^2}\left(\frac{1}{1+\alpha\sin\theta(s)}\right), \tag{2.6.3}$$

where $\nu = \xi/\eta$.

The next step toward mathematical analysis of the bifurcation phenomenon is re-description of hysteresis loop of the mucus. I have the idea of N-type nullcline for the development, but it remains as future work.

Next, we focus on the nonlinear feature of the mucus. As reported by Ewoldt et al. [Ewoldt et al., 2007], a strong nonlinearity at a large amplitude oscillatory shear (LAOS) as shown in Figure 2.7 is observed in dynamic viscoelastic measurement using the mucus of slugs. Although such a nonlinearity is one of the nature which characterizes an viscoelasticity of the mucus, it might be difficult to realize as a synthetic material. In fact, synthetic complex fluids created by Ewoldt et al. [Ewoldt et al., 2007] could not mimic this strain-stiffening. Our model can realize such a strong nonlinearity observed in the result of the mucus of slug, although the model is remarkably-simple and has a lack of the assumption that the recovery D is a jump as shown in Figure 2.16(b). It is also noted that the Lissajous'

figures obtained by our model as shown in Figure 2.28 and 2.29 have asymmetric property which might lead to two different locomotion styles when the parameters were set to appropriate values. By above discussions, it is reasonable to consider that the length of recovery time to elastic property is not essential for realization of migration. However, the recovery of elastic property D is actually performed more slowly compared with the jump B, and it is unclear yet how long the mucus recovers its elasticity. An improved model to describe the recovery time should be considered as a future work since it could influence on velocity and direction of motion.

Finally, let us now look at our results in the context of the research of Chan et al. [Chan et al., 2005]. Our result partially supports their study in that the locomotion of the direct wave can be achieved by the interaction between mucus and muscular contraction. However, they concluded that spontaneous friction control by mucus cannot realize the retrograde wave locomotion. Why did their conclusion differ from ours? Although we cannot say exactly, we suggest the following possibility based on Figure 2.25. That is to say, their model and robots may have the condition that the value of either α or r_{sc} was large. If this were true, we are in agreement with the result that only the direct wave is realized. As described in the section related to bifurcation, Section 2.5, direct wave is independently dominant if α is large. When α is a large value, advantage of direct wave increases with increasing of the value of κ. In their study, a mollusk-like flexible body might not be realized, because they focused on the properties of mucus. They overlooked a significant factor—that the properties of muscle contribute significantly to the choice of movement direction in the mechanism of spontaneous friction control by mucus. Two styles of locomotion may be realized if a robot is made based on our result. Our study would serve as a guideline for the development of such robots.

2.7. Summary and Future Works

The aim of this study was to theoretically verify that mutual interaction between the specific viscoelasticity of the mucus and the propagation of muscular contraction waves can realize adhesive locomotion. Therefore, we built a simple mathematical model that assumed two essential factors. The first was to mimic the propagation of a flexible muscular wave using the spring RTS, and the second was the hysteresis loop for describing the change in the nature of mucus by introducing a switching parameter. Our numerical simulations showed that adequate propulsive force for locomotion could be generated by the interaction of these two factors. Under this mechanism, the mucus has a role in controlling the friction with the ground. It has been also revealed by our numerical results that the features of the mucus and muscle, especially, the yield point of the mucus, stiffness and contraction rate of muscle influence on determination of locomotion strategy, direct wave or retrograde wave. It is noted the properties of muscle, stiffness and contraction rate, are important factors for stability of locomotion styles.

As a future work, we will build a mathematical model with consideration of a healing time in recovery process. By an improved model, we will be

able to investigate how the recovery time affects their locomotion, and how long term can be effective for valid locomotion.

This study reinforces the assertion that mucus has an important role in frictional control for adhesive locomotion. Furthermore, we have obtained new insights into the nature of how the mucus and muscles directly affect the determination of locomotion style. Future experimental research into the yield point of mucus and the ratio of muscle contraction in various species, as well as mathematical investigations into energy efficiency, will reveal the background of the evolutionary acquisition of locomotion strategies in gastropods and their neighboring species.

CHAPTER 3

Spiral Formation on Heterogeneous Excitable Media: Contribution to Solution for Mechanism of Ventricular Fibrillation

Spiral waves may have a negative influence on the functions of living systems. Spiral reentry in the heart as shown in Figure 3.1 is a typical example. In a normal situation, the heart can act as a role of pump by contraction of cardiac cells caused by propagation of action potential with target pattern. If once a spiral wave has been generated, however, the target pattern of action potential will be broken. It is because spiral pattern is the only pattern which could survives on excitable media without an external stimulus. I would like to reveal the mechanism of spiral reentry which happens in the heart, since it is significant life phenomena, i.e., one of the life-threatening ventricular arrhythmia which might induce ventricular fibrillation.

About 50,000 people per year are died by the sudden death in Japan, 60% of which is due to cardiac arrhythmias. A lot of the arrhythmia is

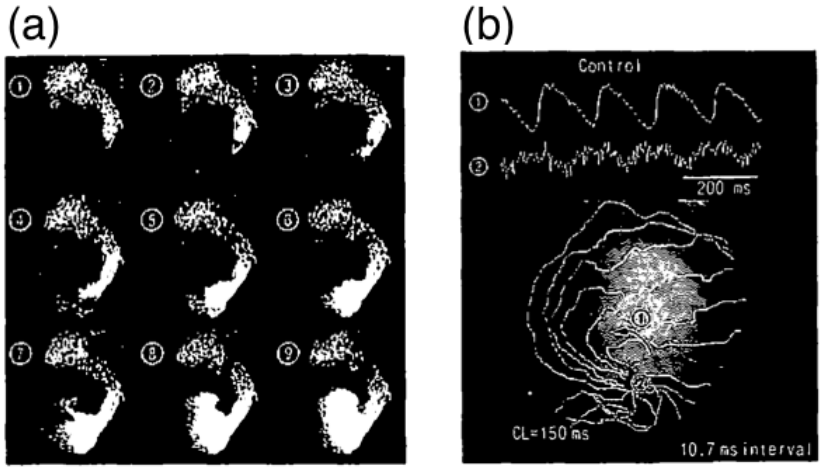

FIGURE 3.1. Spiral reentry in a cultured cardiac cells, quoted from (a) Figure 4.10 and (b) Figure 4.11 of [Inada et al., 2006], respectively. (a) Spiral wave of membrane action potential which was observed by high-speed video camera. (b) Waveform of membrane action potential and example of isochrones view of spiral reentry.

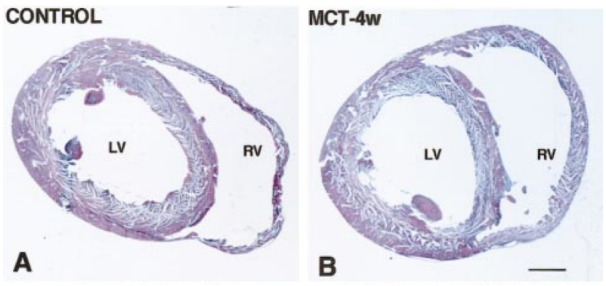

FIGURE 3.2. Macroscopic and microscopic morphology of the heart. Cross section from a control (A) and MCT-treated rat (B) 4 weeks after injection (bar 1 mm), quoted from Figure 2 of [Uzzaman et al., 2000]. The wall of right ventricular in the case of cardiomegalia (B) becomes large compared to a control (A).

ventricular fibrillation. In the United States, about 450,000 lives a year are lost in sudden death, 90% of the cause of death is due to arrhythmia, then the 80% of them is ventricular fibrillation. Not only in the United States and Japan, ventricular fibrillation is a serious problem worldwide.

Heart is constructed of muscle called cardiac muscle cells, and electrical stimulation which is delivered periodically from the sinus node in the right atrium is gradually transmitted to each site, then finally disappear. Through these processes, each part of the heart performs contraction and relaxation in sequence, so the heart can act as a pump to pass the blood into the general circulation. Conversely, if there is an abnormality in propagation of action potential, and spiral reentry which remains winding vortex of electrical stimulation occurs, the heart continues to be stimulated at all times. Therefore, cardiac myocyte can not realize contraction and relaxation, i.e., heartbeat, it means that the heart is unable to function properly as a pump to send the blood, and leads to sudden death. Under present circumstances, a mechanism of spiral reentry which is considered as a cause of ventricular fibrillation has not been elucidated, so we are not able to prevent ventricular fibrillation from occurring.

What is focused on for understanding the mechanism of ventricular fibrillation is that cardiac muscle cell is one of the excitable media. It is reasonable to treat a spiral wave of action potential as the general phenomenon occurring in excitable media. In fact, the concept of spiral reentry was a hypothesis which has been proposed by computer simulations [Moe et al., 1964]. After that M.A. Allessie et al. [Allessie et al., 1977] have found by experiments of rabbits that multiple wavelet observed in cardiac cell is functional reentry, moreover, many researchers have studied the formation mechanism of the functional reentry by analysis of propagation patterns of excitable waves in animal experiment and numerical simulation. For analysis of experiments on animals, the electrode mapping which record multisite extracellular potentials in parallel from the surface of cardiac muscle has mainly been used. More recently, optical mapping is also used, which shoots

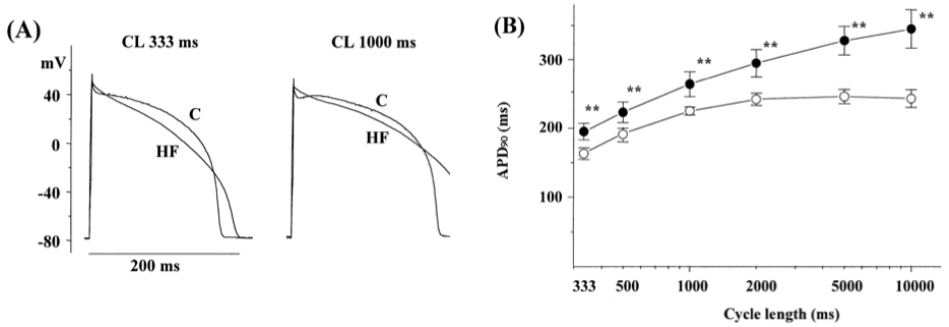

FIGURE 3.3. Frequency response of APD prolongation, quoted from Figure 1 of [Tsuji et al., 2000]. (A) Typical action potentials recorded by ventricular myocytes from a control (C) and a failing heart (HF) at 333 ms (left) and 1000 ms (right) of cycle length (CL). (B) Relationship of cycle length and APD at 90% of repolarization.

simultaneously multi membrane potential signals from myocardial surfaces which are stained with membrane potential-sensitive dyes.

What is needed for generating spiral reentry is that a tip of wave is created by the wave breaking and remains to survive. These factors are induced by non-excitable obstacle such as infarct region and fibrous tissue as well as refractory region which is generated by excitability of the former wave. It is not always true, however, that the spiral pattern is generated when cell necrosis was occurred, i.e., depending on the size of obstacle as reported by [Jalife et al., 1998]. If there is a large obstacle, it is probably reasonable that the spiral waves are occurred. Unfortunately, there are many healthy-looking people among those who died by suddenly death. General example is the case of a player of soccer. The sudden death of Naoki Matsuda in 2011, who was the one of the national team in Japan, is still vivid in our memory. Why does the spiral reentry occur in the healthy heart?

Here indicated point of view is cardiomegalia. Cardiomegalia is that the whole heart is enlarged since the heart is under extreme stress when blood is pumped. There is an explicit difference between heart enlargement and cardiomegalia, that is, cardiomegalia has the feature that the wall of the right ventricular becomes large as shown in Figure 3.2 though heart enlargement enlarges only the heart. Note that in the case of cardiomegalia, the number of cells does not increase but the size of the cell do. Although cardiomegalia is seen in the heart of fat person, overload exercise often induces cardiomegalia such as doing among athletes. Note that ventricular fibrillation would not always happen in the heart of people who has cardiomegalia, but it is a lot of case that the heart whom had died by ventricular fibrillation was enlarged. Why would ventricular fibrillation be caused by cardiomegalia?

The most general change when cardiac muscle enlarged is prolongation of action potential duration (APD) [Tsuji et al., 2000]. Figure 3.3(A) is comparison of wave profile of action potential recorded from myocytes isolated from heart failure (HF) and from normal myocytes as a control (C). It is clearly recognized that action potentials recorded by myocytes of heart

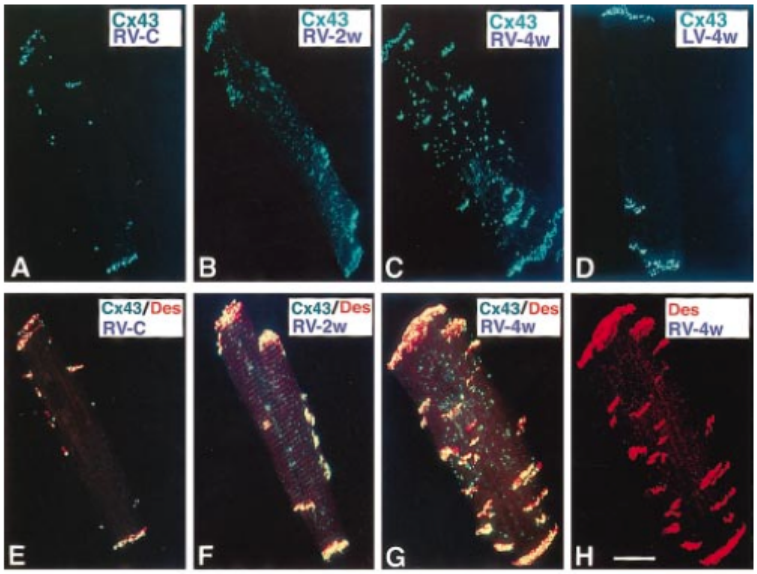

FIGURE 3.4. Localization of gap junctions and desmosomes in isolated ventricular myocytes, labeled for Cx43 (green) (A - D) and desmoplakin (red) (H) and double-labeled for Cx43 (green) and desmoplakin (red) (E - G), quoted from Figure 3 of [Uzzaman et al., 2000]. (A, E)Right ventricular myocytes under control. (B, F) Right ventricular myocytes from monocrotaline (MCT) – treated rats 2 weeks after injection, (C, G, H) 4 weeks after injection. (D) Left ventricular myocytes from MCT – treated rat 4 weeks after injection.

failure were significantly prolonged compared with control. Figure 3.3(B) is relationship between cycle length (CL) and APD at 90% of repolarization. APD_{90} in failing myocytes was significantly increased compared with control at all studied cycle length. It is known that APD prolongation is occurred inhomogeneously at each part of ventricle. That is to say, difference between individual characteristics of each cell which had potentially would become large.

On the other hand, it has been reported that a change would occur in the gap junction which connects electrically and metabolically between cardiac cells [Uzzaman et al., 2000]. Gap junctions are composed of transmembrane proteins that belong to the connexin family. The principal gap junctional protein expressed in the ventricles of mammalian heart is connexin43 (Cx43) [Gros and Jongsma, 1996]. In the earlier stage of enlargement, in general, protein expression of gap junction increases temporally as shown in Figure 3.4B and F. After that, in the advanced stage, i.e., when degree of enlargement became large, and cardiac failure develops, protein expression will decrease. Interestingly, it was indicated, as shown in Figure 3.4C and G, that the array of gap junction changed, furthermore, dissociation from intercalated disc which is in the edge of long axis of cell could be occurred.

In the cardiac muscle such as excitability being reduced, decrease of connection between cells by decrease of gap junction would be a cause of local conduction delay and disruption.

From these previous study, we propose that a cause of spontaneous spiral formation could be induced by heterogeneity of property of each cell or of connection between cells. In order to uncover the essence of spiral reentry expression dealing with one of the behavior of an excitable medium, we focused on a purely chemical system, Belousov-Zhabotinsky reaction, which can reproduce the properties of an excitable medium. For simplify, we consider the heart in two dimension, then investigate using experiments and numerical calculations on wave behavior in inhomogeneous excitable media.

First, the previous study about BZ reaction are covered in the next section. Then, I will introduce the heterogeneity of reaction term, and explain our experiments with photosensitive BZ reaction and a mathematical model of the Oregonator model in section 3.2. Next, in section 3.3, I would mention the second experiments with catalyst-loaded resin beads to realize the heterogeneity of diffusion term. I would discuss in section 3.4 the mechanism of forming spiral waves, and the difference between heterogeneities of reaction and diffusion. Compared the results of our experiments and numerical simulations with the results of numerical calculation using discretized FitzHugh-Nagumo model [Kinoshita et al., 2013], I would investigate an universal sole mechanism of spiral formation regardless of the method of introducing heterogeneities. Furthermore, we would describe a proposed idea based on [Kinoshita et al., 2013] to vanish spiral waves which had generated in heterogeneous excitable media. It would be a clue for prevent from cardiac ventricular fibrillation. Finally, I would summarize this study and describe about future works in section 3.5.

3.1. Introduction: Belousov-Zhabotinsky Reaction

Belousov-Zhabotinsky reaction is one of the oxidation-redox reaction, and is typical example of non-linear reaction. The reaction can indicate the three states, i.e., steady state, oscillatory state, and excitable state, depending on solution condition, and therefore is well-used as a model experiment of excitable media. However, there was long load to win over people's recognition about this reaction. Recent researchers have no problem with this reaction, thanks to a better understanding of non-linear reaction, conversely, about half a century ago, it was common knowledge that chemical reaction would always fall into an eventual equilibrium state. When observation did not fit with the conventional wisdom, we human beings tend to reject and can not believe it.

Now I summarize briefly the history of Belousov-Zhabotinsky reaction, quoting from "The prehistory of the Belousov-Zhabotinsky Oscillator" written by A.T. Winfree [Winfree, 1984] in 1984 and "A history of chemical oscillations and waves" written by A.M. Zhabotinsky [Zhabotinsky, 1991] in 1991. The story began in 1951. It was a little before 1955 that Ilya Prigogine showed that oscillations can exist in far-from-equilibrium systems [Prigogine and Balescu, 1955].

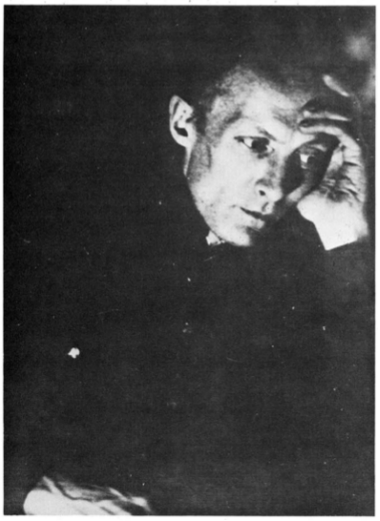

FIGURE 3.5. Photograph of B. P. Belousov at study prior to his discovery of the oscillating reaction (1930-1935), quoted from Figure 2 of [Winfree, 1984].

3.1.1. Temporal Oscillation in Belousov-Zhabotinsky Reaction. Boris Pavlovitch Belousov in Figure 3.5, who was chemist in Russia, had found when he was studying on metabolic (citric acid cycle) pathway of living creatures in 1951 that the color of solution which was reacted citric acid and bromate under cerium (IV) as a catalyst would change periodically between colorless and yellow.

It was started in 1950, when Belousov was 57 years old and the head of a laboratory of Biophysics of the Union of Soviet Socialist Republics (USSR) Ministry of Health. He was interested in biochemistry, and was endeavoring to model catalysis in the Krebs cycle using the metal ion cerium instead of the protein-bound metal ions common in the enzymes of living cells. In his test-tube, surprisingly, a solution of citric acid with bromate as oxidant and yellow ceric ions as catalyst, turned colorless and returned to yellow, and the periodic change repeated for about one hour (at room temperature) while effervescing carbon dioxide. Belousov undertook serious study of this peculiarity, and measured the effects of temperature and acidity on period of oscillation [*from his archives, dated 1951*, 1981]. It had been reported by him that the frequency of oscillations increased with rise of temperature [Belousov, 1959, 1985]. A.P. Safronov who was a colleague of Belousov had perfected the recipe and suggested phenanthroline Fe(II) (ferroin) as a redox indicator/catalyst. Despite their efforts, Belousov's manuscript of 1951 was rejected by the referees. The editor of the journal advised him that his "supposedly discovered discovery" was quite impossible. Belousov had gone back to his laboratory and tried to interpret the mechanism with more care. Although he submitted his comprehensive analysis six years later as a new and enlarged manuscript to another chemical journal, he faced skeptical attitude of the editor. After all, Belousov's manuscript appeared in the

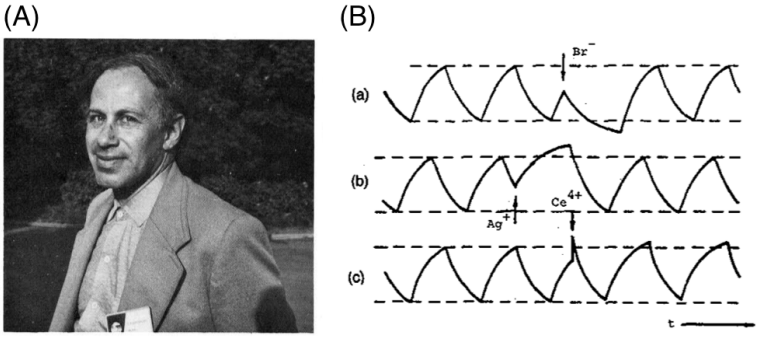

FIGURE 3.6. (A) Photograph of A.M. Zhabotinsky in July 1983, quoted from Figure 1 of [Winfree, 1984]. (B) Phase resetting in the BZ reacrion caused by pulse injection of Br^-, Ag^+, and Ce^{4+}, quoted from Figure 3 of [Zhabotinsky et al., 1991].

proceedings (in Russian) of a symposium on radiation medicine in 1958 [Belousov, 1959]. This abstract contains the recipe and sketchy conjectures about the mechanism, unfortunately without demonstration of the periodic reaction. The paper about this periodic subject had not been published even when he was 64 years old, then he withdrew.

Although Belousov's recipe of 1959 abstract had been circularized in the faculties of Biophysics and Physics at Moscow State University and of the Biophysics Institute of the USSR Academy of Sciences in Puschino, it seems that no one knew where the recipe came from, even Zhabotinsky.

At the end of 1961, Anatol M. Zhabotinsky (Figure 3.6(A)) who was a graduate student of biochemistry at Moscow State University began to do experiment with a citric acid recipe of unknown origin. In the spring of 1962 he sent draft of a manuscript to Belousov, then received reply from Belousov with the development of his original work, enclosing an unpublished manuscript and citation [Belousov, 1959]. Zhabotinsky had investigated vigorously, and reported that similar reaction occurs with malonic acid (MA) instead of citric acid [Zhabotinsky, 1964b] and manganese ions as catalyst [Zhabotinsky, 1964a]. He also has confirmed Br^- is a inhibitor of the autocatalytic oxidation of Ce^{3+} [Vavilin et al., 1973; Zhabotinsky et al., 1991] as shown in Figure 3.6(B), because of its rapid reaction with the autocatalyst $HBrO_2$ [Zhabotinsky, 1964a,b] Moreover he spread the recipe with complex iron ions α,α'-dipyridyl and 1,10-phenanthroline as a catalyst and indicated that complex ions of ruthemium $Ru(phen)_3^{3+}$ and $Ru(dyp)_3^{3+}$ can be used as a catalyst for the autooscillating reaction because those ions have redox potentials similar to those of complex iron ions [Vavilin et al., 1969]. Meanwhile Belousov and Zhabotinsky exchanged letters and talked by phone with progress and advices of the research, they never met. Then, Belousov had died 12 June 1970.

The reaction consists of two main parts, the autocatalytic oxidation of cerous ions Ce^{3+} by bromate and the reduction of ceric ions Ce^{4+} by malonic acid. An oscillatory cycle of the reaction can be described in the following

way [Zhabotinsky, 1964a]. When ceric ion concentration $[Ce^{4+}]$ is sufficiently high, bromide ion will be produced rapidly, and its concentration $[Br^-]$ will also be high. As a result, autocatalytic oxidation is completely inhibited, and the concentration of ceric ion $[Ce^{4+}]$ decreases with reduction of malonic acid. In parallel, the concentration of bromide ions $[Br^-]$ decreases. When the concentration of ceric ions $[Ce^{4+}]$ drops below a lower threshold value, the concentration of bromide ions $[Br^-]$ drops steeply, and the concentration of ceric ions $[Ce^{4+}]$ will increase with beginning rapid autocatalytic oxidation reaction. Finally reaching an upper threshold of the concentration of ceric ions $[Ce^{4+}]$, the concentration of bromide ions $[Br^-]$ increases sharply, and the autocatalytic oxidation reaction is inhibited. Such a cycle is repeated in this reaction.

3.1.2. Spatial Patterns in Belousov–Zhabotinsky Reaction. The Zhabotinsky's achievement had this reaction spread only in Russia, at least ten papers had been published in Russian about this oscillating reaction before the first in English. This reaction became widely known to people other than Russia at the summer 1968 Symposium on Biological and Biochemical Oscillators in Prague, attended by Zhabotinsky and colleagues, but not Belousov. The name "Zhahotinsky reaction" became common in the Western literature, changing to "Belousov-Zhabotinsky" only in recent years.

The most important exploit of Zhabotinsky was to show oscillation in visible ways as spatial patterns. The wave propagation was able to study in two-demensional systems by the introduction of the iron-phenanthroline complex (ferroin) as a catalyst [Vavilin et al., 1969]. Using a thin layer of unstirred solution with the ferroin-catalyzed BZ reaction, Zaikin and Zhabotinsky [Zaikin and Zhabotinsky, 1970] observed periodic propagation of concentric chemical waves generated by point pacemakers. Visualization of the oscillation made BZ reaction spread rapidly.

In two-dimensional field, there are two typical patterns; target pattern as shown in Figure 3.7(a) is concentric ring pattern, and spiral pattern as shown in Figure 3.7(b) forms helix. Because of using a thin layer of unstirred solution, there occur perturbations such as surface and convection

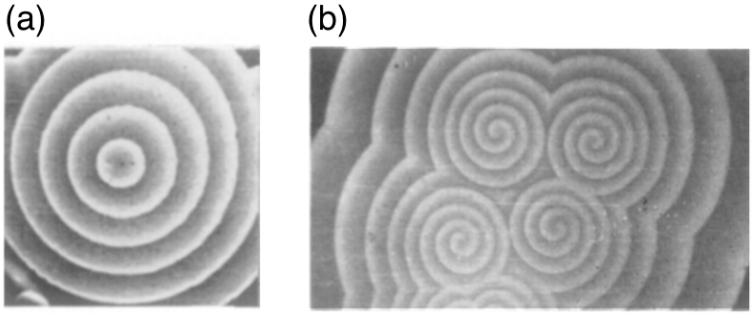

FIGURE 3.7. Two dimensional patterns observed in BZ reaction, (a) target pattern, and (b) spiral pattern, quoted from PLATE I and II of [Zhabotinsky and Zaikin, 1973], respectively.

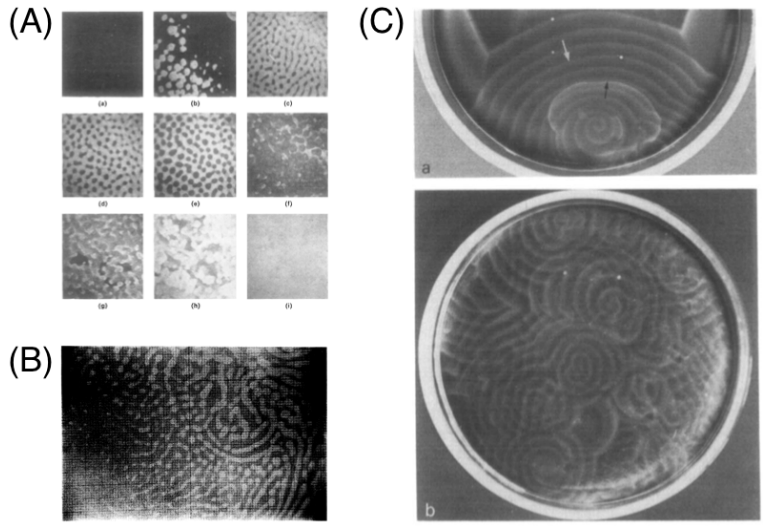

FIGURE 3.8. Complex patterns in two dimensional BZ reaction. (A) Small-cell structure (SPS) quoted from PLATE III of [Zhabotinsky and Zaikin, 1973]. A series of photographs taken at two-minute intervals, the catalyst transited from (a) reduced to (i) oxidized. (B) The patterned oxidation transition at 33.75 min after mixing, quoted from Figure 1 of [Showalter, 1980]. (C) Independent propagation of top (black arrow) and bottom (white) waves about (a) 10 min and (b) 40 min after the start of the experiment, quoted from Figure 2 of [Zhabotinsky et al., 1991].

flows, and production of carbon dioxide bubbles, so that the wave patterns often are formed complexly, i.e., mosaic pattern [Zhabotinsky and Zaikin, 1973; Showalter, 1980] as shown in Figure 3.8(A) and (B), and the pattern as a result of the interaction between top and bottom chemical wave patterns [Zhabotinsky et al., 1991] as shown in Figure 3.8(C). A quantitative study of chemical waves in BZ reaction had also been reported [Wood and Ross, 1985]. It had found that the wave velocity decreases with increasing the initial concentration of ferroin as shown in Figure 3.9(a), conversely, is linear with respect to a function of initial concentration of sulfuric acid and sodium bromate as shown in Figure 3.9(b). The dependence of wave velocity on temperature has been measured as shown in Figure 3.9(c).

On the other hand, the core mechanism of BZ reaction had been elucidated by several authors [Zhabotinsky, 1964a; Vavilin and Zaikin, 1971; Filed et al., 1972]. Especially, the mechanism reported by Field et al. [Filed et al., 1972] is still widely used today, and called "FKN mechanism" named by initials of authors. In section 3.1.4, FKN mechanism will be introduced in detail. The FKN mechanism helped us to understand BZ reaction using mathematical models of chemical kinetics. In 1973, A.M. Zhabotinsky and A.N. Zaikin [Zhabotinsky and Zaikin, 1973] had reported that this oscillatory phenomenon can be understood by a reaction-diffusion equation.

R.J. Field and R.M. Noyes [Field and Noyes, 1974], in next year, had proposed a model of a real chemical reaction with cerium catalyst, subsequently the model became to be called "Oregonator model". Details about Oregonator model will be mentioned in section 3.1.4. A.B. Rovinsky and A.M. Zhabotinsky [Rovinsky and Zhabotinsky, 1984] had suggested a mathematical model of the oscillating bromate-ferroin-bromomalonic acid reaction in 1984, called afterward "Rovinsky-Zhabotinsky model". It will be shown in detail in section 3.1.5. As the most simplified model, cellular automaton (CA) model also had been studied in the field of BZ reaction [Kapral, 1991]. The simple model can be describe the process of generating target pattern and spiral pattern easily, although the model does not consider the details of chemical reaction. The emergence of mathematical model had been made a great deal of progress in understanding of the chemical reaction.

In experimental study, immobilized-catalyst BZ reaction using a thin film as shown in Figure 3.10(a) or beads as shown in Figure 3.10(b) of ferroin-loaded cation-exchange resin had been researched with the object of observing essential behavior of chemical waves [Maselko et al., 1989]. The movement of tip in the spiral pattern formation was examined in detail, as shown in Figure 3.11. First it was indicated by Oregonator model that the patterns of tip movement depend on not physical flow but chemical recipe parameters [Jahnke et al., 1989]. Based on the results of Oregonator model in Figure 3.11(A), the orbit of spiral tip motion in both ferroin [Skinner and Swinney, 1991] (B) and ruthenium bipyridyl [Braune and Engel, 1993] (C) catalyst BZ reaction had been studied.

Additionally, the reaction with cation-exchange resin beads was a cue for considering a reaction in an inhomogeneous reaction field. When the size of beads is small, target and spiral patterns were formed similar to the homogenous film [Maselko and Showalter, 1991], as shown in Figure 3.12(A). Thereafter, various situations of inhomogeneous reaction field were studied with changing the beads size. In the next section, I introduce the feature of BZ reaction in inhomogeneous reaction field.

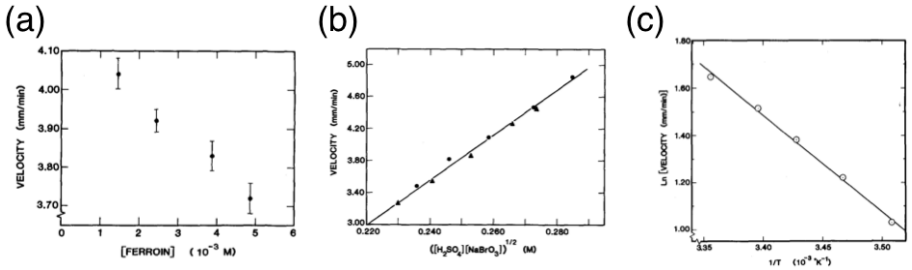

FIGURE 3.9. Plot of wave velocity v.s. (a) initial ferroin concentration, (b) square root of product of initial concentrations of sulfuric acid and sodium bromate. (c) Variation of wave velocity as a function of temperature which was varied five times over a range from 11.9 to 24.8 °C. These figures were quoted from Figure 5, 6, and 11 of [Wood and Ross, 1985], respectively.

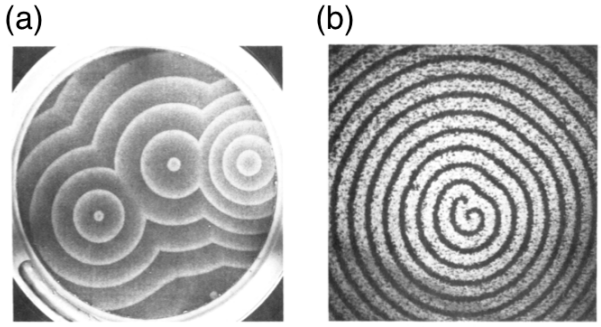

FIGURE 3.10. Chemical waves moving through (a) thin film and (b) beads of ferroin-loaded cation-exchange resin covered with layer of reactant solution, quoted from Figure 1 and 4 of [Maselko et al., 1989], respectively.

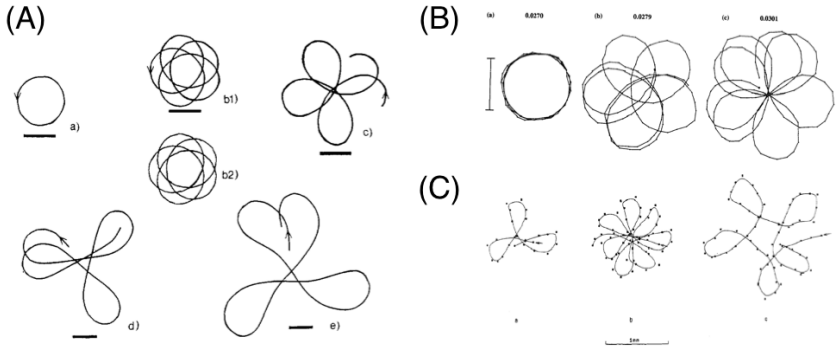

FIGURE 3.11. Spiral tip orbits, obtained from (A) Oregonator model quoted from Figure 4 of [Jahnke et al., 1989], (B) experiment with ferroin-catalyst BZ reaction quoted from Figure 6 of [Skinner and Swinney, 1991], and (C) experiment with ruthenium-catalyst BZ reaction quoted from Figure 3 of [Braune and Engel, 1993]. The tip orbits depend on (B) the potassium bromate concentrations and (C) the light intensity, respectively.

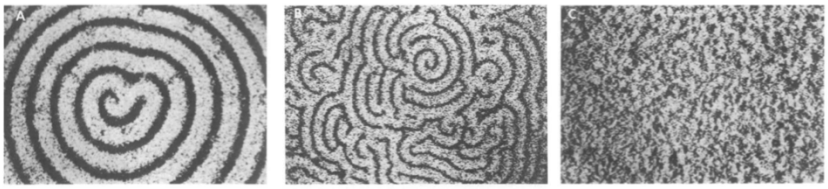

FIGURE 3.12. Difference images of (A) spiral pattern using beads of 38-75 μm diameter, (B) pattern containing closely packed spirals using beads of 106-250 μm diameter, and (C) irregular pattern using beads of 180-425 μm diameter, quoted from Figure 2 of [Maselko and Showalter, 1991].

3.1.3. Chemical Waves on Inhomogeneous Excitable Media. Propagating waves are observed not only in chemical systems [Belousov, 1985; Kapral and Showalter, 1995; Scott, 1994] but also in living creatures [Murray, 1989; Winfree, 1987]. In nature, the system has most often heterogeneities and anisotropy, and these may play an important role in the behavior of biological media. Developments of the research on BZ reaction has enabled to study in inhomogeneous reaction field, then recently BZ reaction is used as a suitable model experiment to understand various phenomena occurred in nature.

Especially, spiral formation is one of the current interests in inhomogeneous systems. It is considered, in general, that spiral pattern in BZ system is formed as a result of an interaction between chemical waves, i.e., due to vulnerability [Starmer et al., 1992; Gesteira et al., 1994; Aliev, 1995]. Vulnerability had been confirmed first in the experimental approach of circus movement in rabbit atrial muscle [Allessie et al., 1973], then reported using FitzHugh-Nagumo model [Keener and Phelps, 1989]. The three classes of responses as following which were found typically in these experiments [Allessie et al., 1973; Keener and Phelps, 1989] had also reported in BZ reaction [Gesteira et al., 1994; Aliev, 1995]. Experimental condition: a conditioning stimulus was input at first, then a test stimulus is input varying a position.

(1) When a test stimulus was input at the place much longer than the restoration time (refractoriness), both pulses can initiate wavefronts that propagate in all directions (the right stimuli pulse of Figure 3.13A).
(2) When a test stimulus was input at the place shorter than the restoration time, the first pulse can initiate a propagating response, but the test pulse disappears (the left stimuli pulse of Figure 3.13A).
(3) When a test stimulus was input at the place slightly larger (several percent) than the restoration time, the test pulses can initiate a propagating response except the direction of the first pulse (the middle stimuli pulse of Figure 3.13A).

Initiating a train of responses by properly timed stimuli is called vulnerability (the middle stimuli pulse of Figure 3.13A) and the range of delays between the waves is called the vulnerable region [Gesteira et al., 1994; Aliev, 1995]. Keener et al. [Keener and Phelps, 1989] came to the conclusion that vulnerability is a characteristic of a discrete anisotropic cellular medium that the wave propagates unidirectionally, and it leads to a permanently rotating wave.

As just described, it had been widely believed that origin of spiral waves is the interaction of traveling waves initially induced physically or chemically, but spiral waves do not occur spontaneously in homogeneous media, despite of the evidence that spiral waves appear spontaneously without specific initial conditions in biological excitable media. Hence, the heterogeneity of an excitable medium has recently been suggested as a probable cause [Steinbock et al., 1995; Tinsley et al., 2011; Toth et al., 2009; Bub and Shrier, 2002; Bub et al., 2002b]. Spiral waves form spontaneously due to, for example, an obstacle [Agladze et al., 1994; Gomez-Gesteira et al., 1994], the

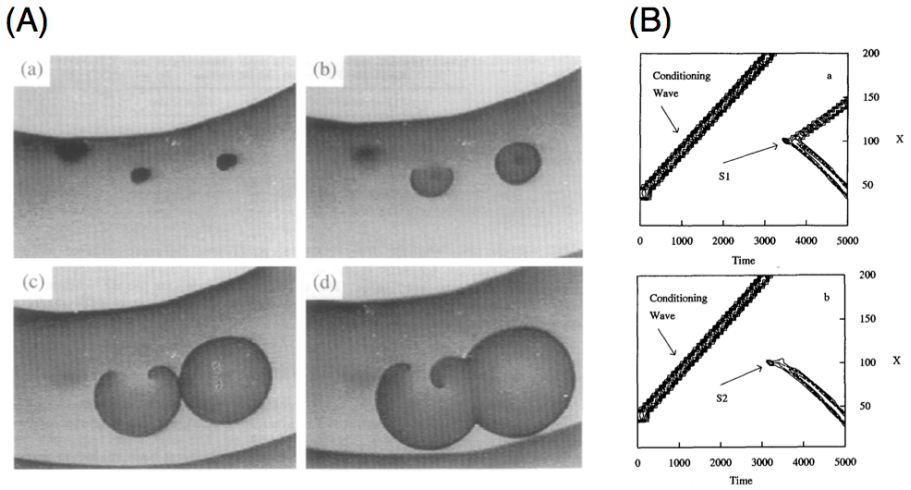

FIGURE 3.13. Vulnerability of waves (A) in 2D BZ reaction quoted from Figure 1 of [Aliev, 1995], and (B) in 1D Oregonator model quoted from Figure 2 of [Gesteira et al., 1994]. In both cases, if a stimuli point was placed in vulnerable region, the wavefront in the direction of preceding wave cannot propagate. In 2D reaction (A), hence, a tip of wave was formed and as a result, spiral formation occurred.

heterogeneity of the medium [Steinbock et al., 1995; Tinsley et al., 2011; Toth et al., 2009], the light intensity gradient in three-dimensional excitable media [Amemiya et al., 1996], and the unidirectional connection of reaction regions [Sendiña-Nadal et al., 2002].

K. Agladze et al. [Agladze et al., 1994] reported that the geometry of the medium necessary for generating a spiral wave spontaneously is sufficient sharpness of corner of the obstacle, and the supercritical frequency of incoming waves, in particular, studied the curvature effect on the propagation of waves in excitable media [Keener, 1991]. The wave velocity decreases with increasing of curvature of the front wave. Furthermore, the main effect of the obstacle is to break the wave into two waves. These waves may go around the obstacle and attach to another boundary as shown in Figure 3.14(B), or form two free ends as shown in Figure 3.14(C). M.G. Gesteira et al. [Gomez-Gesteira et al., 1994] also reported that spiral waves are generated in a BZ medium due to the presence of some inert obstacle. The conditions of generating a spiral have been investigated by varying the excitability and curvature, and discussed using the eikonal equation.

In heterogeneous excitable media which were generated by loading of the catalyst onto the polysulphone membranes with an ink jet printer, the wave propagation has been studied on various patterns as shown in Figure 3.15(A), then it has been reported that spiral waves may occur by the interaction of cells or clusters of cells with different oscillatory frequencies [Steinbock et al., 1995]. It has been also reported that spiral waves are generated spontaneously when a heterogeneous network such a checkerboard pattern is applied to the BZ reaction as shown in Figure 3.15(B) [Toth et al.,

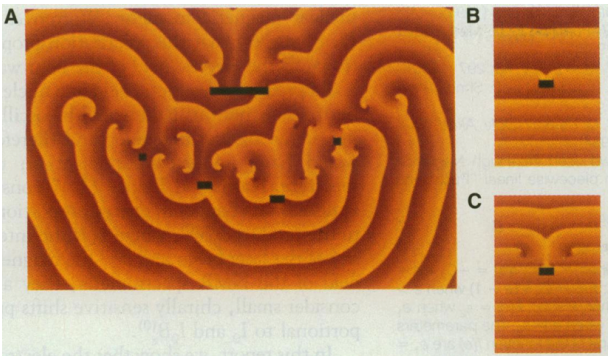

FIGURE 3.14. The wave patterns under high-frequency stimulation in an excitable medium with obstacles quoted from Figure 1 of [Agladze et al., 1994].

2009]. The experiments have been done using two method, the first is to input one wave, and the second is to input two waves varying the period. In the case of one wave, spiral wave was formed at a low network excitability and weakly excitable junctions. Conversely, in the case of two waves, at a high network excitability, stable wave, single spiral, double spirals, and multiple spirals were formed depending on the period. The wave behavior depends sensitively on network excitability, network size, and cell size. A mechanism of spiral formation was confirmed based on unidirectional failure of junctions.

An effect of heterogeneity in BZ system has also been studied using ion-exchange resin particles [Maselko et al., 1989; Maselko and Showalter, 1991; Taylor et al., 2009; Tinsley et al., 2009, 2011], and it has been reported that the complexity of the spatiotemporal patterns increase with increasing bromate concentration [Maselko et al., 1989; Maselko and Showalter, 1991]. The origin of complex behavior in heterogeneous media was explained by the effects of the initial excitability [Maselko and Showalter, 1991], heterogeneity of refractory period [Maselko and Showalter, 1991], and the presence of inactive particles [Wang et al., 2010] or permanently excited particles [Toth and Taylor, 2006]. M.R. Tinsley et al. [Tinsley et al., 2011] suggested using the system as shown in Figure 3.15(C) that heterogeneity of frequency is not an essential for the wave breaking mechanism, but rather the complex patterns occur primarily by heterogeneity of an initial phase, and the spatiotemporal pattern is driven by reentrant circuits placed in the media. Compared with the case of low concentration of bromate, the phase difference is large in the case of high concentration, hence the spiral tip can be formed easily.

Heterogeneity and anisotropy are always in nature. It would be reasonable that such as inhomogeneity has a role for generating spiral spontaneously. What is the mechanism of forming spontaneous spiral pattern?

The topic of this study is the BZ reaction in heterogeneous reaction filed, therefore, we have to deal with complex phenomena. A mathematical model, obviously, is important for understanding a complex phenomenon. Before entering upon a discussion of specific theme, I will describe in the next section about the FKN mechanism [Filed et al., 1972] which elicited essential

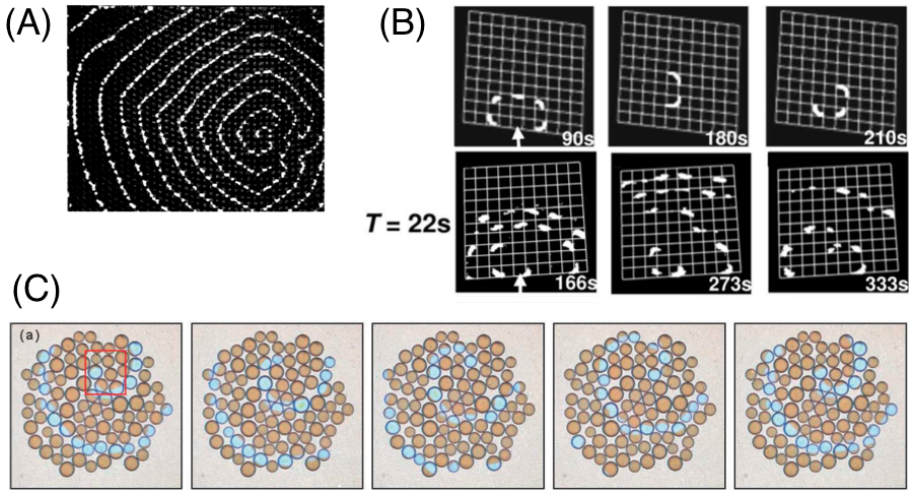

FIGURE 3.15. BZ reaction in inhomogeneous reaction field. (A) Propagating waves with cellular inhomogeneities loading the catalyst onto the membranes with an ink jet printer, quoted from Figure 1B of [Steinbock et al., 1995]. (B) Spiral formation resulting from (top) one wave, or (bottom) two waves input to the checkerboard network quoted from Figure 1(a) and (d) of [Toth et al., 2009]. (C) Typical spiral pattern observed at a low concentration of bromate using catalyst particles quoted from Figure 1(a) of [Tinsley et al., 2011].

process from BZ reaction, and introduce derivations and features of the Oregonator model [Field and Noyes, 1974] and the Rovinsky-Zhabotinsky model [Rovinsky and Zhabotinsky, 1984] which are often used as a model of BZ reaction.

3.1.4. FKN Mechanism and Oregonator Model. The essential mechanism of the BZ reaction are now well understood [Noyes et al., 1972; Filed et al., 1972], and a simplified model, Oregonator, based on five irreversible steps has been developed [Field and Noyes, 1974, 1975; Edelson et al., 1979].

Field, Körös, and Noyes [Filed et al., 1972] studied the temporal oscillations in the Bromate-Cerium-Malonic acid system, observed by earlier researches [Zhabotinsky, 1964b,a], by illustrating the potentiometric behavior of a stirred solution as shown in Figure 3.16. The upper and lower curves in Figure 3.16 recorded the ratio of ceric/cerous ion, ln [Ce(IV)]/[Ce(III)], and bromide ion, ln [Br^-], respectively. According to [Filed et al., 1972], the potentiometric traces in Figure 3.16 can be resolved into six periods, AB ("Bray period"), CD ("induction period"), EF ("slow bromide consumption periods"), FG/BC ("rapid bromide consumption periods"), GH ("slow bromide production periods"), and HE/DE ("rapid bromide production periods").

Field et al. [Noyes et al., 1972; Filed et al., 1972] had carefully considered each period of oscillating behavior, eventually, proposed that the mechanism

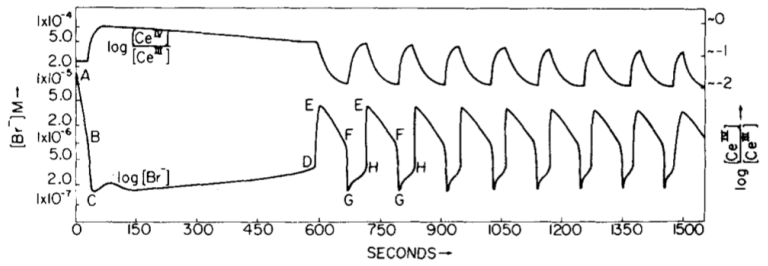

FIGURE 3.16. Potentiometric traces at room temperature of ln $[Br^-]$ and ln [Ce(IV)]/[Ce(III)], quoted from Figure 1 of [Filed et al., 1972].

of oscillating reaction can be described by the following ten component processes.

$$\text{(R1)} \qquad HOBr + Br^- + H^+ \rightleftarrows Br_2 + H_2O$$

$$\text{(R2)} \qquad HBrO_2 + Br^- + H^+ \rightarrow 2HOBr$$

$$\text{(R3)} \qquad BrO_3{}^- + Br^- + 2H^+ \rightarrow HBrO_2 + HOBr$$

$$\text{(R4)} \qquad 2HBrO_2 \rightarrow BrO_3^- + HOBr + H^+$$

$$\text{(R5)} \qquad BrO_3^- + HBrO_2 + H^+ \rightleftarrows 2BrO_2\cdot + H_2O$$

$$\text{(R6)} \qquad BrO_2\cdot + Ce^{3+} + H^+ \rightleftarrows HBrO_2 + Ce^{4+}$$

$$\text{(R7)} \qquad BrO_2\cdot + Ce^{4+} + H_2O \rightarrow BrO_3^- + Ce^{3+} + 2H^+$$

$$\text{(R8)} \qquad Br_2 + CH_2(COOH)_2 \rightarrow BrCH(COOH)_2 + Br^- + H^+$$

$$\text{(R9)} \qquad 6Ce^{4+} + CH_2(COOH)_2 + 2H_2O \rightarrow 6Ce^{3+} + HCOOH + 2CO_2 + 6H^+$$

$$\text{(R10)} \qquad 4Ce^{4+} + BrCH(COOH)_2 + 2H_2O \rightarrow Br^- + 4Ce^{3+} + HCOOH + 2CO_2 + 5H^+$$

These oscillating mechanism today is called "FKN mechanism" derived from the name of the authors, Field, Körös, and Noyes. Figure 3.17 is the outline drawing for the processes of the FKN mechanism. The principle

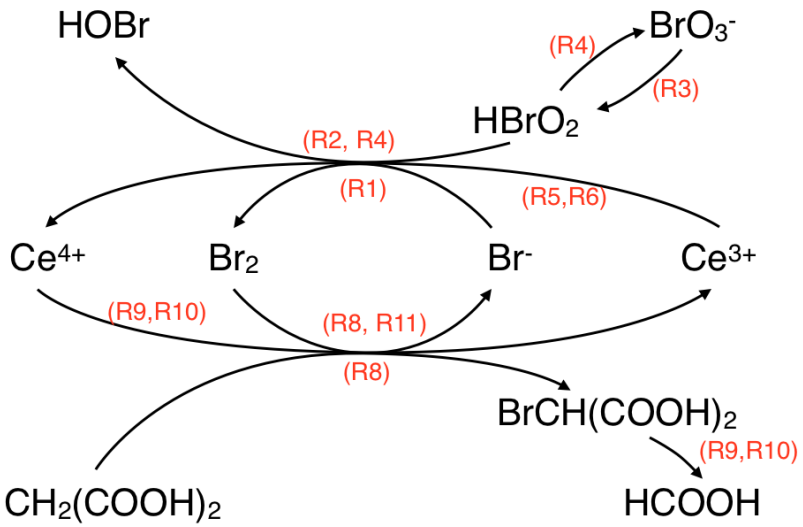

FIGURE 3.17. The processes in oscillatory BZ reaction of FKN mechanism.

overall reaction is written as a bromination of malonic acid by adding the chemical equations (R1)×5, (R2), (R3), (R4)×2, (R5)×4, (R6)×8, (R8)×5, and (R10)×2,

$$3BrO_3^- + 5CH_2(COOH)_2 + 3H^+ \rightarrow 3BrCH(COOH)_2 + 2HCOOH + 4CO_2 + 5H_2O$$

The FKN mechanism for the oscillatory Belousov-Zhabotinsky reaction has been generalized by a model composed of five essential steps, (R3), (R2), (R5)+2(R6), (R4), and (R10), involving three processes by Field and Noyes [Field and Noyes, 1974].

(R3) $BrO_3^- + Br^- + 2H^+ \rightarrow HBrO_2 + HOBr$

(R2) $HBrO_2 + Br^- + H^+ \rightarrow 2HOBr$

(R5)+2(R6)
$BrO_3^- + HBrO_2 + 2Ce^{3+} + 3H^+ \rightarrow 2HBrO_2 + 2Ce^{4+} + H_2O$

(R4) $2HBrO_2 \rightarrow BrO_3^- + HOBr + H^+$

(R10) $BrCH(COOH)_2 + 4Ce^{4+} + 2H_2O \rightarrow 4Ce^{3+} + Br^- + HCOOH + 2CO_2 + 5H^+$

TABLE 3.1. Oregonator scheme [Field and Noyes, 1974; Tyson and Fife, 1980; Keener and Tyson, 1986]

	Reaction	Rate
(O1)	A + Y $\rightarrow$ X + P	k_1
(O2)	X+Y $\rightarrow$ 2P	k_2
(O3)	A + X $\rightarrow$ 2X + 2Z	k_3
(O4)	2X $\rightarrow$ A +P	k_4
(O5)	B+Z $\rightarrow \frac{1}{2}f$Y	k_5

Furthermore, the Oregonator model has been proposed by [Field and Noyes, 1974] as shown in Table 3.1 using the above five chemical equations of the FKN mechanism. Let A = BrO_3^-, B = $BrCH(COOH)_2$, P = HOBr, X = $HBrO_2$, Y = Br^-, and Z = Ce^{4+}, respectively. Invariable numbers k_1, k_2, k_3, k_4, and k_5 are rate constants, and f is a stoichiometric parameter.

If the concentrations of A and B are assumed to be constant, the kinetic behavior of the Oregonator can be described by the following differential equations,

$$\frac{dx}{dt} = k_1 ay - k_2 xy + k_3 ax - 2k_4 x^2, \tag{3.1.1}$$

$$\frac{dy}{dt} = -k_1 ay - k_2 xy + \frac{1}{2} f k_5 bz, \tag{3.1.2}$$

$$\frac{dz}{dt} = 2k_3 ax - k_5 bz, \tag{3.1.3}$$

where [A] = a, [B] = b, [X] = x, [Y] = y, and [Z] = z. Now, we introduce to transfer dimensionless quantities using the method of Tyson and Fife [Tyson and Fife, 1980]. Let $u = x/x_0$, $v = y/y_0$, $w = z/z_0$, and $\tau = t/t_0$, where u, v, and w mean the dimensionless concentrations, and τ means the dimensionless time, respectively.

$$\frac{du}{d\tau} = \frac{k_1 a y_0 t_0}{x_0} v - k_2 y_0 t_0 uv + k_3 a t_0 u - 2k_4 x_0 t_0 u^2, \tag{3.1.4}$$

$$\frac{dv}{d\tau} = -k_1 a t_0 v - k_2 x_0 t_0 uv + \frac{k_5 b f t_0 z_0}{2y_0} w, \tag{3.1.5}$$

$$\frac{dw}{d\tau} = \frac{2k_3 a x_0 t_0}{z_0} u - k_5 b t_0 w, \tag{3.1.6}$$

let the typical numbers t_0, x_0, y_0, and z_0 as follows,

$$t_0 = \frac{1}{k_5 b}, \qquad x_0 = \frac{k_3 a}{2k_4}, \qquad y_0 = \frac{k_3 a}{k_2}, \qquad z_0 = \frac{(k_3 a)^2}{k_4 k_5 b}.$$

Hence, we can obtain the following simple equations by redescribing (3.1.4), (3.1.5), and (3.1.6).

$$\epsilon \frac{du}{d\tau} = qv - uv + u(1-u), \tag{3.1.7}$$

$$\delta \frac{dv}{d\tau} = -qv - uv + fw, \tag{3.1.8}$$

$$\frac{dw}{d\tau} = u - w, \tag{3.1.9}$$

let ϵ, δ, and q as follows,

$$\epsilon = \frac{k_5 b}{k_3 a}, \qquad q = \frac{2k_1 k_4}{k_2 k_3}, \qquad \delta = \frac{2k_4 k_5 b}{k_2 k_3 a}.$$

According to [Tyson and Fife, 1980], the parameters in the case of oscillatory behavior can be estimated by rate constants for the steps (R1)-(R10),

$$\delta \ll \epsilon \ll 1, \qquad q \ll 1, \qquad f \cong 1.$$

The differential equations (3.1.7), (3.1.8), and (3.1.9) are well-used as three-variable Oregonator model. Since v changes on the fastest time scale compared with the reaction scale of u and w, we can assume that the equation (3.1.8) always satisfies $dv/d\tau \approx 0$. Therefore v is determined by u and w according to

$$v \approx \frac{fw}{(q+u)}. \tag{3.1.10}$$

Substituting (3.1.10) into the equation (3.1.7), we can obtain the two-variable Oregonator model with respect to u and w.

$$\epsilon \frac{du}{d\tau} = u(1-u) - fw\frac{u-q}{u+q}, \tag{3.1.11}$$

$$\frac{dw}{d\tau} = u - w, \tag{3.1.12}$$

The two-variable Oregonator model are well-used as a model described the behavior of BZ reaction simply as well as the three-variable one. Keener-Tyson model [Keener and Tyson, 1986] which is reaction-diffusion equations as follows is also well-used in an analysis of wave behavior in two dimensional BZ reaction.

$$\epsilon \frac{\partial u}{\partial t} = \epsilon^2 \nabla^2 u + u - u^2 - fw\frac{u-q}{u+q}, \tag{3.1.13}$$

$$\frac{\partial w}{\partial t} = \epsilon \nabla^2 w + u - w. \tag{3.1.14}$$

3.1.5. Rovinsky-Zhabotinsky Model. Although most of the BZ reaction studies have been investigated using bromate-ferroin-bromomalonic (malonic) acid system from the view point of visualization, the analysis of the mechanism and the mathematical modeling had been performed almost entirely to cerium-catalyzed systems. Using the system of bromate-ferroin-bromomalonic (malonic) acid, the solution is colored red by $Fe(II)(phen)_3^{2+}$ as shown in Figure 3.18(a) in the reduced state, and the one is blue by $Fe(III)(phen)_3^{3+}$ as shown in Figure 3.18(b) in the oxidized state. The color of the solution in Figure 3.18(c) is the case of transition state from blue to red as the medium slowly recovers its reduced state. It is said that there are main two differences of oscillations between the ferroin-catalyzed system and the cerium system. The first is redox potentials of the $Fe(phen)_3^{2+}/Fe(phen)_3^{3+}$ and of the Ce^{3+}/Ce^{4+}, and the second is the presence of ligands in ferroin related to oxidation-reduction process [Rovinsky and Zhabotinsky, 1984].

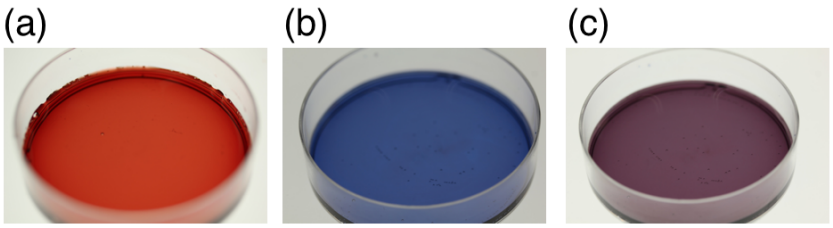

FIGURE 3.18. Temporal oscillation in stirred ferroin-catalyzed BZ reaction. (a) reduction state, (b) oxidation state, and (c) transition state from blue to red, which includes refractory state.

Rovinsky and Zhabotinsky [Rovinsky and Zhabotinsky, 1984] has proposed a mechanism of the oscillatory reaction of the ferroin-catalysed system modified the FKN scheme.

The eleven components are proposed for ferroin-catalyzed system, i.e., the components (R1), (R2), (R3), (R4), and the followings:

$$\text{(F1)} \qquad \mathrm{HBrO_3 + HBrO_2 + H^+ \rightleftarrows HBrO_2^+ + BrO_2\cdot + H_2O}$$

$$\text{(F2)} \qquad \mathrm{BrO_2\cdot + H^+ \rightleftarrows HBrO_2^+}$$

$$\text{(F3)} \qquad \mathrm{Fe(phen)_3^{2+} + HBrO_2^+ \rightleftarrows Fe(phen)_3^{3+} + HBrO_2}$$

$$\text{(F4)} \qquad \mathrm{Fe(phen)_3^{3+} + CHBr(COOH)_2 \rightleftarrows Fe(phen)_2^{2+} + H^+ + \cdot CBr(COOH)_2}$$

$$\text{(F5)} \qquad \mathrm{H_2O + \cdot CBr(COOH)_2 \rightleftarrows H^+ + Br^- + \cdot COH(COOH)_2}$$

$$\text{(F6)} \qquad \mathrm{HOBr + CHBr(COOH)_2 \rightleftarrows CBr_2(COOH)_2 + H_2O}$$

$$\text{(F7)} \qquad \mathrm{Br_2 + CHBr(COOH)_2 \rightleftarrows CBr_2(COOH)_2 + H^+ + Br^-}$$

It is assumed that HOBr and Br_2 are rapidly removed through the step (R1), (F6), and (F7), hence the following seven steps were captured as a essential processes,

$$\text{(F1)+(F2)} \qquad \mathrm{HBrO_3 + HBrO_2 + 2H^+ \rightleftarrows 2HBrO_2^+ + H_2O}$$

$$\text{(F3)} \qquad \mathrm{Fe(phen)_3^{2+} + HBrO_2^+ \rightleftarrows Fe(phen)_3^{3+} + HBrO_2}$$

$$\text{(R4)} \qquad \mathrm{2HBrO_2 \rightarrow BrO_3^- + HOBr + H^+}$$

$$\text{(R2)} \qquad \mathrm{HBrO_2 + Br^- + H^+ \rightarrow 2HOBr}$$

$$\text{(R3)} \qquad \mathrm{BrO_3^- + Br^- + 2H^+ \rightarrow HBrO_2 + HOBr}$$

$$\text{(F4)} \qquad \mathrm{Fe(phen)_3^{3+} + CHBr(COOH)_2 \rightleftarrows Fe(phen)_2^{2+} + H^+ + \cdot CBr(COOH)_2}$$

TABLE 3.2. Rovinsky-Zhabotinsky scheme [Rovinsky and Zhabotinsky, 1984; Rovinsky, 1986]

	Reaction	Rate
(RZ1)	A + X $\rightleftarrows$ 2U	$K_{\pm 1}$
(RZ2)	C+U $\rightleftarrows$ Z+X	$K_{\pm 2}$
(RZ3)	2X $\rightarrow$ A +D	K_3
(RZ4)	Y+X $\rightarrow$ 2D	K_4
(RZ5)	Y+A$\rightarrow$ X+D	K_5
(RZ6)	Z+B$\rightleftarrows$ C+R	$K_{\pm 6}$
(RZ7)	R$\rightarrow$ Y	K_7

(F5) $$H_2O + \cdot CBr(COOH)_2 \rightarrow H^+ + Br^- + \cdot COH(COOH)_2$$

These components can be rewritten by letting X=$HBrO_2$, Y = Br^-, Z = $Fe(phen_3^{3+})$, U = $HBrO_2^+$, R = $\cdot$ $CBr(COOH)_2$, A = $HBrO_3$, B = $CHBr(COOH)_2$, C = $Fe(phen)_3^{2+}$, and D = HOBr as shown in Table 3.2.

Let h_0 is the acidity function, and q is the stoichiometric factor, the following system of equations can be obtained:

$$\begin{aligned}\frac{dx}{dt} &= -K_1h_0ax + K_{-1}u^2 + K_2(c-z)u \\ &\quad -K_{-2}xz - 2K_3h_0x^2 - K_4h_0xy + K_5h_0ay,\end{aligned} \tag{3.1.15}$$

$$\frac{dy}{dt} = -K_4h_0xy - K_5h_0ay + qK_7r, \tag{3.1.16}$$

$$\frac{dz}{dt} = K_2(c-z)u - K_{-2}xz - K_6bz + K_{-6}h_0(c-z)r, \tag{3.1.17}$$

$$\frac{du}{dt} = 2K_1h_0ax - 2K_{-1}u^2 - K_2(c-z)u + K_{-2}xz \tag{3.1.18}$$

$$\frac{dr}{dt} = K_6 bz - K_{-6} h_0 (c - z) r - K_7 r \tag{3.1.19}$$

where [A] = a, [B] = b, [C] + [Z] = c, [X] = x, [Y] = y, [Z] = z, [U] = u, and [R] = r.

Now, the variable u is small and consequently rapid unless $1-(z/c) \ll 1$, and the process related to the variable r is also rapid. Therefore the above equations can be reduced to the x, y, and z variables by $du/dt = 0$ and $dr/dt = 0$. In addition, the term $K_{-1}u^2$ can be omitted and the term K_7 can be neglected as compared with $K_{-6}h_0c$. Hence, we can obtain the following equations,

$$\frac{dx}{dt} = K_1 h_0 ax - 2K_3 h_0 x^2 - K_4 h_0 xy + K_5 h_0 ay, \tag{3.1.20}$$

$$\frac{dy}{dt} = -K_4 h_0 xy - K_5 h_0 ay + q\frac{K_6 K_7}{K_{-6}} \frac{bz}{h_0(c-z)}, \tag{3.1.21}$$

$$\frac{dz}{dt} = 2K_1 h_0 ax - \frac{K_6 K_7}{K_{-6}} \frac{bz}{h_0(c-z)}, \tag{3.1.22}$$

Since y changes on the fastest time scale compared with the reaction scale of x and z, we can assume that the equation (3.1.21) always satisfies $dy/dt \approx 0$. Let $u = x/x_0$, $w = z/z_0$, and $\tau = t/t_0$, where u and w mean the dimensionless concentrations, and τ means the dimensionless time, respectively,

(3.1.23)
$$\frac{du}{d\tau} = K_1 a h_0 t_0 u - 2K_3 h_0 x_0 t_0 u^2 + \frac{(K_5 a - K_4 x_0 u)}{(K_5 a + K_4 x_0 u)} \frac{q t_0 K_6 K_7}{x_0 K_{-6}} \frac{b z_0 w}{h_0 (c - z_0 w)},$$

$$\frac{dw}{d\tau} = \frac{2K_1 a h_0 x_0 t_0}{z_0} u - \frac{K_6 K_7}{K_{-6}} \frac{b t_0}{h_0 (c - z_0 w)} w, \tag{3.1.24}$$

let the typical numbers t_0, x_0, and z_0 as follows,

$$t_0 = \frac{K_3 c}{K_1^2 a^2 h_0}, \qquad x_0 = \frac{K_1 a}{2K_3}, \qquad z_0 = c.$$

Finally, we can obtain the following simple equations by redescribing (3.1.23), (3.1.24).

$$\epsilon \frac{du}{d\tau} = u(1-u) - 2q\alpha \frac{w}{1-w} \frac{u-\mu}{u+\mu}, \tag{3.1.25}$$

$$\frac{dw}{d\tau} = u - \alpha \frac{w}{1-w}, \tag{3.1.26}$$

let ϵ, α, and μ as follows,

$$\epsilon = \frac{K_1 a}{K_3 c}, \qquad \alpha = \frac{K_3 K_6 K_7 b}{K_1^2 K_{-6} a^2 h_0^2}, \qquad \mu = \frac{2K_3 K_5}{K_1 K_4}.$$

This system is called the Rovinsky-Zhabotinsky model, and this model, similar to the Oregonator model, is well-used as a model which supports experimental results since the parameters of the model can be estimated by experimental condition.

Now let us turn to the main topic of this study. As described in earlier section, it would be reasonable that inhomogeneity has a role for generating spiral spontaneously. What is the sole mechanism of forming spontaneous spiral pattern?

In the research of cardiac cells, which has the serious matter of spiral re-entry, there are at least two types of heterogeneity, i.e., dead cells and anisotropy in array of gap junctions [Uzzaman et al., 2000]. From the aspect of reaction-diffusion systems, the former has heterogeneity in the reaction term, and the latter in the diffusion term. The heterogeneity in BZ reaction has been controllable factor by contributions of experimental development, in the reaction by heterogeneous catalyzed membranes [Steinbock et al., 1995; Toth et al., 2009] as well as in the diffusion by catalyst-loaded ion exchange beads [Maselko et al., 1989; Maselko and Showalter, 1991; Taylor et al., 2009; Tinsley et al., 2009, 2011]. It has been reported that a spiral pattern is generated under both heterogeneous conditions [Steinbock et al., 1995; Toth et al., 2009; Tinsley et al., 2011].

In addition to observations of a spiral pattern, it has pointed that unidirectional failure of selected junctions is important for the the mechanism of spontaneous spiral formation in heterogeneous reaction field [Toth et al., 2009]. Furthermore, three different types of wave behavior in heterogeneous excitable medium have been reported using cellular automata model: plane waves propagated without breaking up, plane waves were broken up into spiral waves, and plane waves were blocked [Bub et al., 2002b]. It has also reported by cellular automata model and FitzHugh-Nagumo model added heterogeneities that spiral form at a site of unidirectional block generated by asymmetric narrow, hence, unidirectional block is a necessary condition for beginning to form re-entrant patterns [Bub and Shrier, 2002].

I would like to get to the core of the mechanism on spiral re-entry which occurs in cardiac cells. How is the process of forming spiral waves? How does an unidirectional propagation influence on spiral formation? What is the condition which generates unidirectional site? What is the difference

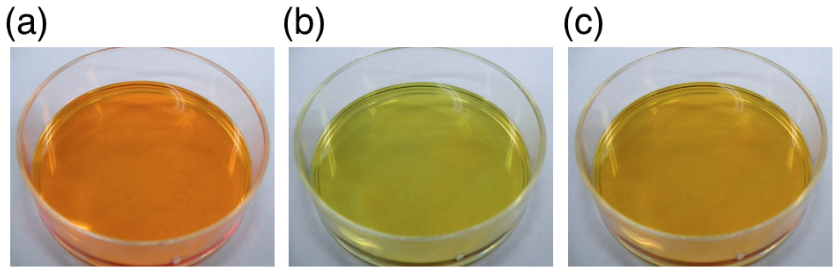

FIGURE 3.19. Temporal oscillation in stirred ruthenium-catalyzed BZ reaction. (a) reduction state, (b) oxidation state, and (c) transition state from green to orange, including refractory state.

of mechanism between heterogeneities of reaction and diffusion? For investigating systematically, the two different heterogeneities were realized by both the experiments of BZ reaction and mathematical models. In the next section, I will introduce the heterogeneity of reaction term, and explain our experiments with photosensitive BZ reaction and a mathematical model of the Oregonator model.

3.2. Wave Behaviors on Two Dimensional Excitable Media with Heterogeneity of Reaction

Now, the spatial heterogeneity of reaction term is introduced. For realization of the experiments in heterogeneous reaction system, the photosensitive BZ reaction system is used. At first, I would start to explain the experiments.

3.2.1. Photosensitive BZ Reaction: Signatures and Experimental Setting. The ruthenium-catalyzed BZ system has been well-studied, especially in researches on spatiotemporal behavior, since the properties of the reaction kinetics (oscillatory, excitation, suppression) can be conveniently controlled varied by adjusting the illumination intensity, and the initiation of chemical wave can also be easily controlled without any physical contact [Gäspär et al., 1983; Kuhnert, 1986; Kuhnert et al., 1989; Jinguji et al., 1990; Amemiya et al., 1996]. It has been reported that the ferroin- and ruthenium-catalyzed systems to be affected by visible light but the cerium-catalyzed system to be unaffected [Gäspär et al., 1983], although the ultraviolet illumination have influences on the cerium-catalyzeted [Vavilin et al., 1968] and the ferroin-catalyzed [Busse and Hess, 1973] systems. In the reduced state the solution in ruthenium-catalyzed BZ system is colored yellow by $Ru(bpy)_3^{2+}$ as shown in Figure 3.19(a), and in the oxidized state the one is green by $Ru(bpy)_3^{3+}$ as shown in Figure 3.19(b). The color of the solution in Figure 3.19(c) is transition state from green to orange as the medium slowly recovers its reduced state.

Chemical waves in photosensitive BZ system tend to be suppressed by high light intensity, since the photo induced to produce bromide ion, i.e., inhibitor. Initially, Kuhnert [Kuhnert, 1986] suggested:

$$6\mathrm{Ru(bpy)_3^{2+*}} + \mathrm{BrO_3^-} + 6\mathrm{H^+} \rightarrow 6\mathrm{Ru(bpy)_3^{3+}} + 3\mathrm{H_2O} + \mathrm{Br^-}$$

Then, Hanazaki [Hanazaki, 1992] proposed:

$$4\mathrm{Ru(bpy)_3^{2+*}} + \mathrm{HBrO_2} + 3\mathrm{H^+} \rightarrow 4\mathrm{Ru(bpy)_3^{3+}} + \mathrm{Br^-} + 2\mathrm{H_2O}$$

and Kádár reported [Kádár et al., 1997]:

(P1) $$\mathrm{Ru(bpy)_3^{2+}} \rightleftarrows \mathrm{Ru(bpy)_3^{2+*}}$$

(P2) $$\mathrm{Ru(bpy)_3^{2+*}} + \mathrm{BrCH_2(COOH)_2} \rightarrow \mathrm{Ru(bpy)_3^{3+}} + \mathrm{Br^-} + \mathrm{org.prod.}$$

(P3) $$\mathrm{Ru(bpy)_3^{3+}} + \mathrm{BrCH_2(COOH)_2} \rightarrow \mathrm{Ru(bpy)_3^{2+}} + \mathrm{Br^-} + \mathrm{org.prod.}$$

On the other hand, chemical waves, interestingly, can be induced by the photo depending on the solution condition [Gäspär et al., 1983; Jinguji et al., 1990; Mori et al., 1993]. This reaction starts by reduction of $\mathrm{BrO_3^-}$ through the autocatalytic reaction of $\mathrm{HBrO_2}$ as following components;

(P4')
$$2\mathrm{Ru(bpy)_3^{2+}} + \mathrm{HBrO_2} + \mathrm{BrO_3^-} + 3\mathrm{H^+} \rightarrow 2\mathrm{Ru(bpy)_3^{3+}} + 2\mathrm{HBrO_2} + \mathrm{H_2O}$$

(P5') $$2\mathrm{Ru(bpy)_3^{2+}} + \mathrm{BrO_3^-} + 3\mathrm{H^+} \rightarrow 2\mathrm{Ru(bpy)_3^{3+}} + \mathrm{HBrO_2} + \mathrm{H_2O}$$

In this study, two dimensional heterogeneity in reaction using the suppression by illumination in photosensitive BZ reaction. Now, I explain the experimental condition briefly, the details are given in Appendix A.

$\mathrm{Ru(bpy)_3Cl_2}$ was used as a catalyst for our system, and the BZ solution consisted of $[\mathrm{NaBrO_3}] = 0.51$ M, $[\mathrm{H_2SO_4}] = 0.34$ M, $[\mathrm{CH_2(COOH)_2}] = 0.16$ M, $[\mathrm{NaBr}] = 0.01$ M, and $[\mathrm{Ru(bpy)_3Cl_2}] = 1.7$ mM. A membrane filter was completely soaked in the ruthenium-catalyzed BZ solution (5 mL) for one minute, then picked up from the petri dish with the BZ solution and wiped by other paper to remove excess solution. The soaked membrane filter was placed on the center of a petri dish with a diameter of 20 mm, and entirely covered by silicone oil (0.4 mL) to keep from drying out. As shown in Figure 3.20, the petri dish with the membrane filter was placed on a glass plate, and irradiated from below. The reaction field on the glass plate was keep at a certain temperature 20 $\pm$1 °C using a water-cooling hose attached to thermostat bath, and the experiments were carried out in an air-conditioned room at 23 °C. A patterned image on a computer was irradiated to the membrane using a liquid crystal projector of which mercury

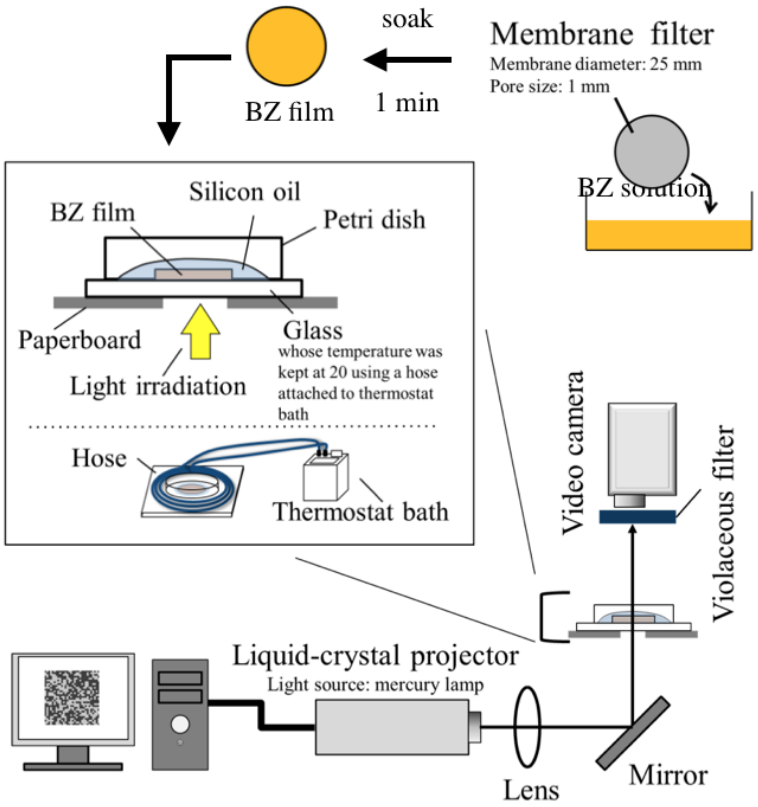

FIGURE 3.20. Schematic illustration of the experimental system (side view) with photosensitive BZ reaction. The details of experimental condition is mentioned in Appendix A.

lamp is as a light source through a magnifying lens to adjust the focus. The wave behavior on the membrane was observed through a blue optical filter using a digital video camera.

The spatial distribution of illumination intensity was controlled by a gray scale with a personal computer using *Microsoft Power Point* which is the presentation software. Three distinguished regions constituted the experimental reaction field as shown in Figure 3.21(a), (A)oscillatory, (B)inhibitory, and (C)excitable regions. The light intensities on each region were 0.16 kLx (A: oscillatory dark region), 74.9 kLx (B: inhibitory bright region), and 8.4 kLx (C: excitable region). A single chemical wave was entered from the oscillatory region (A) outside the excitable region (C) by putting a bridging triangle excitable region as shown in Figure 3.21(b). After the entrance of a wave, the triangle object was removed to prevent other waves from entering to the excitable region. I used a little ingenuity to enter a single wave straightly on excitable region, see Appendix A for more information. The excitable region (C) was a 10-mm square.

The excitable square region was separated in N×N square lattice as shown in Figure 3.22(a), and the spatial distribution of illumination intensity consisting of the excitable (8.4 kLx) and the suppressed (74.9 kLx) cells are placed randomly in the area ratio of excitable region R_{BZ} ($= n/N^2$, where

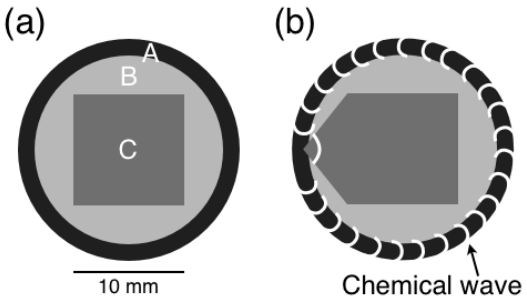

FIGURE 3.21. Schematic illustration of the reaction field on the membrane filter used in the photosensitive BZ reaction. (a) initial setting of the reaction field; (A) oscillatory region with 0.16 kLx light intensity, (B) inhibitory region with 74.9 kLx, and (C) excitable region with 8.4 kLx, respectively. (b) A triangle excitable region was put between the regions of (A) and (C) to enter a single chemical wave.

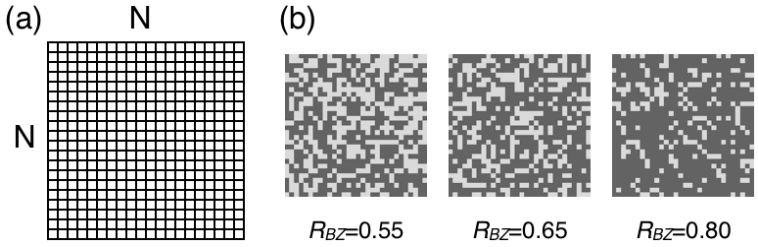

FIGURE 3.22. Schematic illustration of the setting on excitable region in Figure 3.21(C). (a) N×N square lattice. (b) Examples of image figures varying the ratio, R_{BZ}= 0.55 (left), 0.65 (middle), and 0.80 (right), respectively.

n is the number of excitable cells) [Suematsu et al., 2011]. Now let N = 30, since the size of cells is too large compared with the width of chemical waves if N is set to be larger than 40, and the resolution of pictures taken by a digital video camera is not enough to observe wave behaviors if N is set to be smaller than 20. Figure 3.22(b) is panels of examples of image figures varying the ratio R_{BZ}, which are irradiated on excitable region in Figure 3.21(C) from a personal computer.

3.2.2. Experimental Results in Heterogeneous Photosensitive BZ reaction. The behavior of chemical wave depends on the area fraction R_{BZ}, and could be classified into three types as similar to previous study [Bub et al., 2002b]: planar wave propagation, blocked wave propagation, or spiral formation. The wave behaviors were easy to observe by conducting visualization analysis using *ImageJ*[1], which is one of the image processing softwares that is provided free. At the first step, the movie

[1]ImageJ: http://rsbweb.nih.gov/ij/

recorded with a digital video camera was split into red-green-blue channels, all analyses were conducted using a blue channel image.

The first state of wave behaviors is "planar wave propagation", that was observed when R_{BZ} is relatively larger. Figure 3.23 is an example of the case of $R_{BZ} = 0.80$ that a chemical wave is relatively easy to propagate. Using the image analysis[2] to overlay images which split from a movie as shown in Figure 3.23(a), it can be obviously observed that the wave entered from left-hand side arrived at the right-hand side of the medium, where time evolution progresses from red to blue, and the white squares are suppression cells. Figure 3.23(b) is the spatiotemporal plot of certain line parallel to horizontal axis. Noticed that the wave can propagate by coming around from another direction even if the suppression cells exist as an obstacle. This behavior case always occurred when $R_{BZ} > 0.80$, and stochastically observed when $0.6 \leq R_{BZ} \leq 0.77$.

If the value of R_{BZ} was relatively low, however, the wave vanished before it reaches the right-hand side due to a lot of the bright obstacles. It is the second state of wave behavior, "blocked wave propagation", which was always appeared when $R \leq 0.55$, and occurred only infrequently when $0.60 \leq R_{BZ} \leq 0.65$. Figure 3.24 is an example of the case of $R_{BZ} = 0.55$, noticed that the wave cannot propagate by lots of suppression cells enough to prevent a wave from coming around from another direction.

With an appropriate value of R_{BZ}, $0.60 \leq R_{BZ} \leq 0.77$, the third state of wave behavior, "spiral formation", appeared stochastically. Figure 3.25 is an example of the case of $R_{BZ} = 0.77$. Although the behavior of chemical wave in Figure 3.25(a) seems to be similar to the state of planar wave propagation as shown in Figure 3.23, it turned out by Figure 3.25(b) that the wave remained after it has reached to the right-hand side. That is because a wave which came from left-hand side generates a spiral core somewhere by 100 s in excitable region, and spiral pattern was formed spontaneously. Furthermore, Figure 3.25(b) was indicated that a spiral core might have generated around 10 mm from the left-hand side, and that the wave propagated in opposite direction of the initial wave after a spiral has been formed. In fact, the spiral cores were generated at three locations, including the above position, and three spiral waves appeared.

Why has a spiral core been generated spontaneously? In general, it is considered that a spiral core is generated by the interaction between waves [Agladze et al., 1994] or is due to vulnerability [Gesteira et al., 1994; Aliev, 1995], but we propose that the geometric heterogeneity of reaction can generate spiral cores. The process of forming a spiral core can be clearly observed in the enlarged snapshots of the three regions which generated a spiral wave, named region A as shown in Figure 3.26(a), B as shown in Figure 3.27(a), and C as shown in Figure 3.28(a). As shown by overlap the red and blue lines of time progress in the enlarged snapshots of region A in Figure 3.26(a), a spiral core was generated in this region. Furthermore, unidirectional wave propagation was observed in the region A where the spiral core was formed. A chemical wave traveling to the right cannot path downward through the narrow gap in Figure 3.26(c), on the other hand,

[2]Macro for ImageJ: http://www.jaist.ac.jp/ms/labs/hiratsuka/index.php

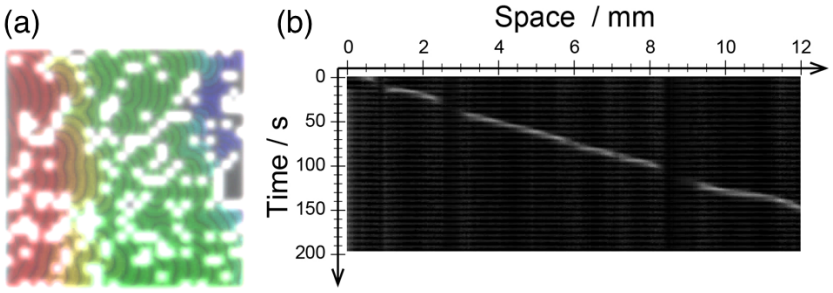

FIGURE 3.23. Example of the state of planar wave propagation when $R_{BZ} = 0.80$. (a) Superimposed image in which the color changes from red to blue as time progresses. (b) Spatiotemporal image. The cause of wave breaking observed in several places is suppression cells.

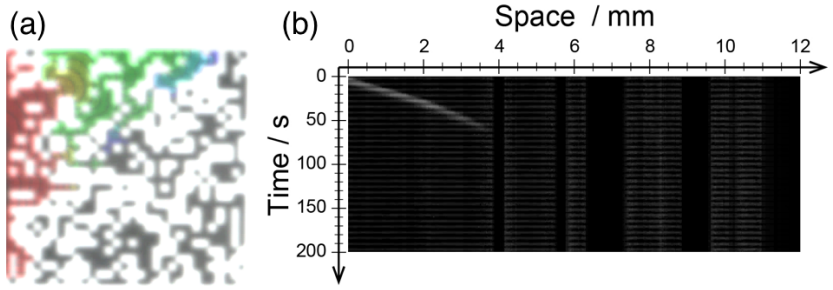

FIGURE 3.24. Example of the state of blocked wave propagation when $R_{BZ} = 0.55$, (a) superimposed image, and (b) spatiotemporal image.

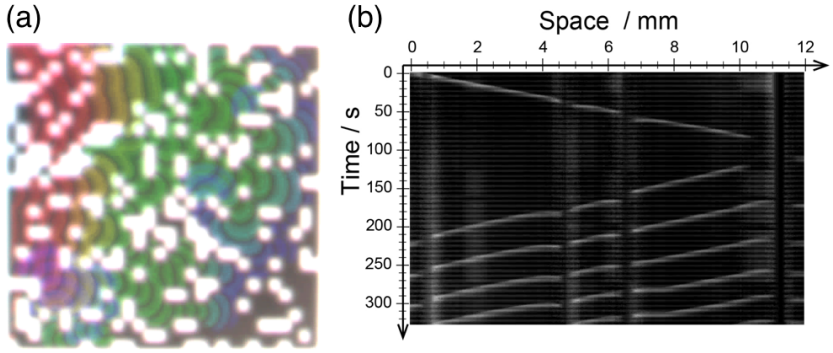

FIGURE 3.25. Example of the state of spiral formation when $R_{BZ} = 0.77$, (a) superimposed image, and (b) spatiotemporal image.

it propagates in a clockwise direction and reaches the narrow gap again, and cannot path upward through the first narrow in Figure 3.26(d) while traveling upward. Interestingly, in this direction, the wave can pass upward through the second narrow gap in Figure 3.26(e).

As similar to the case of the region A, the unidirectional propagation of chemical waves has been observed in both the region B as shown in Figure 3.27 and C as shown in Figure 3.28 where the spiral core was also formed. In the region B as shown in Figure 3.27, a chemical wave came from the left-hand side cannot path downward through the narrow gap which created by two suppression cells in Figure 3.27(c), conversely, it propagates in a clockwise direction around the small island and reaches the narrow gap again. The wave can pass upward through the narrow gap in this direction in Figure 3.27(d). In the region C as shown in Figure 3.28, in spite of three narrow locations exist, the unidirectional propagation appeared in the only one narrow gap, i.e., a chemical wave came from the left-hand side cannot path to right-hand side through only the middle of narrow gap in Figure 3.28(c). The wave could propagate through the below narrow propagates in a counterclockwise, and can pass though the middle of narrow gap in opposite direction in Figure 3.28(d).

As provided clearly by these experimental results, the geometry of the chemical field created by excitable and suppression cells demonstrates the chemical diode system. Original chemical diode system [Agladze et al., 1996] showed as shown in Figure 3.29(a) that unidirectional propagation occurred when two mesoporous glass plates with ferroin loaded were placed in the condition that the one corner side was close to another plane side. This study obviously indicated that the geometrical arrangement of the plates is important for unidirectional system. From numerical calculations with Rovinsky-Zhabotinsky model, it has found that the gap distance between the plates is of great significance in generating unidirectional propagation as shown in Figure 3.29(b). The subsequent researches [Motoike and Yoshikawa, 1999; Motoike et al., 2001] on chemical diode in various geometric field suggested that the direction of chemical wave when entered in the gap also influences on wave propagation.

In our experiments in heterogeneous BZ reaction, such as diode is generated stochastically by the spatial heterogeneity of the excitable media and the spatial distribution of the excitable and suppression cells in the case of an appropriate value of R_{BZ}. The results indicated clearly that a diode is generated by heterogeneity of the reaction field, and it also became evident that a chemical diode can be the genesis of spontaneous spiral formation.

Now, we should clarify the difference between the previous studies on chemical diode [Agladze et al., 1996; Dupont et al., 1998; Sendiña-Nadal et al., 2006] and our experiments. The crucial difference is that there is a gap between catalyst-loaded fields in [Agladze et al., 1996; Dupont et al., 1998; Sendiña-Nadal et al., 2006], but no gap in our experimental system. The unidirectional propagation in no gap system have yet to be elucidated fully, hence I will investigated in detail in the next section using Oregonator model. We focused on the geometric structure in which a spiral pattern was formed since a spiral core is always generated in the same location when the

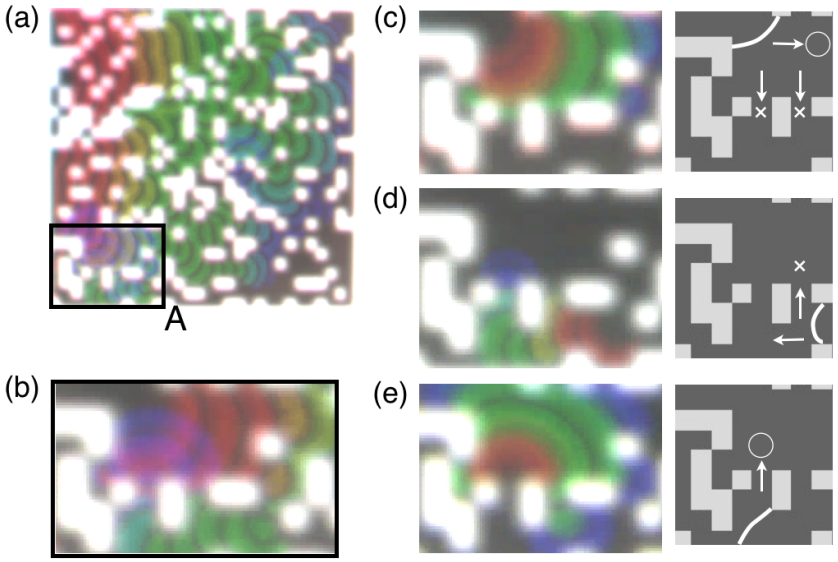

FIGURE 3.26. Snapshots of (a) indicating the region A where a spiral core was formed, (b) enlarged figure of A, and (c)-(d) enlarged figure when unidirectional propagation occurred.

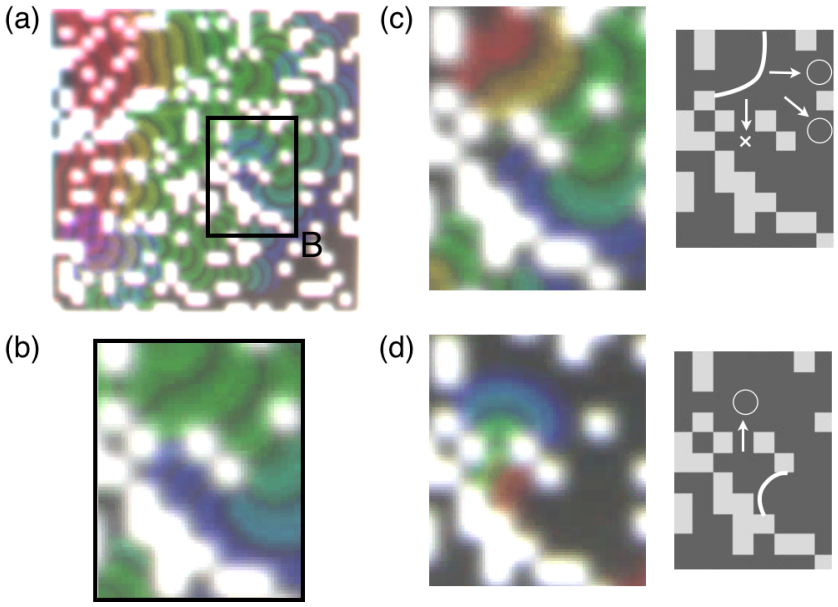

FIGURE 3.27. Snapshots of (a) indicating the region B where a spiral core was formed, (b) enlarged figure of B, and (c)-(d)enlarged figure when unidirectional propagation occurred.

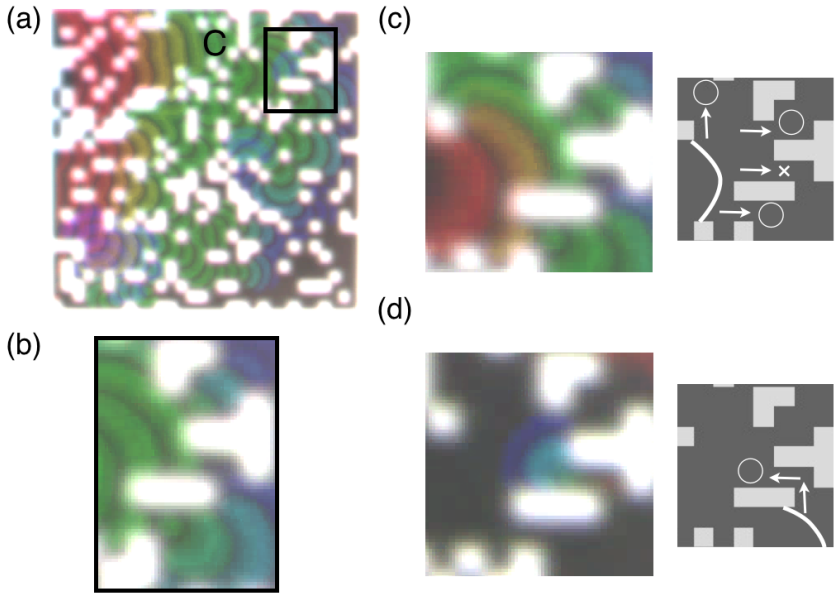

FIGURE 3.28. Snapshots of (a) indicating the region C where a spiral core was formed, (b) enlarged figure of C, and (c)-(d)enlarged figure when unidirectional propagation occurred.

experiments were performed using the same design of heterogeneity. What is the geometric condition to generate unidirectional propagation? What is the relationship between the geometry and other condition, e.g., excitability and effect of diffusion?

3.2.3. Oregonator Model Modified for Photosensitive BZ Reaction. For analysis of the experimental results in photosensitive BZ system, two kinds of models have been suggested as the Oregonator model modified for the ruthenium-catalyzed system, i.e., the one is that the effects of light intensity was introduced into the equation of inhibitor Br^- [Krug et al., 1990; Amemiya et al., 1996], and another is that into the three equations related to Br^-, bromous acid $HBrO_2$, and the catalyst $Ru(bpy)_3^{3+}$ [Kádár et al., 1997; Amemiya et al., 1998]. The simple one of the dimensionless differential equations of Oregonator model modified for photochemical reaction using the Tyson's scaling [Tyson and Fife, 1980] that the only one component was added into the original Oregonator scheme is,

$$\epsilon \frac{du}{d\tau} = qv - uv + u - u^2, \tag{3.2.1}$$

$$\delta \frac{dv}{d\tau} = \phi - qv - uv + fw, \tag{3.2.2}$$

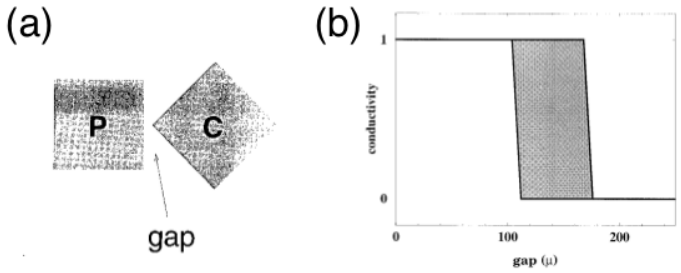

FIGURE 3.29. Chemical diode system, quoted from Figure 1 and 4 of [Agladze et al., 1996], respectively. (a) Two mesoporous glass plates with ferroin loaded. A chemical wave propagates only from the plane side (P) to the corner side (C). (b) Diagram of the state of wave propagation v.s. width of the gap calculated numerically. Unidirectional propagation appears in the painted area.

$$\frac{dw}{d\tau} = u - w, \tag{3.2.3}$$

where u, v, and w are the dimensionless concentrations of $HBrO_2$, Br^-, and $Ru(bpy)_3^{3+}$, respectively; q are scaling parameters, and f is an adjustable stoichiometry parameter. The rate of bromide production from the irradiation is given by ϕ, and this rate is proportional to the applied light intensity [Krug et al., 1990]. This modified Oregonator model has been successful in qualitatively describing various dynamical behaviors observed in the photosensitive BZ systems [Krug et al., 1990; Amemiya et al., 1996].

On the other hand, S. Kádár et al. have revealed the detailed mechanism on the ruthenium-catalyzed BZ system [Kádár et al., 1997]. The chemical reaction equations related to ruthenium are the following six components including the above three equations (P1), (P2), and (P3);

$$\text{(P1)} \qquad Ru(bpy)_3^{2+} \rightleftarrows Ru(bpy)_3^{2+*}$$

$$\text{(P2)} \qquad Ru(bpy)_3^{2+*} + BrCH(COOH)_2 \rightarrow Ru(bpy)_3^{3+} + Br^- + \text{org.prod.}$$

$$\text{(P3)} \qquad Ru(bpy)_3^{3+} + BrCH(COOH)_2 \rightarrow Ru(bpy)_3^{2+} + Br^- + \text{org.prod.}$$

$$\text{(P4)} \qquad Ru(bpy)_3^{2+*} + BrO_3^- + 2H^+ \rightarrow BrO_2\cdot + H_2O + Ru(bpy)_3^{3+}$$

$$\text{(P5)} \qquad BrO_2\cdot + Ru(bpy)_3^{2+} + H^+ \rightarrow HBrO_2 + Ru(bpy)_3^{3+}$$

$$\text{(P6)} \qquad \mathrm{BrO_3^-} + \mathrm{HBrO_2} + \mathrm{H^+} \rightarrow 2\mathrm{BrO_2}\cdot + \mathrm{H_2O}$$

The component of autocatalytic reaction of $HBrO_2$ through the oxidation reaction of ruthenium ion is obtained by adding the equations (P5)$\times$2 and (P6);

$$\begin{aligned} &2\mathrm{Ru(bpy)_3^{2+}} + 3\mathrm{H^+} + \mathrm{BrO_3^-} + \mathrm{HBrO_2} \\ \text{(P4')} \qquad &\rightarrow 2\mathrm{HBrO_2} + 2\mathrm{Ru(bpy)_3^{3+}} + \mathrm{H_2O} \end{aligned}$$

Moreover, the component of production of Br^- through the reduction reaction of ruthenium ion is obtained by adding the equations (P3) and (R8);

$$\begin{aligned} &\mathrm{Ru(bpy)_3^{3+}} + \mathrm{Br_2} + \mathrm{CH_2(COOH)_2} \\ \text{(R10')} \qquad &\rightarrow \mathrm{Ru(bpy)_3^{2+}} + 2\mathrm{Br^-} + \mathrm{H^+} + \text{org.prod.} \end{aligned}$$

Adding the two equations related to ruthenium (P4) and (P5), the following component can be obtained;

$$\begin{aligned} &\mathrm{Ru(bpy)_3^{2+*}} + \mathrm{Ru(bpy)_3^{2+}} + \mathrm{BrO_3^-} + 3\mathrm{H^+} \\ \text{(P7)} \qquad &\rightarrow 2\mathrm{Ru(bpy)_3^{3+}} + \mathrm{HBrO_2} + \mathrm{H_2O} \end{aligned}$$

Hence, the Oregonator Scheme modified for the ruthenium-catalyzed BZ reaction can be described using the seven reaction components of the FKN mechanism (R3), (R2), (P4'), (R4), (R10'), (P2), and (P7) as shown in Table 3.3. Let A = BrO_3^-, B = $BrCH(COOH)_2$, E=$Ru(bpy)_3^{2+*}$, M = $CH_2(COOH)_2$, P = HOBr, X = $HBrO_2$, Y = Br^-, and Z' = $Ru(bpy)_3^{3+}$, respectively. Invariable numbers $k1$, $k2$, $k3'$, $k4$, $k5'$, $r1$ and $r2$ are rate constants, and h is a stoichiometric parameter.

The forward reaction rate r_0 of the photoactivation of $Ru(bpy)_3^{2+}$ in the process of (OP0) in Table 3.3 is proportional to the light flux (Φ), and the reverse reaction is a first-order quenching process with a rate constant of r_{-0} [Amemiya et al., 1998]. The reaction rate equations related to x, y, and z' are as follows by letting the concentrations [X] = x, [Y] = y, [Z'] = z';

$$\frac{dx}{dt} = k_1 ay - k_2 xy + k_3' ax - 2k_4 x^2 + r_2 ea, \tag{3.2.4}$$

$$\frac{dy}{dt} = -k_1 ay - k_2 xy + k_5' hmz' + r_1 eb, \tag{3.2.5}$$

$$\frac{dz'}{dt} = 2k_3' ax - k_5' mz' + r_1 eb + 2r_2 ea, \tag{3.2.6}$$

where [A] = a, [B] = b, [E] = e, and [M] = m. Here the concentration of $\mathrm{Ru(bpy)}_3^{2+*}$, e, can be obtained by assuming the steady-state approximation ($de/dt \approx 0$) [Amemiya et al., 1998], and the reaction rates for the processes (OP1) and (OP2) are the followings as [Kádár et al., 1997; Amemiya et al., 1998],

$$r_1 eb = \frac{b}{0.089 + b + 15[H^+]^2 a}\Phi, \qquad r_2 ea = \frac{15[H^+]^2 a}{0.089 + b + 15[H^+]^2 a}\Phi.$$

Let the Φ coefficients put p_1 and p_2, respectively, i.e.,

$$p_1 = \frac{b}{0.089 + b + 15[H^+]^2 a}, \qquad p_2 = \frac{15[H^+]^2 a}{0.089 + b + 15[H^+]^2 a}.$$

The differential equations (3.2.4), (3.2.5), and (3.2.4) can be nondimensionalized using the Tyson ' s scaling [Tyson and Fife, 1980] as mentioned above. Let $u = x/x_0$, $v = y/y_0$, $w = z'/z_0'$, and $\tau = t/t_0$, where u, v and w

TABLE 3.3. Oregonator scheme for photosensitive BZ reaction

	Reaction	Rate
(O1)	A + Y → X + P	k_1
(O2)	X+Y → 2P	k_2
(O3')	A + X → 2X + 2Z'	k_3'
(O4)	2X → A +P	k_4
(O5')	M+Z' → hY	k_5'
(OP0)	G ⇄ E	$r_{\pm 0}$
(OP1)	E + B → Z' + Y	r_1
(OP2)	E+A → 2Z' + X	r_2

represent the non-dimensional concentrations, and τ is dimensionless time. The dimensionless differential rate law of the concentrations u, v,w related to τ are as follows;

$$\frac{du}{d\tau} = \frac{k_1 a y_0 t_0}{x_0} v - k_2 y_0 t_0 uv + k_3' a t_0 u - 2k_4 x_0 t_0 u^2 + \frac{t_0 p_2 \Phi}{x_0}, \tag{3.2.7}$$

$$\frac{dv}{d\tau} = -k_1 a t_0 v - k_2 x_0 t_0 uv + \frac{k_5' h m z_0' t_0}{y_0} w + \frac{t_0 p_1 \Phi}{y_0}, \tag{3.2.8}$$

$$\frac{dw}{d\tau} = \frac{2k_3' a x_0 t_0}{z_0'} u - k_5' m t_0 w + \frac{t_0 p_1 \Phi}{z_0'} + \frac{2t_0 p_2 \Phi}{z_0'}, \tag{3.2.9}$$

where the characteristic quantities t_0, x_0, y_0, and z_0' are

$$t_0 = \frac{1}{k_5' m}, \qquad x_0 = \frac{k_3 a}{2k_4}, \qquad y_0 = \frac{k_3' a}{k_2}, \qquad z_0 = \frac{(k_3' a)^2}{k_4 k_5' m},$$

hence, the equations (3.2.7), (3.2.8), and (3.2.9) can be redescribed as

$$\epsilon \frac{du}{d\tau} = qv - uv + u - u^2 + p_2 \phi, \tag{3.2.10}$$

$$\delta \frac{dv}{d\tau} = 2hw - qv - uv + p_1 \phi, \tag{3.2.11}$$

$$\frac{dw}{d\tau} = u - w + (\frac{p_1}{2} + p_2)\phi, \tag{3.2.12}$$

where ϵ, δ, q, and ϕ are

$$\epsilon = \frac{k_5' m}{k_3' a}, \qquad q = \frac{2k_1 k_4}{k_2 k_3'}, \qquad \delta = \frac{2k_4 k_5' m}{k_2 k_3' a}, \qquad \phi = \frac{2k_4}{(k_3' a)^2} \Phi.$$

In addition to the above three-variable modified Oregonator, the following two-variable type obtained by stepping down the variable v through comparison of reaction rate is also used.

$$\epsilon \frac{du}{d\tau} = (2hw + p_1\phi)\frac{q-u}{q+u} + u - u^2 + p_2\phi, \tag{3.2.13}$$

$$\frac{dw}{d\tau} = u - w + (\frac{p_1}{2} + p_2)\phi. \tag{3.2.14}$$

3.2.4. Simulation Results with Oregonator Model Modified for Photosensitive BZ System. In this section, the results of numerical simulations using the modified Oregonator model for ruthenium-catalyzed system remodeled for our experiments in two dimensional heterogeneous reaction field are mentioned for the purpose of elucidation of the mechanism on forming unidirectional path spontaneously.

Now, we use the reaction-diffusion system as

$$\frac{du}{d\tau} = D_u\nabla^2 u + \frac{1}{\epsilon}\left((fw + p_1\phi)\frac{q-u}{q+u} + u - u^2 + p_2\phi\right), \tag{3.2.15}$$

$$\frac{dw}{d\tau} = D_w\nabla^2 w + u - w + (\frac{p_1}{2} + p_2)\phi, \tag{3.2.16}$$

where u and w are the dimensionless concentrations and D_u and D_w are the diffusion coefficients of $HBrO_2$ and $Ru(bpy)_3^{3+}$, respectively. As mentioned above, ϵ, f, and q represent the control parameter of the time-scale separation between the two variables, the stoichiometry parameter, and the scaling parameter, respectively. The positive parameters p_1 and p_2 relate to photosensitive chemical reaction, and ϕ corresponds the light intensity. As similar to the experiments, the spatial heterogeneity of reaction field is realized by putting ϕ to two variables, ϕ_1 (excitation) and ϕ_2 (suppression) which are placed randomly in the area ratio of excitable cells R. The numerical calculations were simulated using the Euler method with a time step $\Delta\tau = 10^{-4}$ and the two dimensional difference method of the 150×150 grid mesh with the spatial mesh size $\Delta x = 1.0$. In the calculations, the five lattices correspond to the one cell of the experiments.

Here several constant values can be determined by the initial concentration of our experiment [Amemiya et al., 1998] as $\epsilon = 0.0549$, $\mu = 0.0000952$, $p_1 = 0.00412$, and $p_2 = 0.971$. The stoichiometry parameter is set to $f = 2.0$ for excitable condition [Keener and Tyson, 1986], and the values related to light intensity are set to the excitable condition $\phi_1 = 0.001$ and the suppressed condition $\phi_2 = 0.042$. We set to the diffusion coefficients $D_u = D_w = 1.0$ as similar to previous study [Nakata et al., 2011]. The initial condition of u and w are set to 0.0, and we use the Neumann boundary condition. A single chemical wave were generated by the stimulative perturbation of u in a vertical line at left hand side as $u = 0.1$.

The same results as the experiments, i.e., the three states, are appeared in our simulations depending on the value of R. Figure 3.30 is chronological

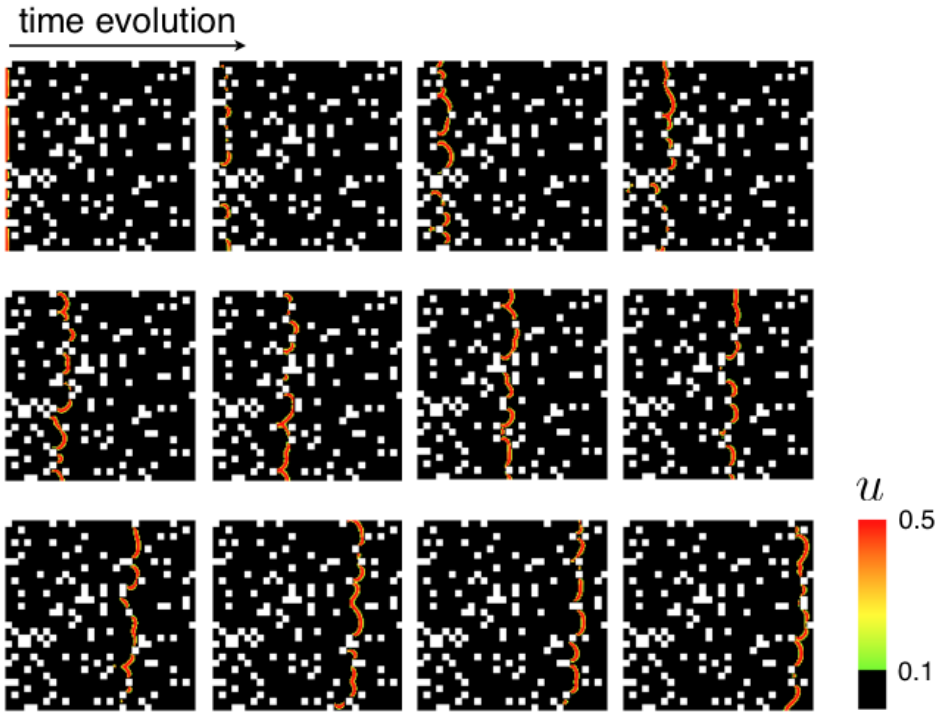

FIGURE 3.30. Chronological snapshots every 2.5 s of the planar wave propagation state in the case of $R = 0.87$. Excitable reaction field was blacked out, and suppressed cells were filled with white boxes. An oxidation single wave generated at the left can propagate to the right hand side.

snapshots of an example of planar wave propagation in the case of $R = 0.87$. In the figures of numerical results, the excitable reaction field was blacked out, and the suppressed cells were filled with white boxes. Since a chemical wave observed in this experiment is the wave of oxidation state, a cell is colored depending on the value of u if $u > 0.1$. A single wave generated at the left hand side can propagate to right hand side as shown in Figure 3.30. Conversely, when R is lower, a wave cannot propagate to the right by suppressed cells blocking as obstacles, e.g., Figure 3.31 is chronological snapshots of an example of thus blocked wave propagation in the case of $R = 0.64$.

A spiral wave formed when R is an appropriate value and the distribution of suppressed cells, created some specific structures. Figure 3.32 is chronological snapshots of an example of spiral formation in the case of $R = 0.87$. A single wave generated at the left hand side broke partially at the lower left, and the edge of wave generated by wave breaking formed a core of spiral. Similar to the results by experiment, spiral patterns are formed spontaneously.

It is stochastic to generate a spiral wave depending on the distribution of suppressed cells. Figure 3.33 is a phase diagram for probability of occurrence of wave behaviors. When R is less than 0.58, the state of blocked propagation

FIGURE 3.31. Chronological snapshots every 1.25 s of the blocked wave propagation state in the case of $R = 0.64$. An oxidation wave generated at the left cannot propagate to the right hand side.

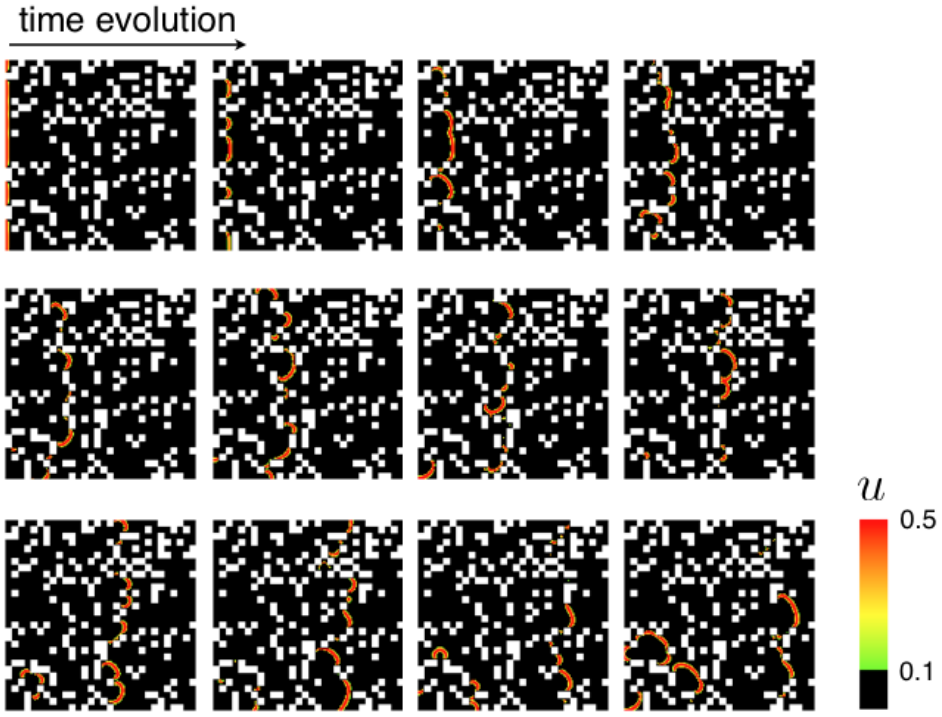

FIGURE 3.32. Chronological snapshots every 2.5 s of the spiral formation state in the case of $R = 0.80$. A spiral core were generated at the lower left while an oxidation single wave generated at the left propagates to the right hand side.

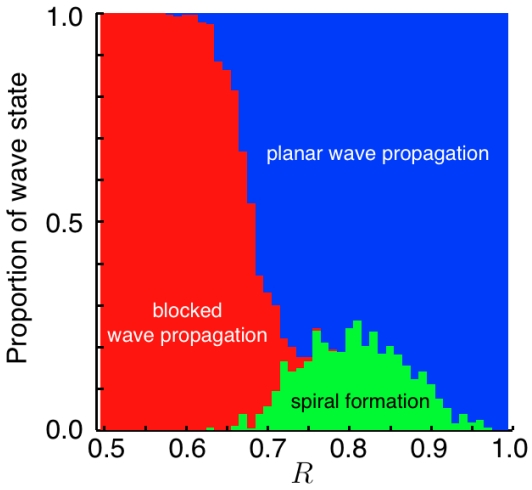

FIGURE 3.33. Phase diagram of occurrence probability of three wave behaviors. Each behavior is colored by red (blocked propagation), blue (planar wave propagation), and green (spiral formation).

is always appeared. It is reasonable that this results was caused by site percolation. With increasing of R, the behaviors of spiral formation and planar wave propagation are appeared although the state of planar wave propagation is perfectly dominant when the value of R is large enough. A peak of probability of occurrence of the state of spiral wave exist around $R = 0.8$. By the stochastic results, it is expected that a specific structure which induces to generate a spiral core tends to create when the value of R is around 0.8.

If there would be a specific structure for inducing to generate a spiral core, spiral formation should be generated in the same distribution as the experiment when a spiral wave appeared. Figure 3.34 is a simulation result by the same distribution of cells as the experiment that spiral formation occurred as shown in Figure 3.25. It has found that a spiral wave was formed predictably in the numerical simulation. More precisely, a spiral core was generated in the same position as the region A of experiment as shown in Figure 3.26.

The same phenomenon occurred at the region A as shown in Figure 3.35, i.e., unidirectional wave propagation was observed. A wave traveling to the right cannot path downward through the narrow gap in Figure 3.35(a), on the other hand, it propagates in a clockwise direction and reaches the narrow gap again, and cannot path upward through the first narrow in Figure 3.35(b) while traveling upward. Interestingly, in this direction, the wave can pass upward through the second narrow gap in Figure 3.35(c). This result clearly showed that unidirectional propagation is essential to generate a spiral core, and a specific structure created by suppressed cells is important for generating unidirectional path. In the next section, I will discuss why the specific structure can generate unidirectional propagation spontaneously to take the structure of the region A as an example.

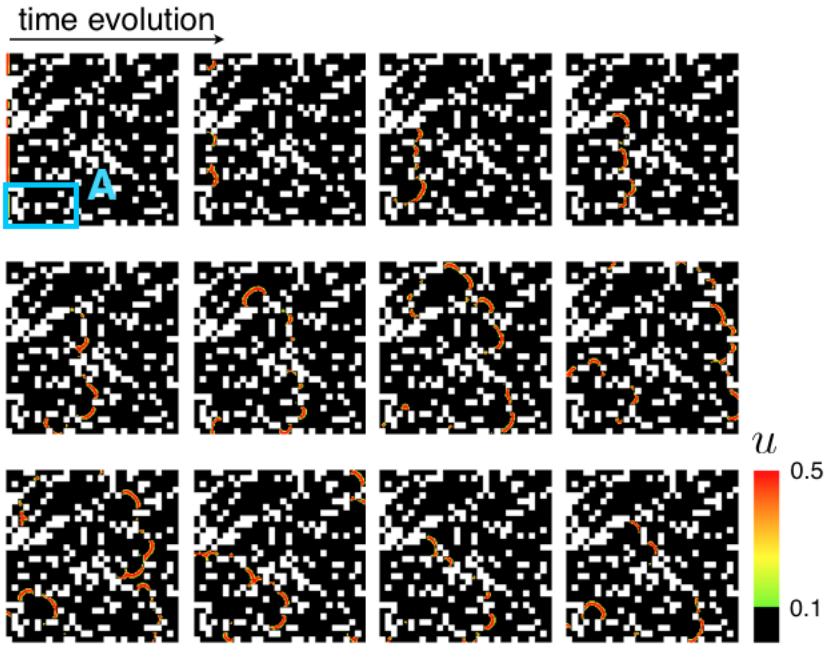

FIGURE 3.34. Chronological snapshots every 2.5 s of the spiral formation state in the case of $R = 0.77$. A spiral core were generated at the region A while an oxidation single wave generated at the left propagates to the right hand side.

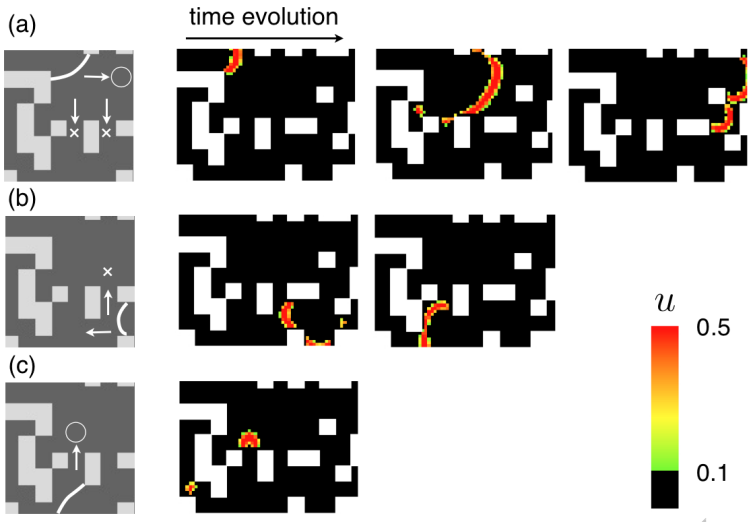

FIGURE 3.35. Chronological snapshots every 2.5 s of wave behavior when spiral was formed in the region A as indicated in Figure 3.34. (a) A wave is unable to pass through the narrow gap from top to bottom. (b) The wave come back to the gap in opposite direction after going around a small island of suppressed cells, and is unable to go through the first gap. (c) At the second gap, the wave can pass through. Unidirectional propagation was appeared.

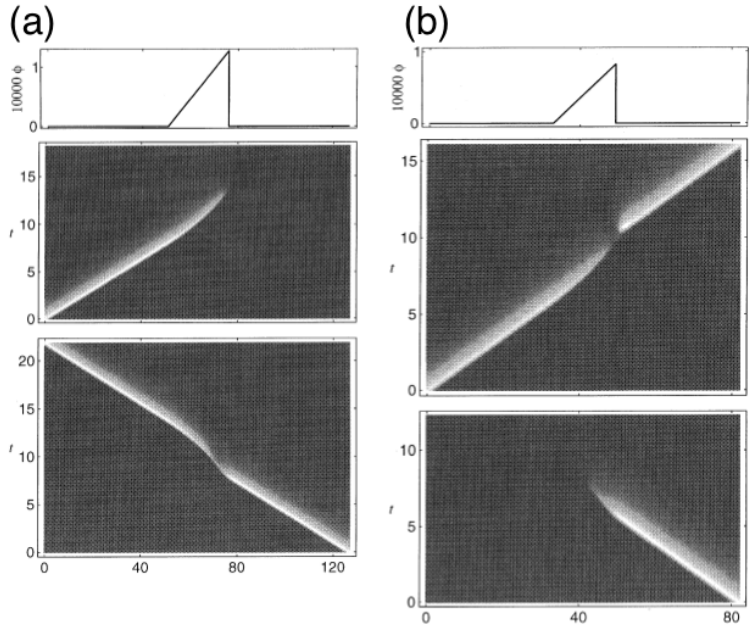

FIGURE 3.36. Unidirectional propagation observed in one dimensional calculations with the Oregonator model modified for photosensitive BZ reaction, quoted from Figure 2 and 3 of [Tóth et al., 2001], respectively. Each panel represents spatial distribution of illumination (top), grayscale visualization of wave propagation with low-side entrance (middle), and with high-side (bottom). The calculations are carried out with the same diffusion coefficient of catalyst and the same gradient of illumination, and with (a) high excitability and long width of gap, and (b) low excitability and short width of gap.

3.2.5. Unidirectional Path Generated by Distribution of Heterogeneity. For investigation on a cause of spontaneous generation of unidirectional path, it is necessary to introduce the previous studies related to chemical diode. The one dimensional calculations with reaction-diffusion system of the Oregonator model modified for photosensitive BZ reaction have shown that a gap of light intensity with gradient could generate unidirectional propagation [Tóth et al., 2001]. Figure 3.36 is simulation results with spatial distribution of light intensity (top). In the panel (a), the wave propagated from the low-side cannot get through the top of the gap (middle). Conversely, the wave propagation from the high-side can succeed in propagating to opposite side (bottom). This phenomenon occurs at higher excitability and higher diffusion of catalyst. On the other hand, the panel (b) is the case of lower excitability and shorter width of gap compared to the case of the panel (a). It is obviously shown that the behavior of a diode appeared in the opposite direction.

Although a cause of direction reversal has not been clear yet, unidirectional propagation could be generated by the time delay with increasing of

gap width, and by the difference between critical widths that complete propagation failure occurs. It is because of asymmetric structure, i.e., the wave propagation depends on the size of the wave [Agladze et al., 1996; Sendiña-Nadal et al., 2006]; the wave from the planar side is larger than the critical size of the propagating wave [Nagy-Ungvarai et al., 1992], but in the other region the wave gradually shrinks as it approaches the corner and is close to the critical size when it reaches the gap. Therefore, an asymmetric excitable field can exhibit diode characteristics. It has been experimentally indicated that the unidirectional propagation of chemical wave, which would occur in high diffusion coefficient of catalyst as shown in Figure 3.36(a), appeared in ruthenium-catalyzed BZ reaction with an asymmetric gap of illumination [Ichino et al., 2009].

Now, let us consider the relationship between these previous researches on a diode with asymmetric gap, and spatial pattern generated by distribution of suppressed cells in our experiments and numerical simulations. In our study, there is no explicit gradient of light intensity on the excitable region which chemical waves go through. As mentioned before, however, photosensitive BZ reaction has the feature that illumination induces generation of inhibitor. It is reasonable to predict that highly-concentrated inhibitor on a suppressed cell diffuses to excitable cells, and generates a gradient of inhibitor.

Since it is difficult to show experimentally that a gradient of inhibitor on excitable region would be created by diffusion, it has been investigated in numerical calculations. Figure 3.37(b) is concentration distribution of inhibitor around the area indicated by Figure 3.37(a) where unidirectional propagation was observed when a spiral core was generated in the region A. It is confirmed that concentration gradient of inhibitor is created on excitable region by inhibitor exuding from suppressed region. A wave has to pass through this narrow gap of inhibitor gradient as shown in Figure 3.37(c).

As indicated by Figure 3.37(d) that shows the average value of inhibitor concentration, the gradient of gap has low-side and high-side entrance. In both experimental and numerical results, as similar to previous study in experiment [Ichino et al., 2009], a wave was able to pass through the narrow gap from high-side entrance, conversely, could not from low-side.

Even if experiments were performed with the same structure created by suppressed cells, spiral patterns were generated stochastically, i.e., unidirectional propagation sometimes did not occur. That is considered an effect of fluctuation. Let us take fluctuation of illumination for example. Figure 3.38 is the case of $\phi_2 = 0.040$, which is slightly lower light intensity than the case of unidirectional propagation. A wave can pass through the narrow gap from top to bottom as shown in Figure 3.38(a) in spite of the concentration gradient of inhibitor as Figure 3.38(b) and (c) similar to the case of generating unidirectional path. Hence, spiral wave was not generated.

On the other hand, Figure 3.39 is the case of $\phi_2 = 0.045$ which is slightly higher than the case of unidirectional path. This case also did not form spiral. Although the result of generating no spiral wave is the same as the case of lower intensity, the wave behavior is extremely different. A wave was not able to pass through the narrow gap from top to bottom as shown in the

top line panels of Figure 3.39(a), and a surviving wave came back to this gap from opposite direction after going around a small island of suppressed cell as shown in the middle panels of Figure 3.39(a). Spiral wave would be formed if the wave could pass through the narrow gap from bottom to top. It was, however, unable to pass through the gap as shown in the bottom panels of Figure 3.39(a).

Despite existence of similar concentration distribution and gradient of inhibitor in the narrow gap, three different types of wave behaviors appeared depending on the light intensity of suppressed cells. We would be able to find a clue about a cause of these differences by superimposed graph of three curves of gradient of inhibitor at narrow gap as shown in Figure 3.40. Both widths of high- and low-side entrances are obviously the same. However, the maximum values of concentration of inhibitor are slightly different. The gradients of both entrances are also different with the difference of maximum value, i.e., it increases with the increase of maximum value. It is clearly indicated that maximum value or gradient of concentration of inhibitor influences on wave propagation. A difference generated by about 5 percent fluctuation make a big influence on wave behavior, therefore, experimental results have stochastic factor. It is considered that such a fluctuation could occur also in excitability and diffusion ratio.

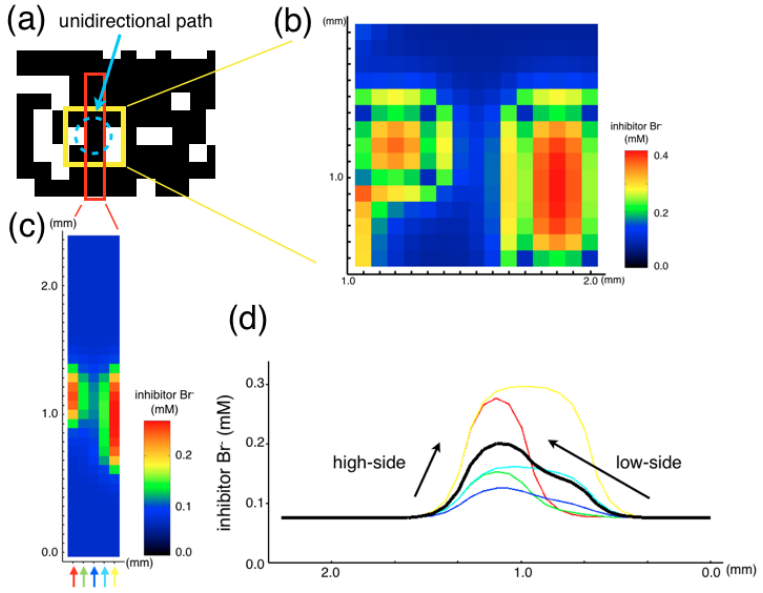

FIGURE 3.37. Concentration distribution of inhibitor when unidirectional propagation occurred. The simulation is carried out with $\phi_2 = 0.042$. (a) The region A where a spiral core was generated. Concentration distribution of inhibitor around (b) unidirectional site and (c) narrow gap. (d) Spatial average concentration gradient of inhibitor on excitable region exuded from suppressed region. The color indicates the position as shown in the bottom of (c).

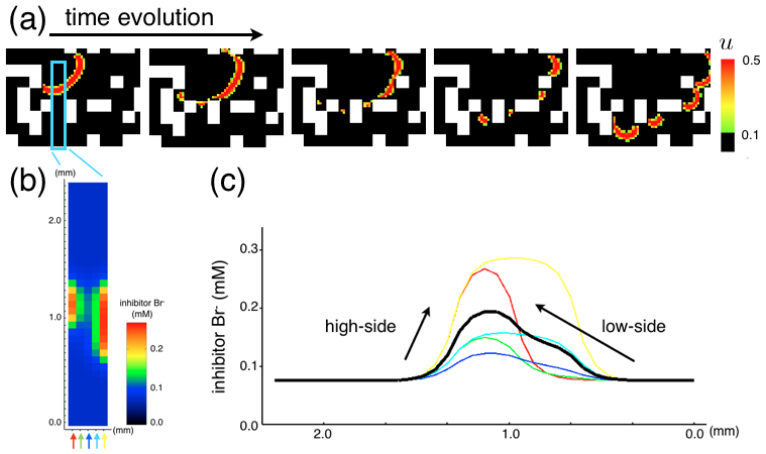

FIGURE 3.38. Wave behavior and concentration distribution of inhibitor in the case of $\phi_2 = 0.040$. (a) Chronological snapshots every 1.25 s. A wave was able to pass through the narrow gap. (b) Concentration distribution of inhibitor in the narrow gap. (c) Spatial average concentration gradient of inhibitor in the gap. The color indicates the position as shown in the bottom of (c).

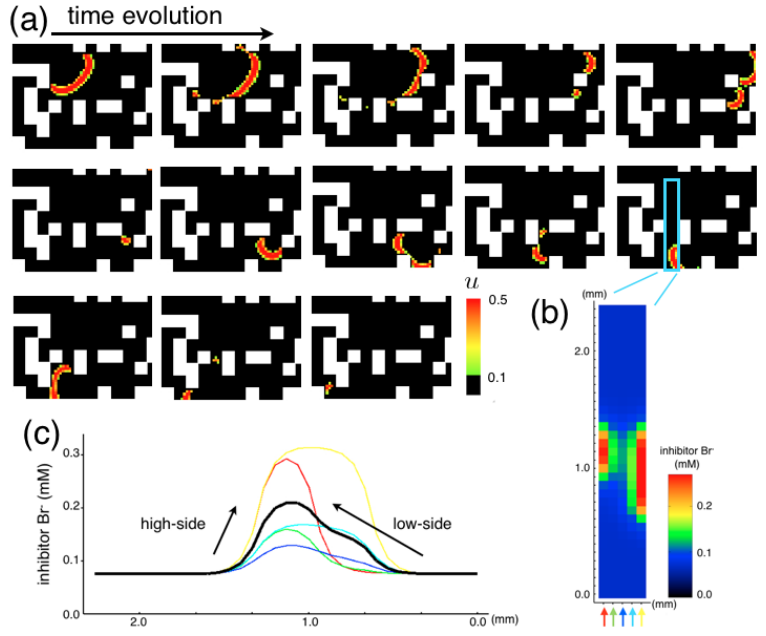

FIGURE 3.39. Wave behavior and concentration distribution of inhibitor in the case of $\phi_2 = 0.045$. (a) Chronological snapshots every 1.25 s. A wave was unable to pass through the narrow gap in both direction. (b) Concentration distribution of inhibitor in the narrow gap. (c) Spatial average concentration gradient of inhibitor in the gap. The color indicates the position as shown in the bottom of (c).

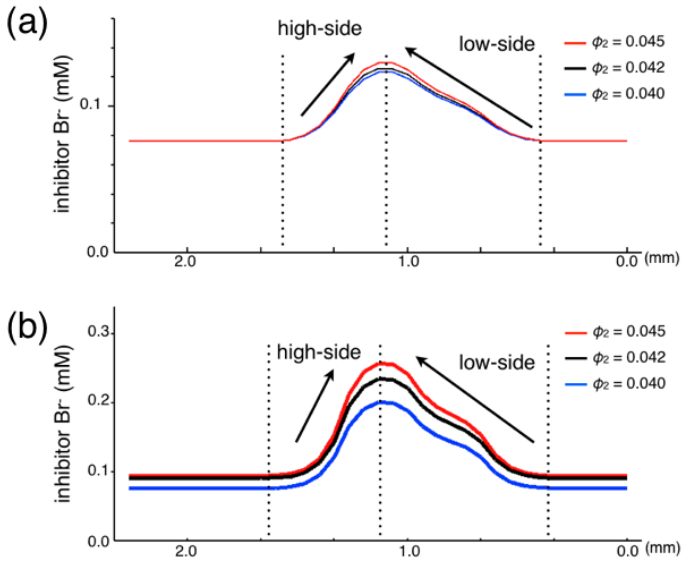

FIGURE 3.40. Concentration gradient of inhibitor at the narrow gap, (a) the middle of gap and (b) the spatial average value (blue and black lines in Figure 3.37, 3.38, and 3.39, respectively), it appears three different types of wave behavior, i.e., planar wave propagation ($\phi_2 = 0.040$), unidirectional propagation ($\phi_2 = 0.042$), and blocked wave propagation ($\phi_2 = 0.045$).

It is noted that the progress direction of wave is also significant to determine wave behavior. That is to say, the wave called planar wave propagation as shown in Figure 3.38 which could progress through the gap has possibility to be unable to pass through from opposite direction. In this case, although the gap has the potential to create unidirectional propagation, spiral wave cannot be generated.

As mentioned above, unidirectional propagation is important mechanism to generate spiral pattern in heterogeneous excitable media. It has been found that gradient of inhibitor created by heterogeneity of reaction can generate the narrow gap which has a potential to generate a unidirectional path. Furthermore, if progress direction of wave is appropriate, a spiral core occurs around the unidirectional path.

In the next section, we focus on diffusion that is the second element of heterogeneity on reaction-diffusion system.

3.3. Wave Behaviors on Two Dimensional Excitable Media with Heterogeneity of Diffusion

Here the spatial heterogeneity of diffusion term is introduced. The ferroin-catalyzed BZ reaction system with catalyst-loaded resin beads is used for realization of the experiments in heterogeneous diffusion system. At first, I would describe about the experiments.

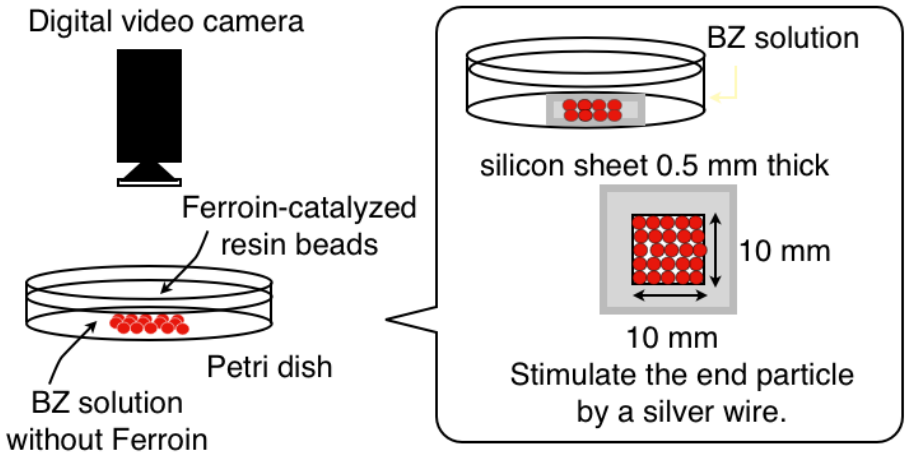

FIGURE 3.41. Experimental condition of beads BZ reaction. See Appendix B for details.

3.3.1. Beads BZ Reaction: Signatures and Experimental Setting. The particles used in the experiment were porous cation-exchange beads of 0.7 - 1.2 mm diameter that were loaded with the BZ catalyst ferroin. We performed the experiments by two conditions, $[\mathrm{Fe(phen)}_3^{2+}]$ = (i) 3.6×10^{-5} mol g^{-1} and (ii) 1.7×10^{-5} mol g^{-1}. The loaded particles were placed into a petri dish enclosed in a 10 mm square by 5 mm thick silicon sheet to prevent it from going all over, as shown in Figure 3.41.

The particles were set in catalyst-free BZ solution [Tinsley et al., 2011, 2009; Toth and Taylor, 2006], with (i) [NaBr] = 0.03 M, $[\mathrm{CH_2(COOH)_2}]$ = 0.3 M, $[\mathrm{H_2SO_4}]$ = 0.45 M, and $[\mathrm{NaBrO_3}]$ = 0.39 M, and (ii) [NaBr] = 0.025 M, $[\mathrm{CH_2(COOH)_2}]$ = 0.2 M, $[\mathrm{H_2SO_4}]$ = 0.36 M, and $[\mathrm{NaBrO_3}]$ = 0.24 M. We selected these concentration conditions for the particles being excitable media. The area ratio A_{BZ} of ferroin-catalyzed region was controlled by the number of particles, and particles were placed randomly. The particles were uniformly illuminated from below and viewed from above using a microscope fitted with a digital camera. The left line particles were stimulated by silver wire at once. The wave behaviors were easy to observe by conducting visualization analysis using *ImageJ*[1] similar to photosensitive BZ reaction. The movie recorded with a digital video camera was split into red-green-blue channels, all analyses were conducted using a green channel image. Details of experimental setting includes in Appendix B.

3.3.2. Experimental Results in Two Dimensional Discretized BZ System. As with the case of all systems which have been reported, three different types of wave behavior, i.e., blocked wave propagation, planar wave propagation, and spiral wave, were observed in 2D beads BZ system.

Figure 3.42(a) is chronological snapshots of the experimental result with concentration condition (i) in the case of blocked wave propagation, where the reduction state is colored by black and the oxidation state is bright gray. For visualization of the oxidation waves, Figure 3.42(b) was obtained

[1]ImageJ: http://rsbweb.nih.gov/ij/

by color image processing that the green channel images were colored green, and overlaid on background images of blue and red channels. A green line of oxidation wave could not propagate at a certain place. Eventually, all waves of oxidation state could not progress to a next particle. This occurs at lower area ratio of catalyzed region.

On the other hand, Figure 3.43 is chronological snapshots of the experimental result with concentration condition (i) obtained by color image processing in the case of planar wave propagation. It is clearly observed that a green line progressed from left to right hand side. This behavior appears at higher area ratio of catalyzed region. It is obviously found that a gap between each particle is smaller than the case of blocked wave propagation.

We could have just only one opportunity of observing spontaneous spiral formation in the experiment of concentration condition (ii). Note for avoiding possible misunderstandings that planar wave propagation and blocked wave propagation were also appeared in the concentration condition (ii). We could not observe the behavior of spiral formation in condition (i). The reason I used the results of condition (i) in the above figures is just from a perspective of viewability.

Figure 3.44 and 3.45 are chronological snapshots of the experimental result with concentration condition (ii) obtained by color image processing in the case of spiral formation. Figure 3.44 is that of the first 30 seconds, and Figure 3.45 is of the sequel 28 seconds.

First, let us look at the former, Figure 3.44. A green line of oxidation wave propagated from left hand side could progress to only downside of the field. We would have to focus on the gap, which was unable to be propagated a wave from bottom to top as indicated by a blue arrow. After a certain period of time, the particle was excited as indicated by a red arrow, then, a wave progressed to the down particle. It turns out that unidirectional propagation occurred. As shown in Figure 3.45, the circuit of wave propagation which was created once remained, and a wave continued to propagate in counter-clockwise.

By the experimental results, especially by the fact that blocked wave propagation appeared, the system with heterogeneity of diffusion has potential to cause time delay and propagation failure. It is difficult to observe a spiral wave in this system, however, since a position of each particle has high degree of freedom, thus, there are a lot of distributions to be considered in two dimensional system. Here, for supporting an existence of time delay and simplifying the phenomenon, let us show a basic experimental result with discretized beads arrayed in one dimension in the next section.

3.3.3. Propagation Failure Generated by Gap. The Ferroin catalyzed resin beads were placed in one dimension as shown in Figure 3.46(a), and fixed by two silicon sheets. A wave of the left edge which was excited by a silver wire has propagated to the next particle through the catalyst-free gap. Figure 3.46(b) is the spatiotemporal plot of the propagation behavior. Although a wave can propagate through the gap if the gap width is shorter than a certain value, propagation failure could occur at a large value of the gap width as shown in Figure 3.46(c). In addition, propagation time tends to increase not linearly but exponentially with respect to the gap width.

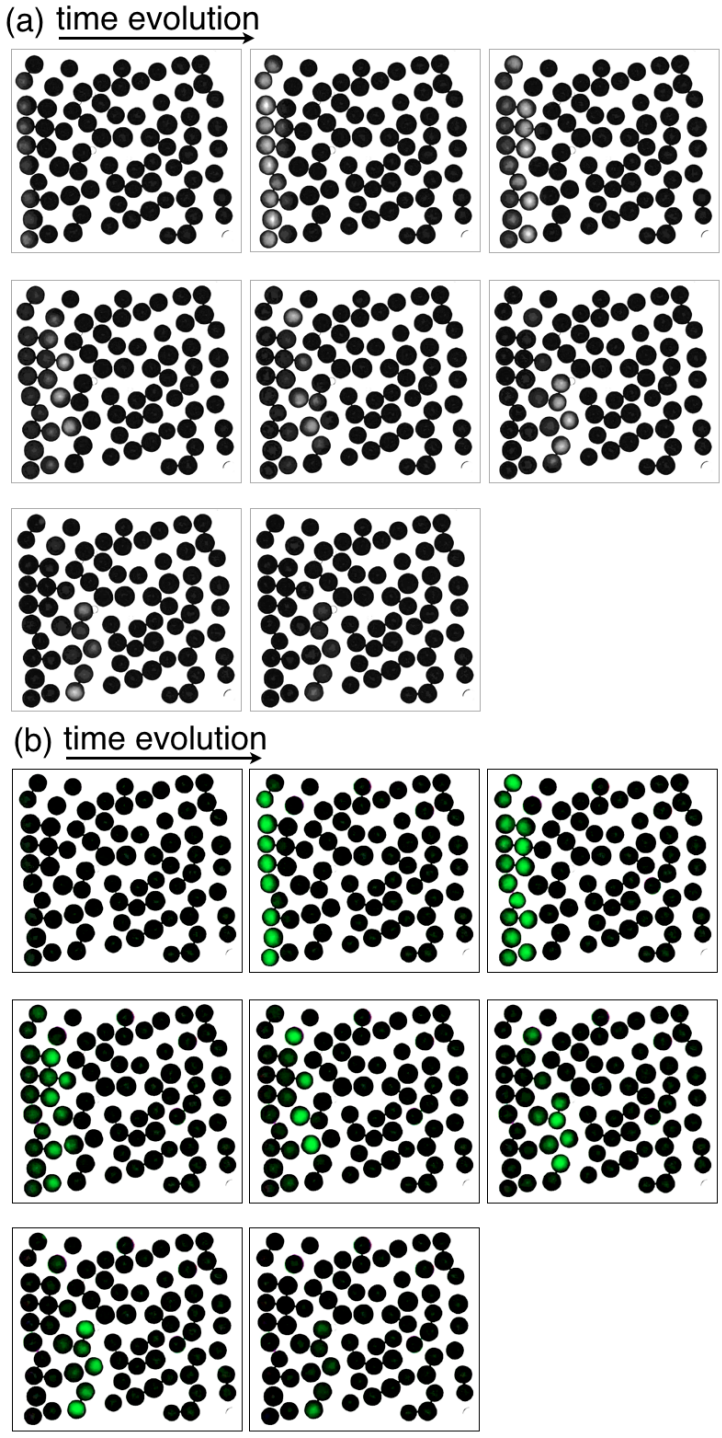

FIGURE 3.42. Chronological snapshots every 1 s of the experimental result with concentration condition (i) in the case of $A_{\mathrm{BZ}} = 0.49$, blocked wave propagation. (a) Green channel images. (b) Enhanced image of oxidation waves by color image processing.

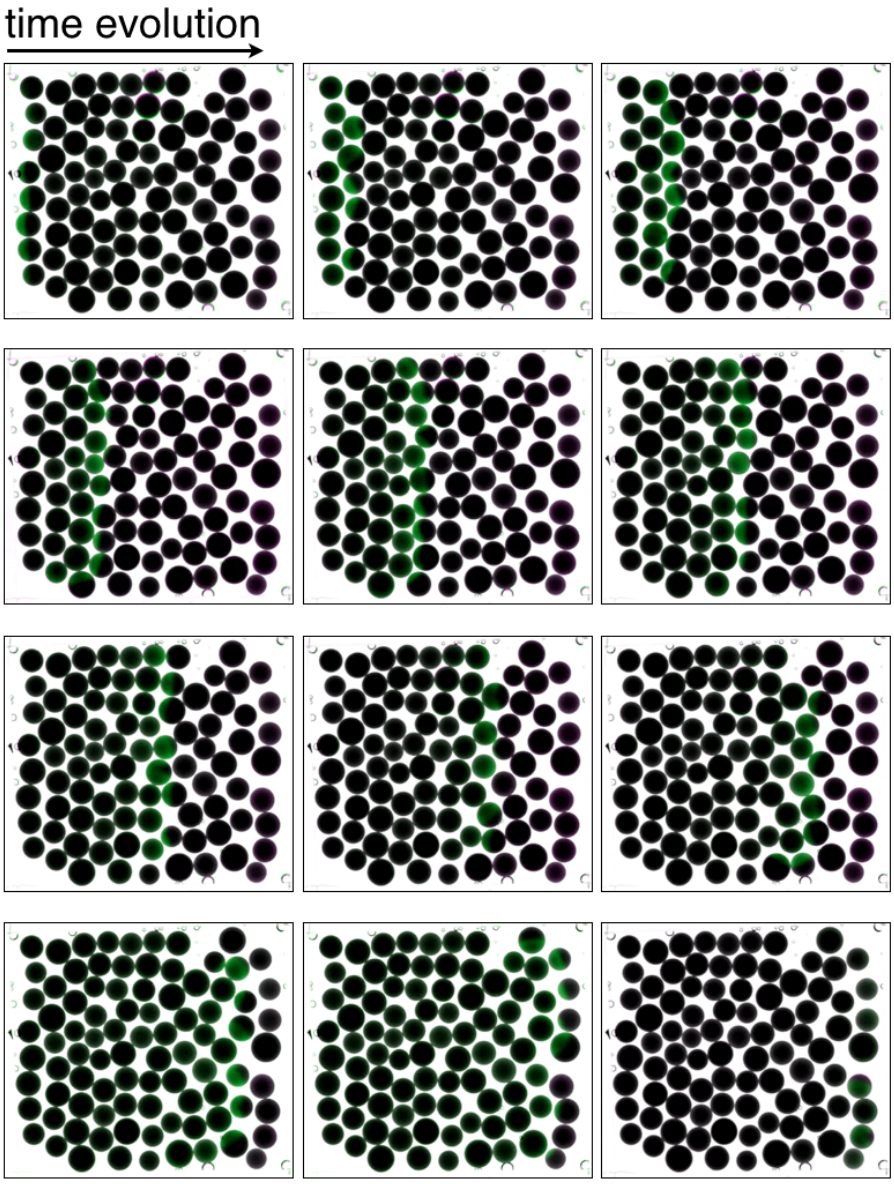

FIGURE 3.43. Chronological snapshots every 1.5 s of the experimental result with concentration condition (i) obtained by color image processing in the case of $A_{\mathrm{BZ}} = 0.61$, planar wave propagation.

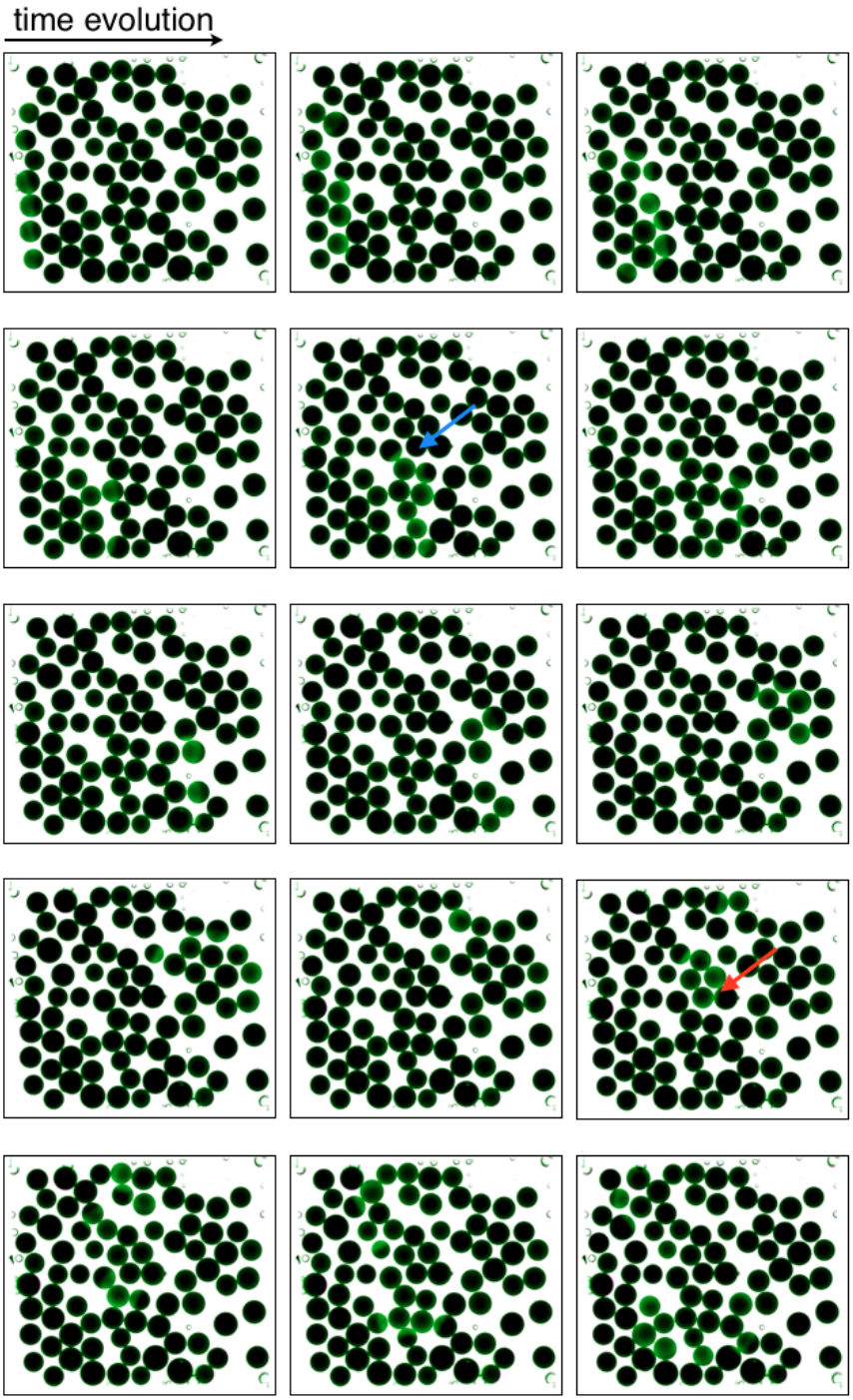

FIGURE 3.44. Chronological snapshots of the first 30 s every 2 s of the experimental result with concentration condition (ii) obtained by color image processing in the case of $A_{\mathrm{BZ}} = 0.55$, spiral formation. A wave was unable to propagate at the gap indicated by a blue arrow from bottom to top. After a certain period of time, the particle at the gap indicated by a red arrow was excited, and a wave was able to propagate from top to bottom.

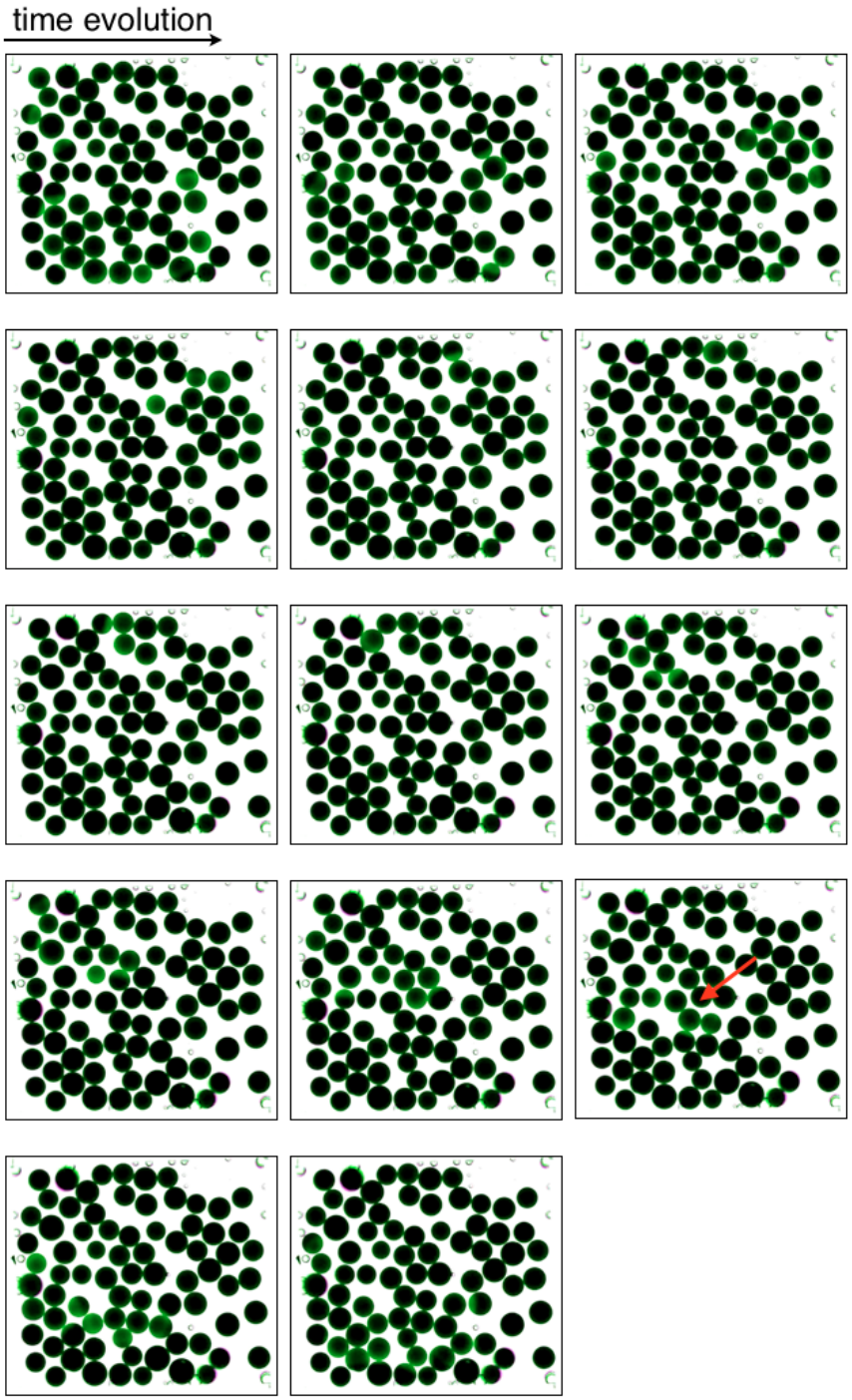

FIGURE 3.45. Chronological snapshots of the sequel 28 s every 2 s of the experimental result with concentration condition (ii) obtained by color image processing in the case of $A_{\mathrm{BZ}} = 0.55$, spiral formation. A wave progresses from top to bottom at the gap indicated by a red arrow, and continued to propagate in counter-clockwise.

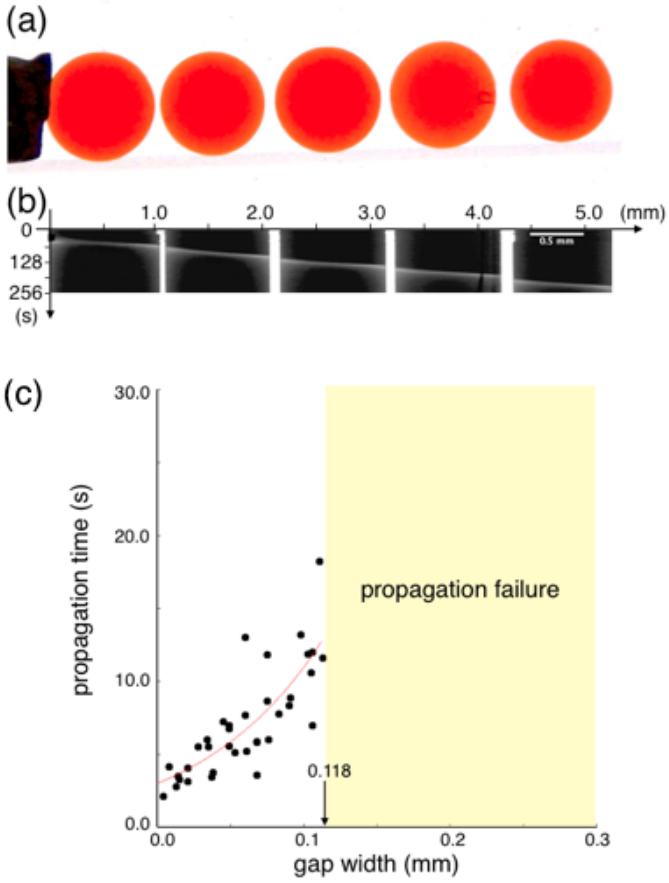

FIGURE 3.46. Experimental result with discretized beads arrayed in one dimension. (a) Beads were placed in one dimension, and the left edge particle was excited by a silver wire. (b) Spatiotemporal plot of wave propagation. (c) Relationship between the gap width and propagation time. Experimental data are plotted by black circles, and fitted curve of exponential function is drawn by red line.

Here, the gap width between particles was 0.172 mm, in the case that unidirectional propagation occurred in two dimensional reaction field as shown in Figure 3.44 and 3.45. This value is the region of propagation failure in one dimension. Although a cause of unidirectional propagation remains as an unsolved matter, it is reasonable to consider that anisotropy of array of particles generated by extension to two dimension is one of the possibility. It is difficult to elucidate the cause because of experimental data deficiency, however. It remains as a future subject.

3.4. Discussions

In all our systems of heterogeneous excitable media including heterogeneity of both reaction and diffusion as shown in Figure 3.26, 3.27, 3.28, 3.35, and 3.44, a unidirectional site was generated and a spiral core formed.

In the systems with heterogeneity of reaction, a wave produced a spiral core by coming into contact with an obstacle of suppression cells (Figure 3.26, 3.27, 3.28, and 3.35), and the wave did not vanish when it reached the same site, due to the diode characteristics. Thus, the spiral core was stabilized. We also have indicated the same behavior in numerical analysis with FitzHugh-Nagumo model [Kinoshita et al., 2013].

In another system with heterogeneity of diffusion, a wave also produced a spiral core by reaching to a comparatively wide gap between catalyzed particles, and the wave did propagate through the gap when it came back to the same location.

The necessary conditions and mechanisms explaining how a unidirectional site is formed have been investigated using the BZ reaction [Toth et al., 2009; Agladze et al., 1996; Motoike and Yoshikawa, 1999; Sendiña-Nadal et al., 2006], i.e., a chemical diode. Furthermore, some researchers have successfully constructed other types of chemical diodes in an excitable medium in which the wave propagation depends on the gradient of the excitability [Tóth et al., 2001; Ichino et al., 2009] or the incident angle of the wave [Motoike and Yoshikawa, 1999]. In our system of heterogeneous reaction, photosensitive BZ reaction, it has been obviously indicated that the wave propagation deeply depends on the gradient of the inhibitor as shown in Figure 3.40.

The unidirectional site hypothesis suggested here is a probable mechanism for spiral formation as well as the vulnerability. We have clarified that the spatial heterogeneity stochastically realizes unidirectional sites in an excitable medium, in which a single traveling wave transforms into a spiral wave. I would like emphasis that this is quite different from vulnerability originated from an interaction between two waves. From the results of the experiments and the numerical simulation, spatial heterogeneities generate unidirectional sites which induce the spiral formation.

Now, let us consider a control of wave behaviors. From medical point of view, it is a great contribution for defibrillating to propose the method of vanishing spiral waves. The current method of removing spiral reentry is to give a heart an electrical shock by the automatic external defibrillator (AED). Unfortunately, the shock is not small enough to protect a body, thus this method could carry a risk for persons whose body have been severely weakened. We should suggest the method using a slight fluctuation. In addition, a realistic one without a difficulty which has to target a necrotic cell or a defective cell is required. Here I describe an effectual method of removing spiral wave which has generated in heterogeneous reaction field along the line suggested in [Kinoshita et al., 2013].

We show using numerical simulation with the FitzHugh-Nagumo model that a unidirectional site near the spiral core is removed, and a spiral wave can be destroyed by a small change in the reaction properties of the excitable medium. The method is explained as follows, as demonstrated in Figure 3.47. At first, the right-hand edge of the media was stimulated, and we observed that the spiral wave that is generated once is rotated recursively near the spiral core before, as shown in Figure 3.47(a) “first stage”. Secondly, at any time, we lowered the excitability of the whole system slightly.

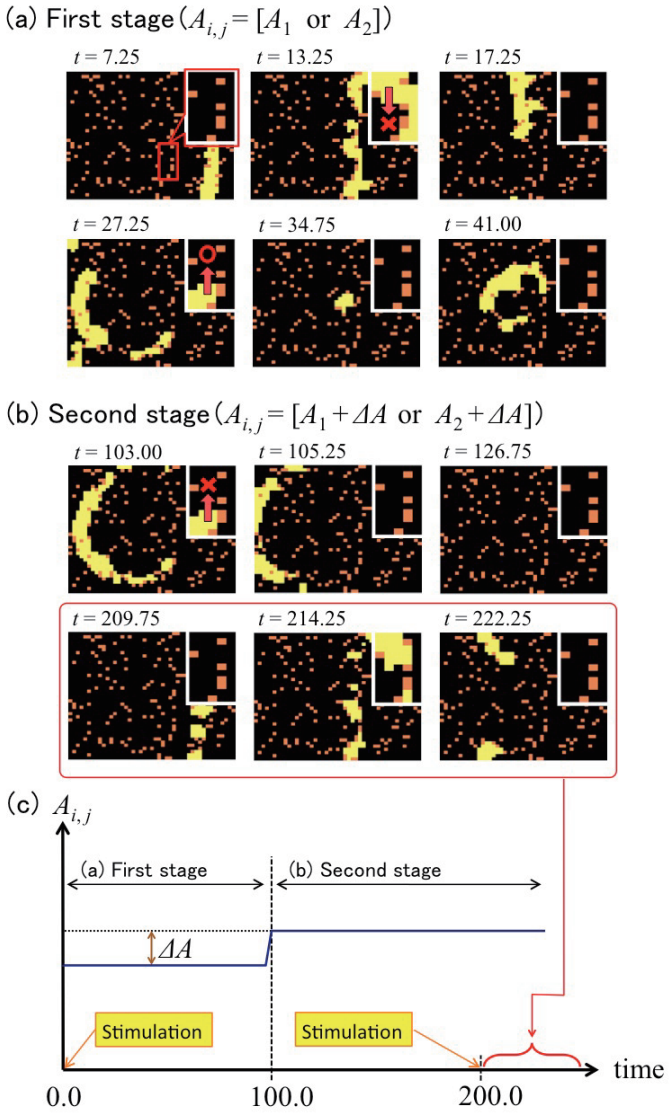

FIGURE 3.47. Snapshots of the demonstration of removing spiral waves, quoted from Figure 4 of [Kinoshita et al., 2013]. In (a) and (b), each panel shows the time sequence of excitable waves, and the insets are enlarged figures of the wave propagation near a spiral core. Orange squares indicate suppression cells, and yellow squares are excitable cells. (a) Unidirectional path has generated at a location indicated by the enlarged figures, and spiral waves are formed. (b) By a small fluctuation at t= 100, i.e., a slight increase of a constant term of inhibitor, spiral waves are removed. A new excitable wave generated by stimulation of the right-hand edge at t=200 was able to propagate normally without spiral formation. (c) A schematic of the demonstration condition.

Specifically, as shown in Figure 3.47(b) "second stage", we increased the value of a constant term of inhibitor, $A_{i,j}$ in all cells at $t = 100.0$. Even though this change is too slight compared with the original value of constants, it was able to prevent a wave from generating unidirectional site. As a result, we can confirm spiral waves are removed. Moreover, we stimulated the right edge of the excitable media at $t = 200.0$ again. In this condition, a wave has not formed a spiral pattern but propagated as a fluctuating planar wave. This demonstration has a meaningful indication that spiral formation generated in heterogeneous excitable media could be removed by a small fluctuation and transformed into a normal wave behavior.

3.5. Summary and Future Works

We have investigated the behavior of a traveling wave in heterogeneous excitable media using experiments of the photosensitive BZ reaction and the BZ reaction with discretized resin particles, and numerical calculations of the Oregonator model. In all systems, three types of wave behaviors were observed with an increase in the ratio of heterogeneity, i.e., blocked wave propagation, spiral formation, and planar wave propagation. These results agree well with other study [Bub and Shrier, 2002; Bub et al., 2002b]. Moreover, from the results of these systems, we found that the heterogeneity locally generated unidirectional sites [Toth et al., 2009; Agladze et al., 1996], which became the origin of the spiral wave. The randomly distributed sites easily generate a chemical diode that usually requires a locally anisotropic spatial configuration. Our findings reveal that Toth et al.'s idea [Toth et al., 2009] is not limited to the unrealistic condition but is a likely scenario in the case of a heterogeneous field including a random distribution. These results strongly support the idea that the generation of unidirectional sites in heterogeneous excitable media is one mechanism for the emergence of spiral waves. In addition, we have demonstrated that spiral waves can be destroyed by a small change in the properties of the excitable media. This result suggests that spiral formation may be controllable in heterogeneous excitable media in a specific parameter region.

However, I fully comprehend that many challenges still exist in both experimental and numerical study. In the experimental study with photosensitive BZ reaction, conditions which induce unidirectional propagation, especially, specific structures which could generate the gradient of inhibitor should be investigated. Additionally, the method of a control of wave behaviors suggested in the paper will be verified using photosensitive BZ reaction. On the other hand, the additional study of spiral formation in discretized resin beads BZ reaction is sufficiently needed. A high degree of freedom of heterogeneity in the system makes this study more difficult to advance. Thus to build a mathematical model which captured the essence of this experimental system has a significant meaning. We have an idea of a network model, and will investigate it. Finally, for the contribution to solution of spiral reentry and ventricular fibrillation, a practicality would be required. In this study, we aimed to reveal a common behavior of excitable waves accurately, therefore two dimensional media were considered. Three dimensional

model which captures essential factor of excitable media will be studied in future.

CHAPTER 4

Conclusion

This dissertation focused on waves and pattern dynamics in nature, and aimed to understand the mechanism of the two nonlinear phenomena, adhesive locomotion in gastropods in Chapter 2 and spiral formation in heterogeneous excitable media in Chapter 3. Mathematical model is a powerful tool to uncover a complete view of complex phenomena, and indicate a new prediction. I classified waves and pattern dynamics in nature into two kinds, i.e., the first is that they have a functional role for life maintenance, and the second is that its patterns are generated as a result of wave propagation.

Wave patterns which have a functional role for life maintenance are seen in animal locomotion, especially, what I dealt with in this dissertation was muscular contraction waves observed in gastropod's pedal foot. Over many years, lots of observations and experiments [Miller, 1974b; Lissmann, 1945a; Gray, 1968; Jones and Trueman, 1970; Parker, 1917; Barr, 1926, 1927; Lissmann, 1945b; Jones, 1973; Miller, 1974a; Trueman, 1983; Alexander, 1992a; Donovan and Carefoot, 1997; Alexander, 2002; Lai et al., 2010] had indicated that its muscular waves are sure to relate to directional motion. It had been also figured out, however, that adhesive locomotion is impossible to realize only by the muscular wave, i.e., there are other forces for motion including sliding force [Lissmann, 1945a]. In the Section 2.2, I have shown a significance of frictional control and a necessity of anisotropic interfacial friction. In my Master's thesis [Iwamoto, 2011], I focused on asymmetry of muscular waves, and proposed a ladder model using a self driven spring, Real-time Tunable Spring (RTS) [Umedachi et al., 2007], which is the same as a model in this dissertation, to compare a effectiveness of asymmetry. It was a weak point that the ladder model needed a central signal to control interfacial friction although muscular contraction waves was described as autonomous distributed system. What is needed about frictional control to achieve a locomotion is that a part of pedal is anchored on the ground and the other part is moved. A mathematical model can realize this two phase by switching between two frictional coefficients, but we should consider how animals can achieve such a frictional control. Although lifting up the pedal has been a dominant theory, it needs a complex signal from the center such as frictional control in ladder model. I considered there exists automatic control of interfacial friction such as the method which had been verified in peristaltic motion of earthworm. Hence, I focused on mucus.

Thixotropic property of mucus in gastropod has been found by M.W. Denny [Denny, 1980a,b; Denny and Gosline, 1980; Denny, 1981]. Thus the mucus of banana slug has the loop of elastic solid and viscous liquid. In the Section 2.3, I proposed a mathematical model which describes hysteresis

loop of mucus by introducing switching parameter and covers lacks of researches in Hosoi's group [Chan et al., 2005; Lauga and Hosoi, 2006; Ewoldt et al., 2007], i.e., flexibility of muscle, and motion of muscular waves depending on surrounding environments, by using RTS. Numerical calculation with our simple mathematical model revealed in the Section 2.4 that the mutual interaction between muscular contraction waves and dynamic viscoelasticity of mucus can realized an efficient locomotion. It was also showed numerically that the motion by both direct wave and retrograde wave could be understood by the same mechanism. The determination to select locomotion styles depends on physical properties. e.g., yield point of mucus, contraction ratio of muscle, and stiffness of muscle. The proposed model is simple but was able to capture essences, for example, a strong nonlinear property of mucus as shown in Lissajous' curve in the Section 2.4.5. I believe that we can deeply understand the locomotion mechanism by dealing with the adhesive locomotion of direct and retrograde waves as a bifurcation phenomenon. Moreover, the numerical results indicates direction of future experimental study on physical features of gastropods. Measurement of contraction ratio of muscle, stiffness of muscle, and of yield point of mucus should be performed. I would like investigate the relationship between methods to control interfacial friction and surrounding environments in the perspective that both of lifting up and mucus are real methods to control friction.

Next, patterns which are generated as a result of wave propagation are seen in the heart. What I focused on was spiral reentry observed in cardiac myocyte when ventricular fibrillation, which one of the cause of sudden death, occurred. Spiral reentry was proposed first by numerical calculation [Moe et al., 1964], then observed in experiments with isolated cardiac cells of animals [Allessie et al., 1977]. Although a heterogeneity of cells is indicated as a cause of spiral formation [Bub and Shrier, 2002; Bub et al., 2002b], the mechanism has not been elucidated yet. I used Belousov-Zhabotinsky (BZ) reaction and some mathematical models related to excitable media for investigating the mechanism thus we can discuss it as general issue of wave behaviors in heterogeneous excitable media. There are two heterogeneities observed in cardiac myocyte; locally decay of excitability caused by necrotic cells and weakened cells [Tsuji et al., 2000], and locally time delay of propagation or propagation failure by a change in the array of gap junctions [Uzzaman et al., 2000]. I deal with these heterogeneities as a heterogeneity of reaction or diffusion in reaction-diffusion system, and reproduced them using two kinds of BZ reaction. The experimental results were analyzed by numerical calculations with the Oregonator model, and additional perspective was gained by numerical calculations with FitzHugh-Nagumo model.

Put simply, regardless of a heterogeneity in the system as shown in the Section 3.2.2, 3.2.4, 3.3.2, and [Kinoshita et al., 2013], we obtained the same three types of wave behaviors, i.e., planar wave propagation, spiral formation, and blocked wave propagation, depending on an increase of the ratio of heterogeneity. In spiral formation, it is necessary to form a spiral core. It had been already indicated that existence of an obstacle and vulnerability

of excitable waves induce to generate a spiral core when spiral wave was formed spontaneously in BZ system [Starmer et al., 1992; Gesteira et al., 1994; Aliev, 1995; Agladze et al., 1994], but we could not understand spiral reentry which is generated by one wave since the proposed mechanism was explained by interaction between waves. In the results of this study, we have found unidirectional propagation as a probable cause of spontaneous spiral formation. In all heterogeneous systems, unidirectional path was generated spontaneously around a location created a spiral core in the process of forming a spiral wave. This is an interesting self-organized example that anisotropy characteristic was generated. The cause of unidirectional path would depend on the kind of heterogeneity. In the photosensitive BZ reaction system which describes a heterogeneity of reaction, it has been revealed by numerical analysis with the Oregonator model in the Section 3.2.5 that concentration gradient of inhibitor could induce unidirectional propagation. In the BZ system with catalyst loaded resin beads, time delay of propagation and propagation failure would relate deeply to it, but a new mathematical model would be needed to explain details. Even though additional researches will be required, fortunately, we have already obtained a ray of light for control of waves. That is to say, we just have to remove the unidirectional path to break spiral waves. We demonstrated the method to remove a spiral wave using FitzHugh-Nagumo model in the Section 3.4; unidirectional path was broken by decreasing a excitability of whole reaction field, then spiral wave was removed. A excitable wave induced by a stimuli again propagated as a planar wave. This method will be considered in future as more safe than the current method to remove spiral waves by automatic external defibrillator (AED). Some questions have still remained, however. A causing structure of unidirectional propagation should be clear.

Finally, I summarize this dissertation simply in Figure 4.1. I took two nonlinear phenomena for example. In animal locomotion, I considered there is a common logic of locomotion mechanism, hence, dealt with adhesive locomotion as the simplest locomotion. In this study, adhesive locomotions of direct wave and retrograde wave were achieved by the mutual interaction between muscular contraction waves and frictional control of mucus. By the result of this study, two factors, i.e., autonomous distributed system with oscillators and (automatic) control of friction, could be suggested as minimum required logic of all adhesive locomotion mechanism. On the other hand, in the study of pattern formation on heterogeneous excitable media, three general behaviors of waves was observed in all inhomogeneous systems including experiments of BZ reaction and some mathematical models. Significantly, unidirectional propagation which was induced spontaneously by heterogeneity was revealed as a common mechanism of spiral formation.

In this dissertation, two different phenomena related to waves and pattern dynamics were taken up. Mathematical models were enable us to generalize each phenomenon in a broad perspective, and to understand that deeply. Additionally, future experimental problems were suggested by numerical results of mathematical model. I believe that science will develop furthermore by understanding complex phenomena using mathematical model, and I hope I will be able to contribute to that.

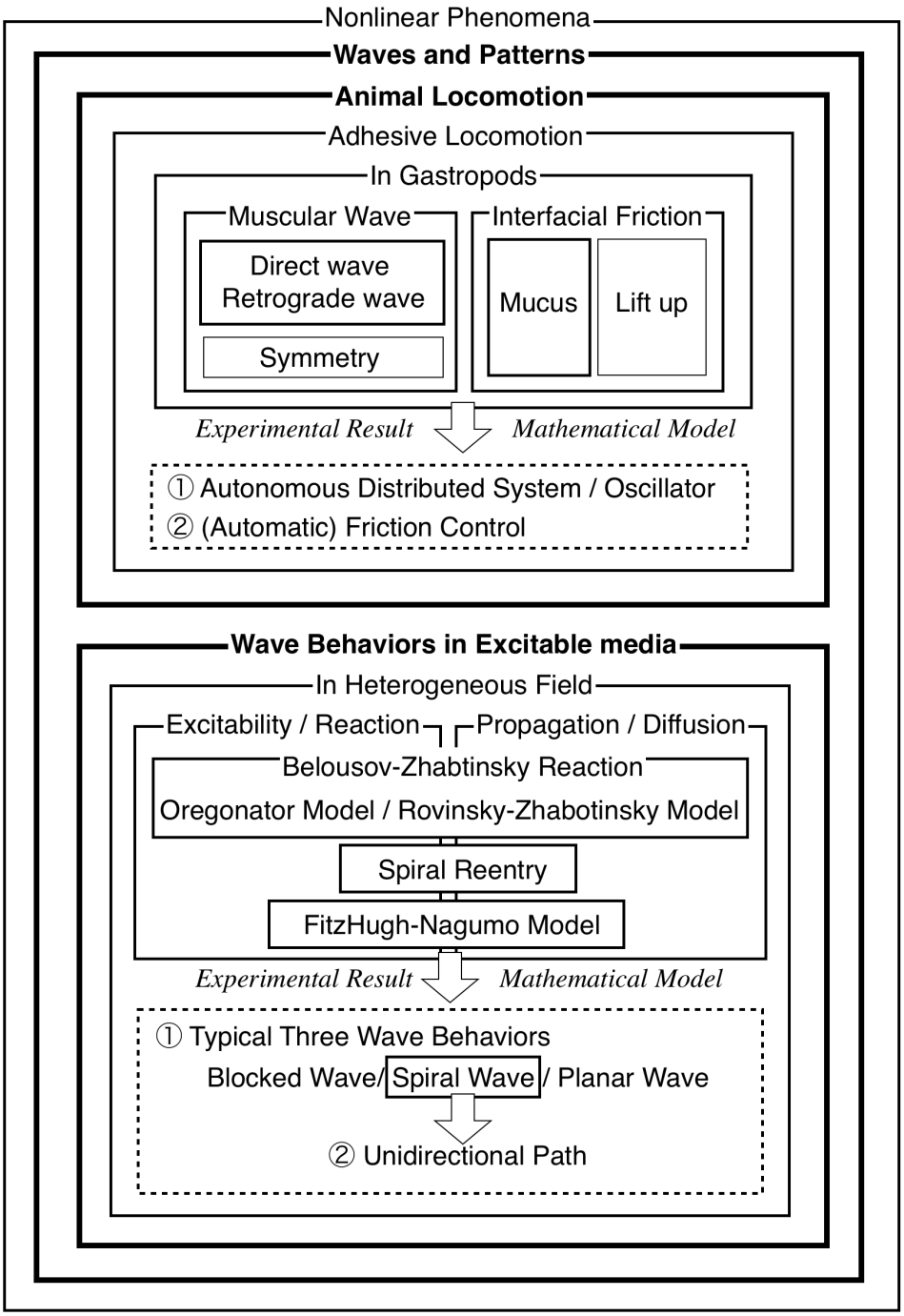

FIGURE 4.1. Summary of this dissertation.

References

Agladze, K., Aliev, R., Yamaguchi, T., and Yoshikawa, K. (1996). Chemical diode. *J. Phys. Chem.*, 100:13895–13897.

Agladze, K., Keener, J. P., Müller, S. C., and Panfilov, A. (1994). Rotating spiral waves created by geometry. *Science*, 264:1746–1748.

Alexander, R. M. (1992a). *Exploring Biomechanics: Animals in Motion.* Freeman and Company, New York, NY/Oxford, UK.

Alexander, R. M. (1992b). *Exploring Biomechanics: Animals in Motion (in Japanese).* NIKKEI SCIENCE Inc. A. Azuma (trans.).

Alexander, R. M. (2002). *Principles of Animal Locomotion*, pages 86–90, 166–180. Princeton University Press, Princeton, NJ/Oxford, UK.

Aliev, R. R. (1995). Heart tissue simulations by means of chemical excitable media. *Chaos, Solitons & Fractals*, 5:567–574.

Allessie, M. A., Bonke, F. I., and Schopman, F. J. (1977). Circus movement in rabbit atrial muscle as a mechanism of tachycardia. iii. the "leading circle" concept: a new model of circus movement in cardiac tissue without the involvement of an anatomical obstacle. *Circ. Res.*, 41:9–18.

Allessie, M. A., Bonke, F. I. M., and Scopman, T. Y. G. (1973). Circus movement in rabbit atrial muscle as a mechanism of tachycardia. *Circ. Res.*, 33:54–62.

Amemiya, T., Kádár, S., Kettunen, P., and Showalter, K. (1996). Spiral wave formation in three-dimensional excitable media. *Phys. Rev. Lett.*, 77:3244–3247.

Amemiya, T., Ohmori, T., Nakaiwa, M., and Yamaguchi, T. (1998). Two-parameter stochastic resonance in a model of the photosensitive belousov-zhabotinsky reaction in a flow system. *J. Phys. Chem. A*, 102:4537–4542.

Ball, P. (2011). *Shapes Nature's patterns (in Japanese).* Hayakawa Pub. Co., Ltd. M. Hayashi (trans.).

Barr, R. A. (1926). Some observations on the pedal gland of *milax*. *Q. J. Microsc. Sci.*, 70:647–667.

Barr, R. A. (1927). Some notes on the mucous and skin glands of *arion ater*. *Q. J. Microsc. Sci.*, 71:503–525.

Belousov, B. P. (1959). A periodic reaction and its mechanism (in russian). *Sb. Ref. Radiats. Med. za 1958, Medgiz. Moacow*, 1:145.

Belousov, B. P. (1985). *Oscillations and traveling waves in chemical systems*, chapter A periodic reaction and its mechanism. Wiley-Interscience, New York.

Bolotnik, N., Pivovarov, M., Zeidis, I., and Zimmermann, K. (2011). The undulatory motion of chain of particles in a resistive medium. *ZAMM*, 91(4):259–275.

Braune, M. and Engel, H. (1993). Compound rotation of spiral waves in a light-sensitive belousov-zhabotinsky medium. *Chem. Phys. L.*, 204(3-4):257–264.

Bub, G. and Shrier, A. (2002). Propagation through heterogeneous substrates in simple excitable media models. *Chaos*, 12:747.

Bub, G., Shrier, A., and Glass, L. (2002a). Spiral wave generation in heterogeneous excitable media. *Phys. Rev. L.*, 88:058101.

Bub, G., Shrier, A., and Glass, L. (2002b). Spiral wave generation in heterogeneous excitable media. *Phys. Rev. Lett.*, 8:058101.

Budrene, E. O. and Berg, H. C. (1991). Complex patterns formed by motile cells of *escherichia coli*. *nature*, 349:630–633.

Burghes, D. N. and Borrie, M. S. (1981). *Modelling with Differential Equations (Mathematics and Its Applications)*. Ellis Horwood Ltd., Publisher.

Burghes, D. N. and Borrie, M. S. (1990). *Modelling with Differential Equations (Mathematics and Its Applications) (in Japanese)*. Nihon Hyoron Sha Co., Ltd. T. Kakita (trans.) and H. Ohmachi (trans.).

Busse, H. and Hess, B. (1973). nformation transmission in a diffusion-coupled oscillatory chemical system. *Nature*, 244:203–305.

Chan, B., Balmforth, N. J., and Hosoi, A. E. (2005). Building a better snail: lubrication and adhesive locomotion. *Phys. Fluids*, 17:113101.

Chernous'ko, F. L. (2011). Analysis and optimization of the rectilinear motion of two-body system. *Appl. Math. Mech.*, 75(5):493–500.

Denny, M. W. (1980a). Locomotion : the cost of gastropod crawling. *Science*, 208:1288–1290.

Denny, M. W. (1980b). The role of gastropod pedal mucus in locomotion. *Nature*, 285:160–161.

Denny, M. W. (1981). A quantitative model for the adhesive locomotion of the terrestrial slug, *ariolimax columbianus*. *J. Exp. Biol.*, 91:195–217.

Denny, M. W. and Gosline, J. M. (1980). The physical properties of the pedal mucus of the terrestrial slug, *ariolimax columbianus*. *J. Exp. Biol.*, 88:375–393.

Donovan, D. A. and Carefoot, T. H. (1997). Locomotion in the abalone haliotis kamtschatkana: pedal morphology and cost of transport. *J. Exp. Biol.*, 200:1145–1153.

Dubois, R. and Vles, F. (1907). Locomotion des gasteropodes. *Compt. Rend. Acad. Sci. Paris*, 144:658–659.

Dupont, C., Agladze, K., and Krinsky, V. (1998). Excitable medium with left—right symmetry breaking. *Physica A*, 249:47—52.

Dvorak, V. F. (1984). Tropical cyclone intensity analysis using satellite data. *NOAA technical report NESDIS*, 11.

Edelson, D., Noyes, R. M., and Field, R. J. (1979). Mechanistic details of the belousov-zhabotinsky oscillations. ii. the organic reaction subset. *Int. J. Chem. Kinetics*, 6:155–164.

Ertl, G. (1991). Oscillatory kinetics and spatio-temporal self-organization in reactions at solid surfaces. *Science*, 254:1750–1755.

Ewoldt, R. H., Clasen, C., Hosoi, A. E., and McKinley, G. H. (2007). Rheological fingerprinting of gastropod pedal mucus and synthetic complex fluids for biomimicking adhesive locomotion. *Soft Matter*, 3:634–643.

Field, R. J. and Noyes, R. M. (1974). Oscillations in chemical systems. iv. limit cycle behavior in a model of a real chemical reaction. *J. Chem. Phys.*, 60:1877.

Field, R. J. and Noyes, R. M. (1975). Mechanistic details of the belousov-zhabotinskii oscillations. *Inter. J. Chem. Kinet.*, 7:417–432.

Filed, R. J., Körös, E., and Noyes, R. M. (1972). Oscillations in chemical systems. ii. through analysis of temporal oscillation in the bromate-cerium-malonic acid system. *J. Am. Chem. Soc.*, 94(25):8649–8664.

from his archives, dated 1951, B. P. B. (1981). *Autowave Processes in Systems with Diffusion (in Russian)*, page 178. USSR Academy of Sciences lnstitute of Applied Physics, Gorky.

Fujikawa, H. and Matsushita, M. (1989). Fractal growth of *bacillus subtilis* on agar plates. *J. Phys. Soc. Japan*, 58(11):3875–3878.

Gäspär, V., Bazsa, G., and Beck, M. (1983). The influence of visible light on the belousov-zhabotinskii oscillating reactions applying different catalysts. *Z. Phys. Chem. (Leipzig)*, 264:43–48.

Gesteira, M. G., Garcia, G. F., Mufiuzuri, A. P., Prrez-Mufiuzuri, V., Krinsky, V. I., Starmer, C. F., and Perez-Villar, V. (1994). Vulnerability in excitable belousov-zhabotinsky medium: from 1d to 2d. *Physica D*, 76:359.

Gomez-Gesteira, M., del Castillo, J. L., Vazquez-Iglesias, M. E., Perez-Munuzuri, V., and Perez-Villar, V. (1994). Influence of the critical curvature on spiral initiation in an excitable medium. *Phys. Rev. E*, 50:4646–4649.

Gray, J. (1968). *Animal Locomotion*. George Weidenfeld and Nicolson Ltd., London, UK.

Gray, J. and Lissmann, H. W. (1938). Studies in locomotion. vii. locomotory reflexes in the earthworm. *J. Exp. Biol.*, 15:506—517.

Gray, R. A. and Jalife, J. (1996). Spiral waves and the heart. *International Journal of Bifurcation and Chaos*, 6:415.

Grimm-Jorgensen, Y., Ducor, M. E., and Piscatelli, J. (1986). Surface mucus production in gastropods is dependent on environmental salinity and humidity. *Comp. Biochem. Physiol.*, 83A(3):415–419.

Gros, D. B. and Jongsma, H. J. (1996). Connexins in mammalian heart function. *Bioessays.*, 18:719–730.

Hanazaki, I. (1992). Cross section of light-induced inhibition and induction of chemical oscillations. *J. Phys. Chem.*, 96:5652–5657.

Ichino, T., Fujio, K., Matsushita, M., and Nakata, S. (2009). Wave propagation in the photosensitive belousov-zhabotinsky reaction across an asymmetric gap. *J. Phys. Chem.*, 113:2304–2308.

Inada, H., Kodama, I., Sakuma, I., and Nakazawa, K. (2006). *Why So Cardiac Arrhythmias Occur? – Experimental, In-silico, and Clinical Approach – (in Japanese)*. CORONA PUB. CO., LTD.

Iwamoto, M. (2011). Experimantal and mathematical researches on crawling locomotion in gastropods (in japanese). Master thesis (Hiroshima University, Japan).

Iwamoto, M., Ueyama, D., and Kobayashi, R. (2013). The advantage of mucus for adhesive locomotion in gastropods. submitted.

Jahnke, W., Skaggs, W. E., and Winfree, A. T. (1989). Chemical vortex dynamics in the belousov-zhabotinsky reaction and in the two-variable oregonator model. *J. Phys. Chem.*, 93:740–749.

Jalife, J., Gray, R. A., Morley, G. E., and Davidenko, J. M. (1998). Self-organization and the dynamical nature of ventricular fibrillation. *Chaos*, 8:79–93.

Jensen, N. O. and Agee, E. M. (1978). Vortex cloud street during amtex 75. *Tellus*, 30:517–523.

Jinguji, M., Ishihara, M., and Nakazawa, T. (1990). Photoinduced formation of spatial patterns in the belousov-zhabotinskii reaction. *J. Phys. Chem.*, 94:1226–1229.

Jones, H. D. (1973). The mechanism of locomotion in *agriolimax reticulatus* (mollusca; gastropoda). *J. Zool., Land.*, 171:489–498.

Jones, H. D. and Trueman, E. R. (1970). Locomotion of the limpet, *patella vulgata l. J. Exp. Biol.*, 52:201–216.

Kádár, S., Amemiya, T., and Showalter, K. (1997). Reaction mechanism for light sensitivity of the ru(bpy)$_3^{2+}$-catalyzed belousov-zhabotinsky reaction. *J. Phys. Chem. A*, 101:8200–8206.

Kapral, R. (1991). Discrete models for chemically reacting systems. *J. Math. Chem.*, 6:113–163.

Kapral, R. and Showalter, K., editors (1995). *Chemical Waves and Patterns*. Kluwer, Dordrecht, Netherlands.

Keener, J. P. (1991). An eikonal-curvature equation for action potential propagation in myocardium. *J. Mathe Biol.*, 29:629–651.

Keener, J. P. and Phelps, F. M. (1989). Consequences of the cellular, znisotropic structure of myocardium. *in: Lectures on Mathematics in Life Sciences*, 21:151–181.

Keener, J. P. and Tyson, J. J. (1986). Spiral waves in the belousov-zhabotinskii reaction. *Physica D*, 21:307–324.

Kim, K., Kim, Y., and Kim, D. (2010). Adhesion characteristics of the snail foot under various surface conditions. *Inter. J. Pre. Eng. Man.*, 11(4):623–628.

Kinoshita, S., Iwamoto, M., Tateishi, K., Suematsu, N. J., and Ueyama, D. (2013). Mechanism of spiral formation in heterogeneous discretized excitable media. *Phys. Rev. E*, 87:062815.

Klausmeier, C. A. (1999). Regular and irregular patterns in semiarid vegetation. *Science*, 284:1826–1828.

Kobayashi, R., Tero, A., and Nakagaki, T. (2006). Mathematical model for rhythmic protoplasmic movement in the true slime mold. *J. Math. Biol.*, 53:273—286.

Kondo, S. and Asai, R. (1995). A reaction-diffusion wave on the skin of the marine angelfish *pomacanthus*. *Nature*, 376:765–768.

Krug, H. J., Pohlmann, L., and Kuhnert, L. (1990). Analysis of the modified complete oregonator accounting for oxygen sensitivity and photosensitivity of belousov-zhabotinsky systems. *J. Phys. Chem.*, 94:4862–4866.

Kuhnert, L. (1986). A new optical photochemical memory device in a light-sensitive chemical active medium. *Nature*, 319:393–394.

Kuhnert, L., Agladze, K. I., and Krinsky, V. I. (1989). Image processing using light-sensitive chemical waves. *Nature*, 337:244–247.

Lai, J. H., del Alamo, J. C., Rodríguez-Rodríguez, J., and Lasheras, J. C. (2010). The mechanics of the adhesive locomotion of terrestrial gastropods. *J. Exp. Biol.*, 213:3920–3933.

Lancaster, N. (1995). *Geomorphology of desert dunes*. London: Routledge.

Lauga, E. and Hosoi, A. E. (2006). Tuning gastropod locomotion: modeling the influence of mucus rheology on the cost of crawling. *Phys. Fluids*, 18:113102.

Lechleiter, J. D., John, L. M., and Camacho, P. (1998). Ca^{2+} wave dispersion and spiral wave entrainment in *xenopus laevis* oocytes overexpressing ca^{2+} atpases. *Bio. Chem.*, 72:123–129.

Lissmann, H. W. (1945a). The mechanism of locomotion in gastropod molluscs. i. kinematic. *J. Exp. Biol.*, 21:58–69.

Lissmann, H. W. (1945b). The mechanism of locomotion in gastropod molluscs. ii. kinetics. *J. Exp. Biol.*, 22:37–50.

Lister, M. (1694). *Exercitatio Anatomica in qua de Cochleis maxime terrestribuset Limacibus agitur*. London.

Lovis, F., Smolinsky, T., Locatelli, A., Niño, M., and Imbihl, R. (2012). Chemical waves and rate oscillations in the $h_2 + o_2$ reaction on a bimetallic rh(111)/ni catalyst. *Phys. Chem. C*, 116:4083–4090.

Macfadyen, W. A. (1950). Vegetation patterns in the semidesert plains of british domaliland. *Geog. J.*, 116(4):199–211.

Maselko, J., Reckley, J. S., and Showalter, K. (1989). Regular and irregular spatial patterns in an immobilized-catalyst belousov-zhabotinsky reaction. *J. Phys. Chem.*, 93:2774–2780.

Maselko, J. and Showalter, K. (1991). Chemical waves in inhomogeneous excitable media. *Physica D*, 49:21–32.

McBRIDE, E. F. (2003). Pseudofaults resulting from compartmentalized liesegang bands: update. *Sedimentology*, 50:725—730.

Meinhardt, H. (1982). *Models of biological pattern formation*. London Academic Press.

Meinhardt, H. and Klingler, M. (1987). A model for pattern formation on the shells of molluscs. *J. theor. Biol.*, 126:63–89.

Miller, S. L. (1974a). Adaptive design of locomotion and foot form in prosobranch gastropods. *J. exp. Biol. Ecol.*, 14:99–156.

Miller, S. L. (1974b). The classification, taxonomic distribution, and evolution of locomotor types among prosobranch gastropods. *Proc. Malac. Soc. Lond.*, 41:233–261.

Moe, G. K., Rheinboldt, W. L., and Abildskov, J. A. (1964). A computer model of atrial fibrillation. *Am. Heart J.*, 67:200–220.

Mori, Y., Nakamichi, Y., Sekiguchi, T., Okazaki, N., Matsumura, T., and Hanazaki, I. (1993). Photo-induction of chemical oscillation in the belousov-zhabotinsky reaction under the flow condition. *Chem. Phys. Lett.*, 211:421–424.

Motoike, I. and Yoshikawa, K. (1999). Information operations with an excitable field. *Phys. Rev. E*, 59:5354–5360.

Motoike, I. N., Yoshikawa, K., Iguchi, Y., and Nakata, S. (2001). Real-time memory on an excitable field. *Phys. Rev. E*, 63:036220.

Murray, J. D. (1981). A pre-pattern formation mechanism for animal coat markings. *J. Theor. Biol.*, 88:161–199.

Murray, J. D. (1989). *Mathematical biology*. New York: Springer-Verlag.

Nagy-Ungvarai, Z., Ungvarai, J., Müller, S. C., and Hess, B. (1992). The role of curvature and pulse width for transition to unstable wave fronts in the belousov-zhabotinsky reaction. *J. Chem. Phys.*, 97:1004.

Nakata, S., Matsushita, M., Sato, T., Suematsu, N., Kitahata, H., Amemiya, T., and Mori, Y. (2011). Photoexcited chemical wave in the ruthenium-catalyzed belousov-zhabotinsky reaction. *J. Phys. Chem. A*, 115:7406–7412.

Noyes, R. M., Filed, R. J., and Körös, E. (1972). Oscillations in chemical systems. i. detailed mechanism in a system showing temporal oscillations. *J. Am. Chem. Soc.*, 94(4):1394–1395.

Parker, G. H. (1911). The mechanism of locomotion in gastropods. *J. Morphol.*, 22:155–170.

Parker, G. H. (1917). The pedal locomotion of the sea-hare *aplysia californica*. *J. Exp. Zool.*, 24:139–145.

Prigogine, I. and Balescu, R. (1955). Sur les proprétés différentielles de la production d'entropie ii. *Bull. Cl. Sci. Acad. Roy. Belg.*, 41:917.

Rovinsky, A. B. (1986). Spiral waves in a model of the ferroin catalyzed belousov-zhabotinsky reaction. *J. Phys. Chem.*, 90:217–219.

Rovinsky, A. B. and Zhabotinsky, A. M. (1984). Mechanism and mathematical model of the oscillating bromate-ferroin-bromomalonic acid reaction. *J. Phys. Chem. L.*, 88(25):6081–6084.

Schwämmle, V. and Herrmann, H. J. (2003). Solitary wave behaviour of sand dunes. *Nature*, 426:619–620.

Scott, S. K. (1994). *Oscillations, Waves, and Chaos in Chemical Kinetics*. Oxford Univ. Press, Oxford.

Sendiña-Nadal, I., de Castro, M., and Gesteira, M. G. (2006). Kinematic description of wave propagation through a chemical diode. *Chaos*, 16:033110.

Sendiña-Nadal, I., de Castro, M., Sagués, F., and Gesteira, . M. G. (2002). Unidirectional mechanism for reentrant activity generation in excitable media. *Phys. Rev. E*, 66:016215.

Shajahan, T. K., Borek, B., Shrier, A., and Glass, L. (2011). Scaling properties of conduction velocity in heterogeneous excitable media. *Phys. Rev. E*, 84:046208.

Shoji, H., Mochizuki, A., Iwasa, Y., Hirata, M., Watanabe, T., Hioki, S., and Kondo, S. (2003). Origin of directionality in the fish stripe pattern. *Dev. Dyn.*, 226:627–633.

Showalter, K. (1980). Pattern formation in a ferroinbromate system. *J. Chem. Phys.*, 73:3735.

Shreif, Z., Mandalian, L., Abi-Haydar, A., and Sultan, R. (2004). Taming ring morphology in 2d co(oh)$_2$ liesegang patterns. *Phys. Chem. Chem. Phys.*, 6:3461—3466.

Simroth, H. (1879). Die bewegung unserer landschnecken, hauptsachlich erortert an der sohle des. *Limax. Z. Wiss. Zool.*, 22:284.

Skinner, G. S. and Swinney, H. L. (1991). Periodic to quasiperiodic transition of chemical spiral rotation. *Physica D*, 48:1–16.

Smyth, W. D. and Moum, J. N. (2012). Ocean mixing by kelvin-helmholtz instability. *Oceanography*, 25(2):140–149.

Starmer, C. F., Krinsky, V. I., Romashko, D. S., Aliev, R. R., and Stepanov, M. R. (1992). *Pulse chemistry of vortices suppression in cardiac muscle*, pages 254–256. Projekt Verlag.

Steigenberger, J. and Behn, C. (2012). *Worm-Like Locomotion Systems - An intermediate theoretical Approach*. Oldenbourg, München.

Steinbock, O., Kettunen, P., and Showalter, K. (1995). Anisotropy and spiral organizing centers in patterned excitable media. *Science*, 269:1857–1860.

Suematsu, N. J., Sato, T., Motoike, I. N., Kashima, K., and Nakata, S. (2011). Density wave propagation of a wave train in a closed excitable medium. *Phys. Rev. E*, 84:046203.

Tanaka, Y., Ito, K., Nakagaki, T., and Kobayashi, R. (2011). Mechanics of peristaltic locomotion and role of anchoring. *J. R. Soc. Interface*, 9:222–233.

Taylor, A. F., Tinsley, M. R., Wang, F., Huang, Z., and Showalter, K. (2009). Dynamical quorum sensing and synchronization in large populations of chemical oscillators. *Science*, 323:614–617.

Tinsley, M. R., Taylor, A. F., Huang, Z., and Showalter, K. (2009). Emergence of collective behavior in groups of excitable catalyst-loaded particles: Spatiotemporal dynamical quorum sensing. *Phys. Rev. Lett.*, 102:158301.

Tinsley, M. R., Taylor, A. F., Huang, Z., and Showalter, K. (2011). Complex organizing centers in groups of oscillatory particles. *Phys. Chem. Chem. Phys.*, 13:17802–17808.

Tomchik, K. J. and Devreotes, P. N. (1981). Adenosine 3',5' - monophosphate waves in *dictyostelium discoideum*: A demonstration by isotope dilution – fluorography. *Science*, 212(4493):443–446.

Tóth, A., Horvátha, D., and Yoshikawa, K. (2001). Unidirectional wave propagation in one spatial dimension. *Chemical Physics Letters*, 345:471–474.

Toth, R., de Lacy Costello, B., Stone, C., Masere, J., Adamatzky, A., and Bull, L. (2009). Spiral formation and degeneration in heterogeneous excitable media. *Phys. Rev. E*, 79:035101(R).

Toth, R. and Taylor, A. F. (2006). Loss of coherence in a population of diffusively coupled oscillators. *J. Chem. Phys.*, 125:224708.

Trueman, E. R. (1983). Locomotion in gastropods. *Mollusca*, 4:155–198.

Tsuji, Y., Opthof, T., Kamiya, K., Yasui, K., Liu, W., Lu, Z., and Kodama, I. (2000). Pacing-induced heart failure causes a reduction of delayed rectifier potassium currents along with decreases in calcium and transient outward currents in rabbit ventricle. *Cardiovascular Research*, 48:300—309.

Turing, A. M. (1952). The chemical basis of morphogenesis. *Philos. Trans. R. Soc. Lond. Ser. B Biological*, 237:37–72.

Tyson, J. J. and Fife, P. C. (1980). Target patterns in a realistic model of the belousov-zhabotinskii reaction. *J. Chem Phys.*, 73:2224–2237.

Umedachi, T., Yamada, Y., and Ishiguro, A. (2007). Development of a real-time tunable spring -toward independent control of position and stiffness of joints. *J. Robo. Mech.*, 19:27–33.

Uzzaman, M., Honjo, H., Takagishi, Y., Emdad, L., Magee, A. I., Severs, N. J., and Kodama, I. (2000). Remodeling of gap junctional coupling in hypertrophied right ventricles of rats with monocrotaline-induced pulmonary hypertension. *Circ. Res.*, 86:871–878.

Valentin, C., d'Herbès, J. M., and Poesen, J. (1999). Soil and water components of banded vegetation patterns. *CATENA*, 37:1–24.

van Capelle, F. J. L., Janse, M. J., Varghese, P. J., Freud, G. E., Mater, C., and Durrer, D. (1972). Spread of excitation in the atrioventricular node of isolated rabbit hearts studied by multiple microelectrode recording. *Circulation Research*, 31:602–616.

Vavilin, V. A., Gulak, P. V., Zhabotinsky, A. M., and Zaikin, A. N. (1969). Complex iron ions as catalysts for the autooscillating oxidation of malonic acid and its analogs with bromate. *Proc. Acad. Sci. UUUR, Ser Chem.*, 11:2618.

Vavilin, V. A. and Zaikin, A. N. (1971). The effect of solution stirring on the rate of autocatalytic reaction. *Kinet. Catal.*, 12:1045.

Vavilin, V. A., Zhabotinsky, A. M., and Zaikin, A. N. (1968). Effect of ultraviolet radiation on the self-oscillatory oxidation of malonic acid derivatives. *Russ. J. Phys. Chem.*, 42:3091–3094.

Vavilin, V. A., Zhabotinsky, A. M., and Zaikin, A. N. (1973). A study of a self-oscillatory chemical reaction i. the autonomous system, in biological and biochemical oscillators (proceedings of a conference on biological and biochemical oscillators, prague, 1968). In et al., B. C., editor, *Biological and Biochemical Oscillators*, page 71. Academic, Newyork.

Wang, G., Wang, Q., He, P., Pullela, S., Marquez, M., and Cheng, Z. (2010). Target-wave to spiral-wave pattern transition in a discrete belousov-zhabotinsky reaction driven by inactive resin beads. *Phys. Rev. E*, 82:045201.

Winfree, A. T. (1984). The prehistory of the belousov-zhabotinsky ocsillator. *J. Chem. Ed.*, 61(8):661–663.

Winfree, A. T. (1987). *When time breaks down: The three-dimensional dynamics of electrochemical waves and cardiac arrhythmias*. Princeton University Press (Princeton, N.J.).

Wood, P. M. and Ross, J. (1985). A quantitative study of chemical waves in the belousov-zhabotinsky reaction. *J. Chem. Phys.*, 82:1924.

Zaikin, A. N. and Zhabotinsky, A. M. (1970). Concentration wave propagation in two-dimensional liquid-phase self-oscillating system. *Nature*, 225:535.

Zhabotinsky, A. M. (1964a). Periodic liquid phase reactions. *Proc. Ac. Sci. USSR*, 157:392–395.

Zhabotinsky, A. M. (1964b). Periodical oxidation of malonic acid in solution (a study of the belousov reaction kinetics). *Biofizika*, 9:306–311.

Zhabotinsky, A. M. (1991). A history of chemical oscillations and waves. *Chaos*, 1:379.

Zhabotinsky, A. M., Müller, S. C., and Hess, B. (1991). Pattern formation in a two-dimensional reaction-diffusion system with a transversal chemical gradient. *Physica D*, 49:47–51.

Zhabotinsky, A. M. and Zaikin, A. N. (1973). Autowave processes in a distributed chemical system. *J. Theor. Biol.*, 40:45–56.

Zimmermann, K., Zeidis, I., and Behn, C. (2009). *Mechanics of Terrestrial Locomotion - With a Focus on Non-pedal Motion Systems*. Springer, Berlin.

Zimmermann, K., Zeidis, I., and Pivovarov, M. (2013). Dynamics of two interconnected mass point in a resistant medium. *Differential equations and dynamical systems*, 21:21–28.

Publications

– Refereed papers published in journals or books

1 Tsubasa Masui, Akiyasu Tomoeda, Mayuko Iwamoto, & Daishin Ueyama (2013) "Arch-Shaped Equilibrium Solutions in Social Force Model", pp.179-186 in "Traffic and Granular Flow '11" Springer.

2 Shu-ichi Kinoshita, Mayuko Iwamoto, Keita Tateishi, Nobuhiko J. Suematsu, & Daishin Ueyama (2013) "Mechanism of spiral formation in heterogeneous discretized excitable media", Phys. Rev. E 87, 062815.

3 Tsubasa Masui, Akiyasu Tomoeda, Mayuko Iwamoto, & Daishin Ueyama (2011) "Analysis of Arch-shaped Equilibrium Solutions in Escape Panic" in Japanese, pp.121-124. in *Proceedings of the 17th Symposium on Simulation of Traffic Flow*, The Mathematical Society of Traffic Flow.

– Unrefereed papers published in local conference proceedings.

4 Mayuko Iwamoto, Daishin Ueyama, & Ryo Kobayashi (2013) "Mechanism of Crawling Locomotion with Mucus in Gastropods" in Japanese, No.1853 pp.217-224 in *Proceedings of "Theory of Biomathematics and Its Applications IX"*, Research Institute for Mathematical Sciences (RIMS), Kyoto University.

5 Shu-ichi Kinosita, Keita Tateishi, Mayuko Iwamoto, Nobuhiko J. Suematsu, & Daishin Ueyama (2013) "Review of the origin of spiral formation in heterogeneous excitable media using cellular automaton model" in Japanese, No.1853 pp.210-216 in *Proceedings of "Theory of Biomathematics and Its Applications IX"*, Research Institute for Mathematical Sciences (RIMS), Kyoto University.

Appendix A Photosensitive BZ Reaction

Details of experimental conditions of photosensitive BZ reaction are described here. All experiments performed using the reagents mentioned in Table 5.1 and the experimental instruments in Table 5.2. For maintaining the temperature, reaction field was always cooled by a hose connected to the Low Temperature Bath. The images on personal computer illuminated by the Liquid-Crystal Projector were displayed to a membrane filter through the Magnifying Lens and the Mirror. All experiments were observed through the Colored Glass Filter for enhancing blue color, and recorded by the Digital Video Camera.

Table 5.1. Reagents used in photosensitive BZ reaction.

Reagent	Manufacturer	Molecular Formula	Molecular Weight
Tris(2,2'-bipyridine)ruthenium(II) chloride hexahydrate	Alfa Aesar (ALF)	$C_{30}H_{24}Cl_2N_6Ru{\cdot}6H_2O$	748.63
Sodium Bromate	Wako	$NaBrO_3$	150.89
Sulfuric acid	Wako	H_2SO_4	98.08
Malonic Acid	Wako	$HOOCCH_2COOH$ 3	104.06
Sodium Bromide	Wako	NaBr	102.89
Silicone Oil	TORAY		

Table 5.2. Experimental instruments in photosensitive BZ reaction.

Production	Manufacturer	Details
Membrane Filter	ADVANTEC	MIXED CELLULOSE ESTER A100A025A pore size : 1.0 μm diameter: 25 mm
Colored Glass Filter	Newport.	FSQ-BG40 50.8 μm$\times$ 50.8 μm Blue Bandpass thickness: 3.0 mm
Liquid-Crystal Projector	EPSON	LCD Projector EB-1771W
Digital Video Camera	JVC	Everio GZ-E265
Low Temperature Bath	EYELA	NCB-2500

A excitable wave entered from oscillatory region of outside was designed to keep a shape close to a planar wave. A wave has a high curvature as

shown in Figure 5.2(a), where the time progresses from red to blue, if it was entered without a ingenuity. To decrease the curvature and achieve a wave close to a planar wave, the three large suppression rhombuses as shown in Figure 5.2(b) were placed at near the entrance before a wave reaches the designed heterogeneous reaction field. At first, convexity at middle of a wave was broken by the largest rhombus (A), and convexity at middle of two separated waves were broken by each rhombus (B). Compared with no-obstacle condition (Figure 5.2(a)), a wave in Figure 5.2(b) is clearly shown that a wave became a shape close to planar.

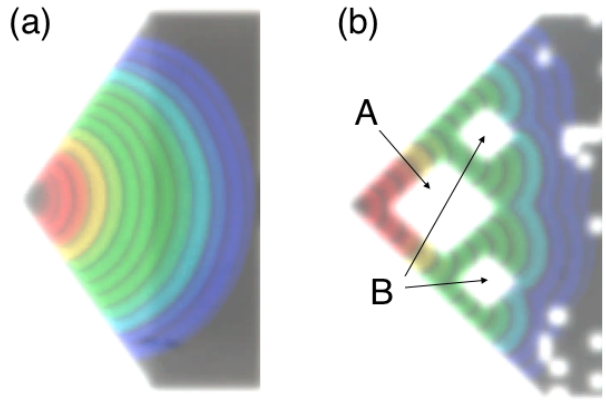

FIGURE 5.2. Superimposed image to show an experimental ingenuity to make a wave become a shape close to a planar wave, where the time progresses from red to blue. (a) No ingenuity condition. A wave has a high curvature. (b) By putting the three obstacle, the shape of a wave became close to a planar wave.

All superimposed color images which tracked a motion of wave were created using the Image J macro developed by Prof. Y. Hiratsuka's laboratory of Japan Advanced Institute of Science and Technology (JAIST)[1].

[1]Macro for ImageJ: http://www.jaist.ac.jp/ms/labs/hiratsuka/index.php

Appendix B BZ Reaction in Ion-Exchange Resin

Details of experimental conditions of the BZ reaction in ion-exchange resin beads are described here. All experiments performed using the reagents mentioned in Table 5.3 and the experimental instruments in Table 5.4. Ferroin was loaded on ion-exchange resin beads by soaked in stirred ferroin solution (dissolved 1,10-Phenanthroline Anhydrous with water) for one hour. All experiments were recorded every 5 seconds using time lapse function of the Digital Camera.

TABLE 5.3. Reagents used in BZ reaction in ion-exchange resin beads.

Reagent	Manufacturer	Molecular Formula	Molecular Weight
1,10-Phenanthroline Anhydrous	Wako	$C_{12}H_8N_2$	180.21
Sodium Bromate	Wako	$NaBrO_3$	150.89
Sulfuric acid	Wako	H_2SO_4	98.08
Malonic Acid	Wako	$HOOCCH_2COOH$ $_3$	104.06
Sodium Bromide	Wako	NaBr	102.89

TABLE 5.4. Experimental instruments in BZ reaction in ion-exchange resin beads.

Production	Manufacturer	Details
Ion-exchange resin	SIGMA-ALDRICH	DOWEX 50WX4-50
Digital Camera	Canon	EOS Kiss X4